



UNIVERSITY OF  
BIRMINGHAM

EFFECT OF FREQUENCY ON THE  
FAILURE OF ARTICULAR  
CARTILAGE

by

**HAMID SADEGHI**

A thesis submitted to  
University of Birmingham  
for the degree of  
DOCTOR OF PHILOSOPHY

Department of Mechanical Engineering  
University of Birmingham

June 2017

UNIVERSITY OF  
BIRMINGHAM

**University of Birmingham Research Archive**

**e-theses repository**

This unpublished thesis/dissertation is copyright of the author and/or third parties. The intellectual property rights of the author or third parties in respect of this work are as defined by The Copyright Designs and Patents Act 1988 or as modified by any successor legislation.

Any use made of information contained in this thesis/dissertation must be in accordance with that legislation and must be properly acknowledged. Further distribution or reproduction in any format is prohibited without the permission of the copyright holder.

## ABSTRACT

Articular cartilage in synovial joints can become damaged due to mechanical loading, trauma or wear and tear. The initiation and progression of damage in cartilage may lead to degenerative changes of the joint. However, links between mechanical loading and the initiation/progression of damage in cartilage remain poorly understood.

In this thesis, the damaging effects of loading frequencies representative of normal (1 Hz), above normal (10 Hz) and rapid heel-strikes (100 Hz) on cartilage/cartilage-on-bone were assessed and compared to test the hypothesis that failure can be influenced by frequency. Bovine cartilage was used as a model for human cartilage. Materials testing machines were used to apply sinusoidally varying loads at different frequencies and altered maximum forces under different loading types. A metal indenter was used to apply cyclic loading on cartilage-on-bone specimens to produce failure on the surface of cartilage-on-bone specimens in compression. Fatigue failure of cartilage-on-bone specimens were determined using cyclic three-point bending. Propagation of an initial crack across the area of cartilage specimens with respect to increasing number of loading cycles were measured and compared under tension.

The results from this thesis indicated that failure increases significantly ( $p < 0.05$ ) in cartilage-on-bone specimens with increasing the loading frequency under compression and bending. Strain experienced by the cartilage specimens at higher frequency, e.g. 100 Hz, caused a greater crack growth under tension. The results from this work have many potential implications in the early onset of osteoarthritis. This is because rapid heel-strike rise times have been implicated in the early onset of osteoarthritis.

## **ACKNOWLEDGEMENT**

I would like to start with thanking my supervisors; Professor Duncan Shepherd and Dr Daniel Espino for giving me this opportunity. Their constant help, patience and availability were determinant for the accomplishment for the work presented in this thesis.

I would like to thank the mechanical engineering technical staff of University of Birmingham: Mr Carl Hingley, Mr Peter Thornton, Mr Lee Gauntlett, Mr Jack Garrod and Mr Simon Rowan for their valuable suggestions and technical support on the experimental aspect of this thesis.

To all the members of the Biomedical Engineering Research Group of the department of Mechanical Engineering of University of Birmingham. I am grateful for their always prompt help, whenever I needed it.

Lastly, i would like to thank my family and friends for their support and encouragement.

# TABLE OF CONTENTS

<b>Chapter 1. Introduction</b> .....	<b>1</b>
1.1 Thesis overview.....	4
<b>Chapter 2. Background</b> .....	<b>5</b>
2.1 Chapter overview .....	5
2.2 Articular cartilage .....	5
2.3 Cartilage loading .....	13
2.4 GRF and HS.....	16
2.5 GRF at HS rise times during gait and OA .....	17
2.6 Experimental failure of articular cartilage .....	21
2.6.1. Dynamic testing .....	24
2.7 Chapter summary .....	26
<b>Chapter 3. Effect of the variation of loading frequency on surface failure of articular cartilage-on-bone</b> .....	<b>27</b>
3.1 Introduction .....	27
3.2 Material and methods .....	28
3.2.1. General methods .....	28
3.2.2. Preliminary experiments .....	31
3.2.3. Analysis of cartilage surface damage .....	37
3.3 Cyclic experiments.....	46
3.4 Cyclic experiment results .....	50
3.5 Discussion.....	56
3.4 Chapter summary .....	60
<b>Chapter 4. Fatigue strength of bovine articular cartilage-on-bone under bending: the effect loading frequency</b> .....	<b>61</b>
4.1 Introduction .....	61
4.2 Material and methods .....	62
4.2.1. General methods .....	62
4.2.2. Preliminary experiments .....	65
4.3 Cyclic three-point bend testing .....	75

4.4 Cyclic three-point bend results .....	76
4.5 Discussion .....	81
4.6 Chapter summary .....	86
<b>Chapter 5. The effect of frequency on crack growth in articular cartilage under tension .....</b>	<b>87</b>
<b>5.1 Introduction .....</b>	<b>87</b>
<b>5.2 Material and methods .....</b>	<b>88</b>
5.2.1 General methods .....	88
5.2.1. Preliminary tensile experiments .....	92
5.2.3. Crack growth experiments .....	95
5.2.4. Crack growth analysis .....	96
5.2.5. Crack growth experiments results.....	97
<b>5.3 Discussion .....</b>	<b>106</b>
<b>5.4 Chapter summary .....</b>	<b>110</b>
<b>Chapter 6. Overall discussion and conclusions .....</b>	<b>111</b>

## LIST OF FIGURES

<b>Figure 2.1.</b> Illustration of synovial joints shown in a model skeleton. The knee (a), hip (b) and shoulder joint (c).....	6
<b>Figure 2.2.</b> MRI images of a human knee joint. Cartilage layer within the joint is shown with arrows.....	6
<b>Figure 2.3.</b> Articular cartilage surface of medial tibial plateau. (Dotted lines denotes the edge of meniscus). Healthy cartilage is white, and its surface is smooth and glistening. ....	7
<b>Figure 2.4.</b> Cells (a and c) and collagen fibrils (b) are classified within the cartilage tissue into superficial, middle, and deep zones, consisting of 10 %-20 %, 40 %-60 %, and 20 %-50 % of the overall tissue depth, respectively. ....	8
<b>Figure 2.5.</b> SEM (Scanning Electron Microscopy) image of the collagen fibril organization in the superficial zone of bovine articular cartilage.....	9
<b>Figure 2.6.</b> SEM images of the collagen fibril organization of deep zone of bovine cartilage .....	10
<b>Figure 2.7.</b> Geometric relationship between the terms; storage ( $E'$ ), loss ( $E''$ ), dynamic ( $E^*$ ) modulus and phase angle ( $\delta$ ).....	11
<b>Figure 2.8.</b> The vertical (Y) axis displays the value of the vertical GRF as a function of body weight (BW), and the horizontal (X) axis shows time in milliseconds. The GRF associated with foot contact have been studied and are divided into the following components: anterior-posterior, horizontal, and vertical. Of these, the vertical GRF is the greatest in the magnitude. (repsoduced with permission from Larson <i>et al.</i> , 2012). ....	14
<b>Figure 2.9.</b> OA of a rabbit (leporine) patellofemoral groove, showing a defect (shown with arrow). (reproduced with permission from CRC Press/Taylor & Francis Group, LLC (Athanasίου, 2013)). ....	18
<b>Figure 2.10.</b> Sinusoidally varying force a) at 92 Hz (rise time 5.4 ms); b) at 1 Hz (rise time 500 ms).....	20
<b>Figure 3.1.</b> Dissection (a) Bovine shoulder joint (b) humeral head removed from the shoulder joint. ....	29
<b>Figure 3.2.</b> Cartilage samples (a) Two 50 × 50 mm areas were selected from the central region of the humeral head after its removal from the shoulder joint (b) side view of a cartilage-on-	

bone specimen obtained from the humeral head using a hacksaw. Cartilage-on-bone specimens were selected from the central flat surface of the humeral head. Flattest regions were selected for testing only. The scale bar is in mm. .... 30

**Figure 3.3.** India ink (a) A sample image taken from the cartilage surface of a cartilage-on-bone specimen. This image shows the glistening nature of the cartilage surface. (b) India ink was applied on the cartilage surface. (c) Any damage on the cartilage surface (shown with arrows) is visible after the India ink was rinsed off the surface. Damaged areas are highlighted as cracks and fissures on the cartilage surface and were not used for testing. .... 30

**Figure 3.4.** Mechanical testing (a) Bose ELF 3200 testing machine (b) test rig fitted into the testing machine with cartilage-on-bone specimen bathed into ringer’s solution secured using acrylic cement. .... 31

**Figure 3.5.** Diagram of the experimental set-up used during the testing procedure. .... 32

**Figure 3.6.** Load against displacement of a cartilage-on-bone specimen subjected to compression. The cartilage surface was damaged at a load ( $F$ ) of 123 N corresponding to the failure displacement ( $\delta$ ) of 0.58 mm. .... 33

**Figure 3.7.** Three sites were chosen on a cartilage-on-bone specimen to perform compression tests. The cartilage surface damage was highlighted with the aid of India ink. Cracks appeared on the cartilage surface following testing. Black circles inserted in the image are 5.2 mm in diameter, the same diameter as the indenter. Scale bar is 1 cm. .... 34

**Figure 3.8.** Figure 3.8. Images taken from the cartilage surface of three cartilage-on-bone specimens. The black circles show the loaded region. Loading ranges included were (a) 6-60 N, (b) 9-90 N and (c) 12-120 N. The increase in crack length with increasing maximum load and frequency can be observed from left to right. India ink was applied to the cartilage surface to easily distinguish the surface cracks. Scale bar is 1 cm. .... 36

**Figure 3.9.** Drawing a 10 mm line on the scale bar manually. .... 38

**Figure 3.10.** Maximum crack length. (a) Figure 3.8-c (b)The maximum crack length at each testing site was selected from visual observations. In this image, maximum crack lengths were highlighted using red lines. .... 39

**Figure 3.11.** The length of the maximum cracks was measured. .... 40

**Figure 3.12.** Images were converted into 8-bit grayscale before the application of threshold. .... 41

**Figure 3.13.** A threshold was applied to the image to enable quantitative evaluation of the damage induced. .... 42

<b>Figure 3.14.</b> Threshold was increased from 116 (a) to 156 (b).....	42
<b>Figure 3.15.</b> The area of damage was identified at each individual test site as shown by the rectangular box.....	43
<b>Figure 3.16.</b> The white areas represent damage with the area of damage identified objectively. ....	44
<b>Picture 3.17.</b> Total crack length (a) Cartilage surface cracks highlighted with the aid of India ink. (b) Red lines were drawn along the surface cracks to highlight damaged areas. ....	45
<b>Figure 3.18.</b> The individual length of each crack was measured manually (in mm). ....	46
<b>Figure 3.19.</b> Number of independent observations ( <i>n</i> ) used for calculating the 95% confidence intervals in Figures 3.25 and 3.26. Each load range was tested at three loading frequencies on distinct test sites (120 test).....	49
<b>Figure 3.20.</b> Representative images taken from cartilage samples following cyclic loading. The black circles show the loaded region. Loading ranges included were (a) 6-60 N, (b) 9-90 N, (c) 10-100 N, (d) 12-120 N and (e) 16-160 N. The formation and increase in crack length can be generally observed with increasing load and frequency. India ink was applied to the cartilage surface to easily distinguish the surface cracks. A scale bar is included in every image in order to measure the surface features. ....	51
<b>Figure 3.21.</b> Total crack length plotted against the logarithm (with base 10) of the loading frequency for testing on one tissue sample. Three selective data points have been chosen from load ranges of 6-60 N (□), 9-90 N (□), 10-100 N (▼), 12-120 N (Δ) and 16-160 N (■). ....	52
<b>Figure 3.22.</b> Mean total crack length plotted against the logarithm (with base 10) of the loading frequency for the load ranges of 6-60 N (□), 9-90 N (□), 10-100 N (▼), 12-120 N (Δ) and 16-160 N (■). Second order polynomials (see equation 3.1) fitted the data well. Error bars represent 95% confidence intervals, for clarity only positive error bars have been included. When error bars are not visible they are smaller than the symbols used to represent the data point.....	53
<b>Figure 3.23.</b> Mean total crack length plotted against the maximum load for loading frequencies of 1 Hz (●), 10 Hz (○) and 100 Hz (▼). Each point in this graph represents the mean crack length of 8 measurements. The crack length is described by linear curve fits (see equation 3.2). <i>P</i> -value for all lines were $p < 0.05$ which indicates that lines are statistically significant. $R^2$ is the squared correlation coefficients and shows how well the lines fit the data point. $R^2$ value for loading frequencies of 1, 10 and 100 Hz are 0.87, 0.97 and 0.99, respectively. Uncertainty of estimates is presented in the form of 95% confidence intervals for clarity only positive error	

bars have been included. When error bars are not visible it is because they are smaller than the symbols used to represent the data point. .... 55

**Figure 4.1.** Cartilage-on-bone specimen (a) Sample image of the top view of a cartilage-on-bone specimen used to perform bending tests (b) side view of the same specimen showing the depth of the specimen. The scale bar is in mm. .... 63

**Figure 4.2.** Bending test configurations (a) Three-point bend and (b) four-point bend test rig with a cartilage-on-bone specimen in the starting test position. The distances between the inner and outer supports of the four-point bending test were 10 and 20 mm, respectively. .... 64

**Figure 4.3.** Bose ELF3300 material testing machine. (a) Computer (b) Bending test rig fitted into the testing machine (c) Machine (d) Power tower. .... 66

**Figure 4.4.** Load against displacement of a cartilage-on-bone specimen under three-point bending. Failure occurred at a load ( $F$ ) of 89 N corresponding to a failure displacement ( $\delta$ ) of 1.85 mm. .... 67

**Figure 4.5.** Load against displacement of a cartilage-on-bone specimen under four-point bending. Failure occurred at the load ( $F$ ) of 304 N corresponding to the failure displacement ( $\delta$ ) of 3.24 mm. .... 68

**Figure 4.6.** Images taken from six cartilage-on-bone specimens after failure under bending. (a) Failure occurred at the centre of the specimens tested in a three-point bending configuration. (b) Failure occurred at the point of the outer contacts for specimens tested in four-point bending suggesting that stress is concentrated at these points. .... 69

**Figure 4.7.** An initial crack of 0.5 mm depth was cut into the centre of the cartilage-on-bone specimen. .... 70

**Figure 4.8.** Three specimens subjected to sinusoidally varying forces of 7-70 N at 10 Hz. Specimen (a) fractured after the first application of load. Specimens (b) and (c) fractured at 4,715 and 5,242 cycles, respectively. However, the point at which the specimens fractured was not where the pre-existing crack was introduced (marked with arrows). .... 71

**Figure 4.9.** Sample images taken from cartilage-on-bone (specimen c from figure 4.7). a) specimen at the starting position b) specimen after the application of 5,000 loading cycles. A pre-existing crack showing minimal growth after the application of 5,000 loading cycles. The scale bar is in mm. .... 71

**Figure 4.10.** Initial crack was introduced at the centre of each specimen. Two of the cartilage-on-bone specimens fractured at 2,102 (a) and 3,454 (b) of loading cycles. However, one of the specimens reached run-out (c). The scale bar is in mm. .... 72

**Figure 4.11.** Sample images taken from cartilage-on-bone specimen (b) from figure 4.9. (a) specimen at the starting position (b) specimen after the application of 5,000 loading cycles. A pre-existing crack showing minimal growth after the application of 5,000 loading cycles. The scale bar is in mm. .... 73

**Figure 4.12.** Cyclic three-point bending (a) Cartilage-on-bone specimen at the starting position for three-point bending (b) Specimen deflecting under cyclic three-point bending subjected to a force range of 7-70 N at a frequency of 10 Hz. .... 74

**Figure 4.13.** Fractured cartilage-on-bone specimens. (a) Cartilage-on-bone specimen subjected to three sinusoidally varying force ranges of 7-70, (b) 10-100 and (c) 13-130 N after their fracture. The scale bar is in mm. .... 74

**Figure 4.14.** Maximum force plotted against the number of cycles to failure, with the number of cycles on a logarithmic scale (base 10) at loading frequencies of 1 Hz (a), 10 Hz (b), 50 Hz (c) and 100 Hz (d). Specimens that failed were plotted with (●) and specimens that reached run-out were plotted with (○). Details of the regression curves are included in Table 1. Solid curve fits indicate best curve fit for specimens that failed before 10,000 cycles were completed. Dashed curve fits also include the specimens that reached run-out. .... 77

**Figure 4.15.** Mean number of cycles plotted against loading frequency, with the number of cycles on a logarithmic scale (base 10). Specimens that have reached run-out are included in the analysis of this plot as 10,000. .... 80

**Figure 4.16.** Cartilage surface crack observed on specimens that reached run-out at loading frequencies of 1 Hz and 10 Hz (a) Top view of the selected specimens after run-out was reached at a loading frequency of 1 Hz and (b) 10 Hz. Both specimens in these images were loaded between 6-60 N. .... 81

**Figure 5.1.** Cartilage surface crack observed on specimens that reached run-out at loading frequencies of 1 Hz and 10 Hz (a) Top view of the selected specimens after run-out was reached at a loading frequency of 1 Hz and (b) 10 Hz. Both specimens in these images were loaded between 6-60 N. .... 88

**Figure 5.2.** Cartilage specimen extraction. a) Mandoline slicer used to remove cartilage from cartilage-on-bone specimens from Figure 5.1. b) Sample image taken from two cartilage specimens with 1 mm depth from the articular surface. .... 89

**Figure 5.3.** Tensile testing configuration. (a) Dimensions of the cartilage specimen (b) Cartilage specimen placed in grips, ready for testing. All units are in mm. .... 90

**Figure 5.4.** Cartilage testing in tension (a) Bose ELF 3200 testing machine used to test cartilage specimens in tension (b) Cartilage specimen secured in the testing grips with the aid of emery paper..... 91

**Figure 5.5** Load against displacement of a cartilage specimen under tension. Failure occurred at the load ( $F$ ) of 14.8 N corresponding to the failure displacement ( $\delta$ ) of 4.3 mm. The initial crack in this cartilage specimen extended from 2.26 mm to 2.39 mm during this ramp test... 93

**Figure 5.6.** Cartilage specimens after being subjected to 10,000 cycles of continuous tensile strain. 2.26 mm initial crack extended up to 3.1, 4.2 and 4.8 mm at loading frequencies of 1, 10 and 100 Hz, respectively..... 94

**Figure 5.7.** Schematic of the cartilage specimen. Crack growth ( $\delta c$ ) and necking ( $\delta h$ ) were measured for each image acquired from cartilage specimens at several stoppages during cyclic testing..... 97

**Figure 5.8.** Specimen images taken at 0, 20, 50, 100, 500, 1,000, 5,000 and 10,000 cycle. Each specimen was subjected to a maximum strain of 20 % undertaken at loading frequencies of a) 1 Hz, b) 10 Hz and c) 100 Hz. Increasing the loading frequency caused a higher crack growth in cartilage specimens..... 98

**Figure 5.9.** Individual specimen crack growth ( $\delta c$ ) plotted against the natural logarithm of number of cycles ( $N$ ) at the three tested frequencies. Three specimens were selected from each loading frequency. Cartilage specimens 2, 6 and 7 were tested at a frequency of 1 Hz (in black) specimens 11, 12 and 13 at 10 Hz (in white) and specimens 24, 25 and 26 were tested at 100 Hz (in gray)..... 100

**Figure 5.10.** Mean crack growth ( $\delta c$ ) against the natural logarithm of the number of cycles ( $N$ ). Logarithmic curves (equation 5.3) fitted the data points well. Error bars represent 95% confidence intervals for the samples. For clarity only positive error bars are include..... 101

**Figure 5.11.** Sample images taken from cartilage specimen number 8, tested at a frequency of 1 Hz at the initial testing position and following 10,000 cycles. Vertical lines were inserted in each image in order to show the displacement of the sides of the cartilage specimen relative to their initial position..... 103

**Figure 5.12.** Mean necking ( $\delta h$ ) against the natural logarithm of the number of cycles ( $N$ ). Logarithmic curves (equation 5.4) fitted the data points well. The  $R^2$  and  $p$  values of this figure are included in table 2. Error bars represent 95% confidence intervals for the samples. For clarity only positive error bars are include..... 104

## LIST OF TABLES

<b>Table 3.1.</b> Details of the constants from the mean total crack length against frequency curve fits (Figure 3.22) .....	54
<b>Table 4.1.</b> Constants from the curve fit correlations of Figure 4.14. ....	78
<b>Table 5.1.</b> Details of the constants from the mean crack growth against number of cycles curve fits (Figure 5.10). Units for <i>A</i> and <i>B</i> are in mm .....	102
<b>Table 5.2.</b> Details of the constants from the mean necking against number of cycles curve fits (Figure 5.12). Units for <i>C</i> and <i>D</i> are in mm.....	105

## ACRONYMS

GRF .....	Ground Reaction Forces
HS .....	Heel-strike
OA .....	Osteoarthritis
RHS .....	Rapid Heel-strike

## Chapter 1: Introduction

Articular cartilage is a load bearing material in human joints such as the hip and knee. These joints can be affected by degenerative diseases such as osteoarthritis (OA) which can lead to the degeneration and loss of cartilage tissue, which includes initiation and progression of damage across cartilage. Initiation and progression of damage can cause failure in the articular cartilage of joints. The work in this thesis aims to further understand the link between mechanical loading and cartilage failure. Understanding the mechanism associated with the failure of articular cartilage is important to help identify strategic solutions which curtail such failure mechanisms. Understanding such failure mechanisms was achieved by investigating the effect of the variation of loading frequency on the failure of cartilage under different types of loading and testing configurations.

OA appears as a combination of small cracks in the articular surface, with the loss of the tissue's matrix leading to deleterious reduction in its thickness, and it has been hypothesized that these microcracks propagate over time as a constituent of the development/progression of OA (Meachim *et al.*, 1972; Natoli *et al.*, 2008). The lack of blood vessels and cells that can repair significant tissue damage limits the ability of cartilage to repair damage (Buckwalter *et al.*, 1991). Disorders of articular cartilage represent some of the most common and debilitating diseases encountered in orthopaedic practice. Therefore, maintaining the mechanical integrity of articular cartilage is of considerable importance, and the most direct way of doing this is to ensure that the forces applied to joints do not exceed the mechanical tolerance of the component tissues.

Moreover, it is current clinical practice to repair articular cartilage damage using integration of repair cartilage with the host cartilage (LeBaron *et al.*, 2000). However, there is little cohesion between the two tissues. This is because the mechanical properties of the repair tissue are inferior to the original material (Ahsan *et al.*, 1999). Thus, study into the failure mechanisms of bovine articular cartilage as a model for human cartilage would provide the grounds for future comparison of the recipient to the repair tissue. The variation of articular cartilage damage with frequencies

relevant to normal, above normal and rapid heel-strike (RHS) rise times during gait, and how this relationship is altered by the maximum stresses were assessed and compared in this work. The experiments involved using suitable materials testing machines to subject cartilage/cartilage-on-bone specimens to sinusoidally varying force ranges at different frequencies.

The average person takes approximately 2 million steps per year. Thus, a lower limb joint undergoes 1 million loading cycles during this time. Age has been suggested to be the main factor which predisposes cartilage to damage due to mechanical loading (Weightman *et al.*, 1976). Although the mechanisms responsible for OA remain poorly understood, factors such as obesity and heritable genetics have been suggested to be involved in the progression of the disease (Griffin *et al.*, 2005). Moreover, a transversal study of Kraus *et al.* (2017) recently investigated targeting a set a biomarker as predictors of clinically relevant OA. This study reported that risk of progression of OA in articular cartilage was also associated with low serum levels of PIIANP among patients characterized by mild or moderate knee OA. Kraus *et al.* (2017) also showed that knee OA progression was associated with isomered forms of CTX-I epitope level in urine from patients with late-stage OA.

Several studies have established that, in human beings, there is often an impulsive foot-ground reaction at the instant of heel-strike (HS) (Simon *et al.*, 1981; Radin *et al.*, 1991). Cartilage is typically subjected to loading with a HS rise time of 100 to 150 ms (Shepherd *et al.*, 1997). A subset of the population with HS rise times from 5 to 25 ms has been identified as being linked to the onset of OA (Radin *et al.*, 1986). The timing of these HS corresponds to loading frequencies of 3–5 Hz for normal and up to 90 Hz for RHS rise times (Fulcher *et al.*, 2009). Previous studies (Radin *et al.*, 1973; Dekel *et al.*, 1978; Radin *et al.*, 1978) have also suggested that the frequency of loading of a joint might be important with respect to the possibility of damage to articular cartilage. These suggestions were made in terms of the association between mechanical loading and OA. Cartilage injuries can result from impact and cyclic loading, and these can occur under a wide range of loads, timescales, and frequencies. Previous studies have focused on a specific type

of loading and observed crack formation on the cartilage surface following single impact (Jeffrey *et al.*, 1995; Torzilli *et al.*, 1999) or during cyclic compression (Kerin *et al.*, 2003). However, other similar studies have investigated the crack propagation through the cartilage depth and the underlying bone following impact (Silyn-Roberts *et al.*, 2009; Borrelli *et al.*, 1997) or through the depth of cartilage specimens during static tension (Stok *et al.*, 2003 & 2007). Determining thresholds that can induce failure into articular cartilage particularly in terms of the loading frequency and maximum load has not been investigated to date.

The durability of articular cartilage is a crucial factor associated with its functionality within joints. Fatigue testing applies cyclic loading until the specimen fails (Ker *et al.*, 1999; Simon & Mark *et al.*, 1990). Usually a specific type of loading is selected, such as compression, bending, tension, or shear, and repeated cycles are applied until the specimen is noticeably affected by the formation of cracks and fissures. Fatigue life is defined as the number of cycles necessary to produce failure in a specimen. Thus, some caution must be exercised when interpreting the results of experiments in which a large stress/strain is applied to produce failure of specimens removed from the joint. This is because the stress/strain is applied to cause failure maybe greater than experienced *in vivo* (Weightman & Kempson, 1979). In addition, failure could be defined as merely large cracks on the surface of cartilage-on-bone specimens under compression (Fick *et al.*, 2011) or the complete rupture of dumbbell-shaped cartilage specimens subjected to cyclic tension (Bellucci *et al.*, 2001). Fatigue life of articular cartilage may depend on the applied stress, strain and frequency.

## 1.1 Thesis overview

Chapter 2 explains the background knowledge needed to understand the following chapters in this thesis. The background covers articular cartilage, heel-strike during gait, and links between rapid heel-strike rise times and osteoarthritis as well as comparable studies on experimental failure of articular cartilage that have been carried out previously.

Chapter 3 details a study on the effects of the variation of loading frequency on surface failure of cartilage-on-bone specimens. This chapter also provides the preliminary static and cyclic tests performed in order to induce damage on the cartilage surface. The chapter is based on the work published in *Osteoarthritis and Cartilage* titled ‘Effect of the variation of loading frequency on surface failure of bovine articular cartilage’; 2015, Volume 23, Number 12, Pages 2252-2258.

Chapter 4 investigates the effect of variation of loading frequency on fatigue strength of rectangular cartilage-on-bone specimens. In this chapter, the fatigue strength of cartilage-on-bone specimens was obtained via cyclic three-point bending tests. This chapter is based on the work published in *BMC Musculoskeletal Disorders* titled ‘Fatigue strength of bovine articular cartilage-on-bone under three-point bending: the effect of loading frequency’; 2017, Volume 18, Number 142.

Chapter 5 investigates the crack growth of an initial crack across the area of cartilage specimens under tension at various frequencies. Crack growth of cartilage specimens was achieved by applying cyclic strains to the cartilage specimens. The work in this chapter is based on the work submitted to the *Journal of Mechanical Behaviour of Biomedical Materials* titled ‘Effect of frequency on crack growth in articular cartilage’.

Chapter 6 provides the overall discussion and conclusions.

## **Chapter 2: Background**

### **2.1 Chapter overview**

This chapter introduces articular cartilage. It starts with a brief description of the tissue and its function in articulating joints within the body. Section 2.2 describes the role of the articular cartilage in the body and its structure. Section 2.3 defines gait, HS, ground reaction forces (GRF), HS rise times and section 2.4 explains the relationship between GRF at HS and cartilage loading. Section 2.5 describes the association between RHS rise times and OA. Section 2.6 details the methods that have been used to perform experimental injury on articular cartilage. Section 2.7 provides the chapter summary.

### **2.2 Articular cartilage**

Articulating joints between the bones of the mammalian skeleton are structured to do specific functions. These functions usually involve coordination of stability and mobility (Figure 2.1). Covering the end of the bones (epiphyses) in the joints is the articular cartilage tissue. This layer functions to facilitate load support and load transfer while allowing for translation and rotations between bones (Figure 2.2) (Mow & Ratcliffe, 1997). In addition to load distribution, cartilage provides a smooth articular surface, through a combination of a surface roughness of 80-170 nm (Ghosh *et al.*, 2013) and lubrication regimes (McNary *et al.*, 2012), that allows relative motion between bones with extremely low friction (Figure 2.3) (Mow & Ratcliffe, 1997).

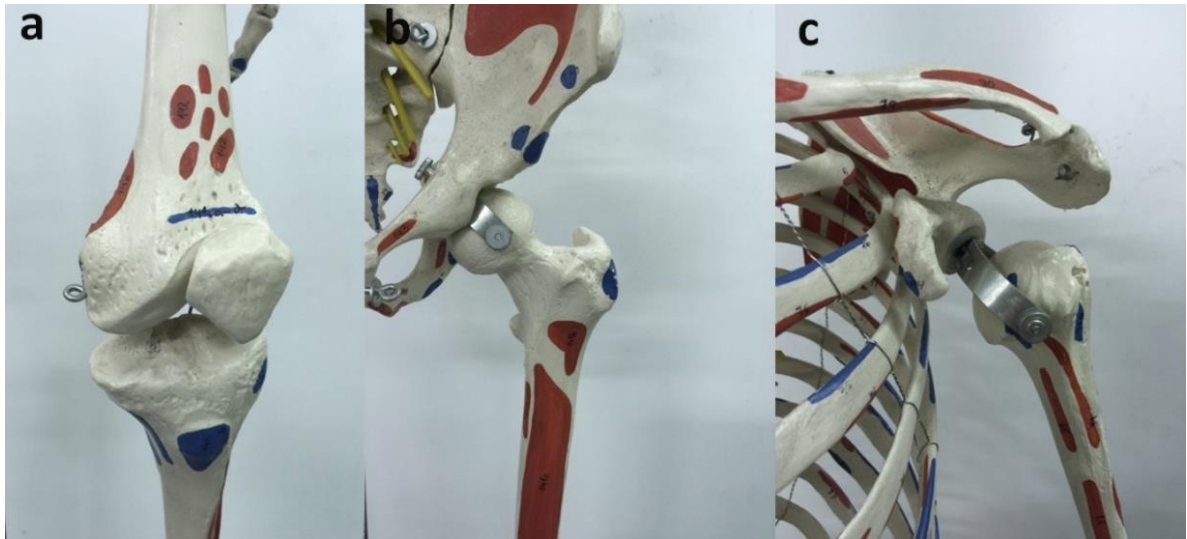


Figure 2.1. Illustration of synovial joints shown in a model skeleton. (a)The knee, (b) hip and (c) shoulder joint.



Figure 2.2. MRI images of a human knee joint. Cartilage layer within the joint is shown with arrows.



Figure 2.3. Bovine articular cartilage surface of medial tibial plateau. (Dotted lines denotes the edge of meniscus). Healthy cartilage is white, and its surface is smooth and glistening.

Articular cartilage is mostly composed of extracellular matrix. The extracellular matrix has three principal constituents: collagen, proteoglycans, and water. Water is the most abundant component of cartilage, contributing between 60-80 % of the tissue's wet weight (Shrive & Frank *et al.*, 1999). However, collagen and proteoglycans make up 60-70 % (Maroudas *et al.*, 1968) and 30 % (Eyre *et al.*, 1991) of the tissue's dry weight, respectively. Articular cartilage also contains cells, called chondrocytes, embedded in the extracellular matrix; however, this only constitutes around 2 % of the total volume of articular cartilage (Alford *et al.*, 2005). Unfortunately, chondrocytes have limited potential for replication, a factor that contributes to the limited healing capacity of cartilage in response to injury (Sophia Fox *et al.*, 2009).

The structure of articular cartilage is often described in terms of four zones between the articular surface and the subchondral bone. These are the superficial zone, intermediate zone, deep zone and the calcified zone (Jeffrey *et al.*, 1991). The zones of articular cartilage from the

articulating surface down to the subchondral bone can be seen in Figure 2.4. The superficial zone contains highly packed, collagen fibrils that are parallel to the articular surface (Figure 2.5). In the intermediate (transitional) zone, collagen is randomly organized. The deep zone is typically characterized by collagen fibrils that are perpendicular to the articular surface (Figure 2.6) (Sophia Fox *et al.*, 2009).

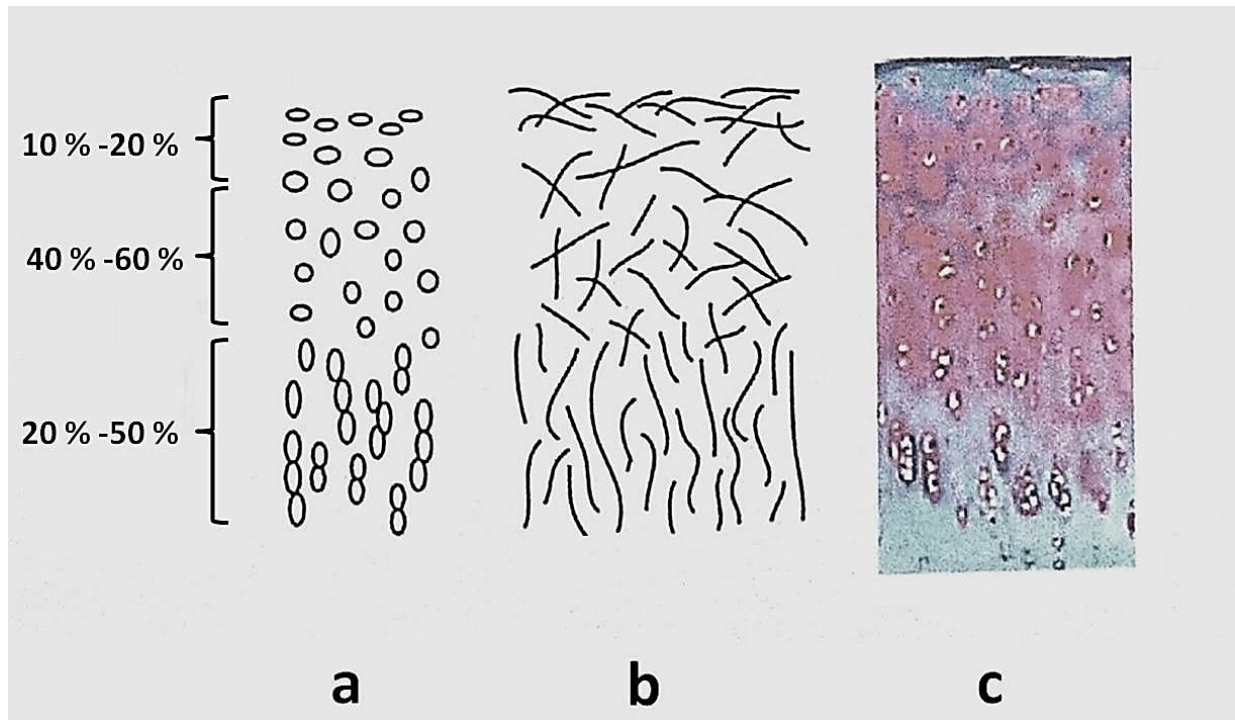


Figure 2.4. Cells (a and c) and collagen fibrils (b) are classified within the cartilage tissue into superficial, intermediate, and deep zones, consisting of 10 %-20 %, 40 %-60 %, and 20 %-50 % of the overall tissue depth, respectively. (reproduced with permission from CRC Press/Taylor & Francis Group, LLC (Athanasίου, 2013)).

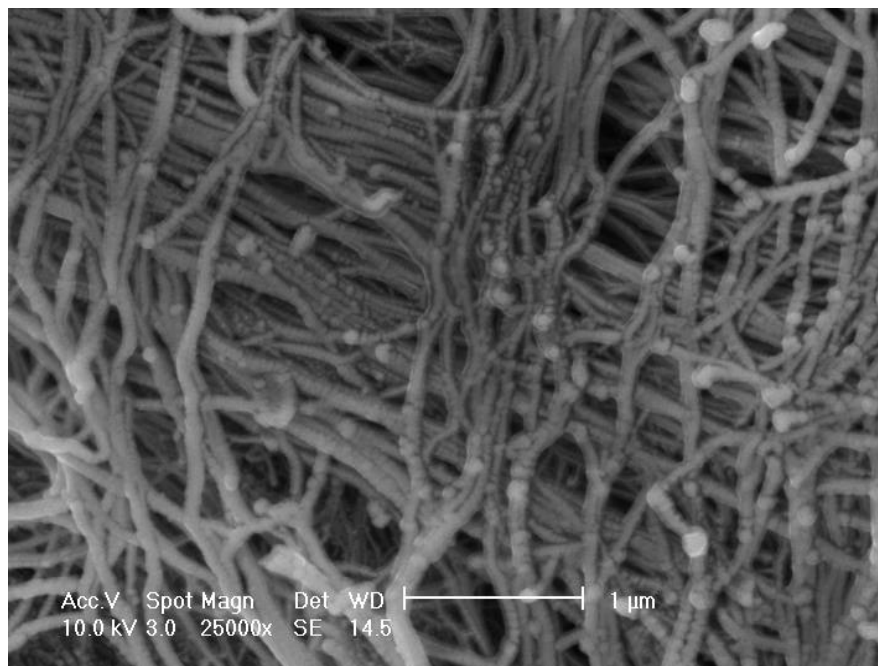
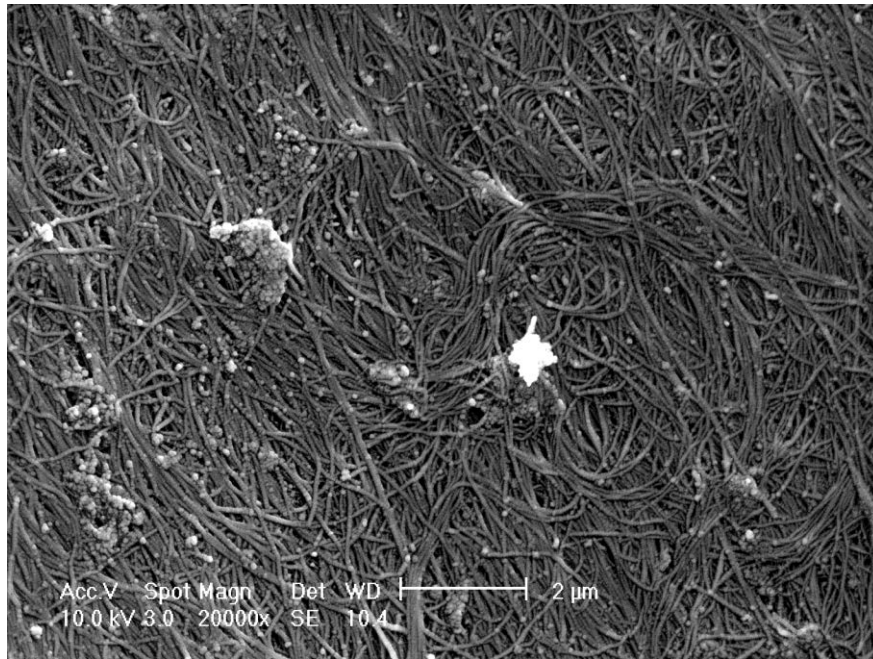


Figure 2.5. SEM (Scanning Electron Microscopy) image of the collagen fibril organization in the superficial zone of bovine articular cartilage. (Images courtesy of Siddharth Ghosh)

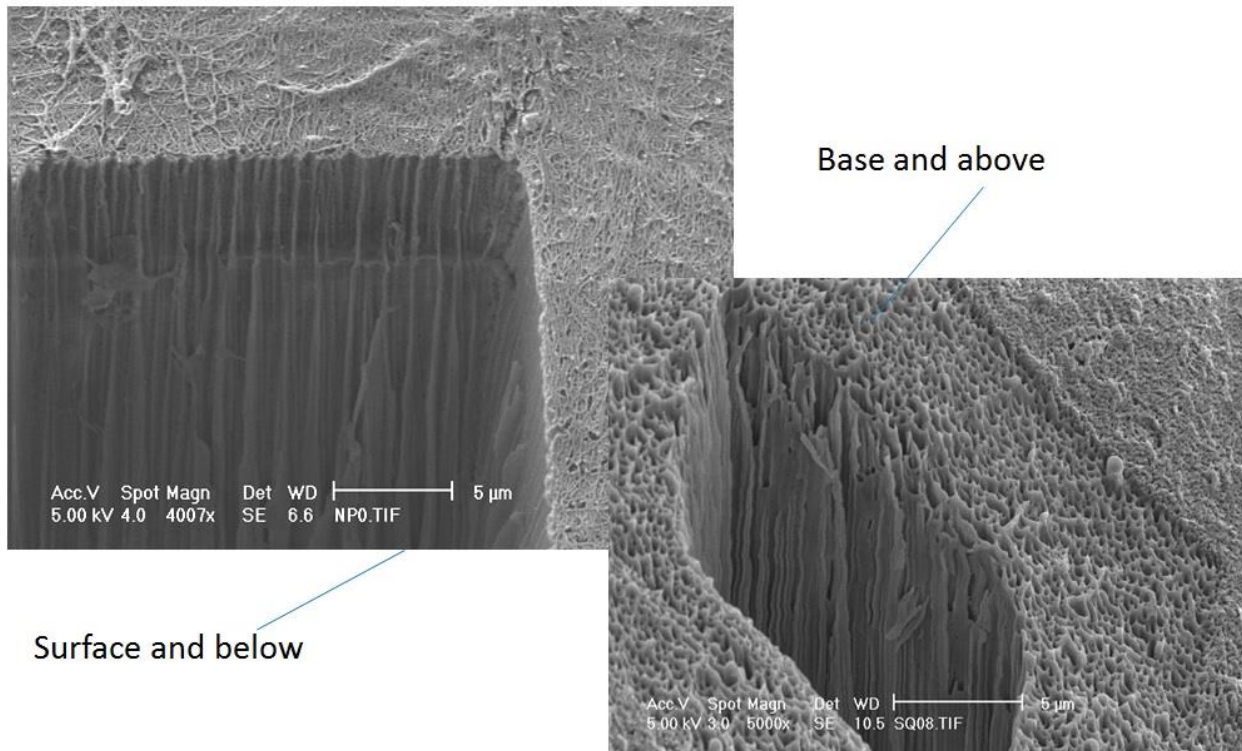


Figure 2.6. SEM images of the collagen fibril organization within the deep zone of bovine cartilage. (Images courtesy of Siddharth Ghosh)

Cartilage is assumed as a biological example of a fiber-composite material in which the strong and stiff collagen fibrils reinforce a mechanically weak proteoglycan gel (Hukins *et al.*, 1985). The extracellular matrix consists of collagen fibrils surrounded by a highly hydrated gel (Hukins *et al.*, 1985). This gel contains a proteoglycan gel and negatively charged glycosaminoglycans (GAGs) chains (Muir, 1995). These GAGs attract water into the tissue, via the Donnan osmotic effect, and so form a gel which tends to swell as more water is attracted (Hukins *et al.*, 1984).

Articular cartilage is a mechanically complex structure that includes both elastic-like and viscous-like properties. In an ideal linearly elastic material, stress and strain are directly proportional, whereas in a viscous material, deformation follows applied load by a measurable time lag. In an elastic material, the work done by loading is stored as potential strain energy which is released when the load is removed. This allows the material to return to its original dimensions. In

contrast, mechanical loading of a viscous material causes larger scale molecular movement that results in energy dissipation (Wainwright *et al.*, 1976). Articular cartilage is a viscoelastic material since it combines the ability to store potential strain energy, but also experience energy dissipation while loaded (Hayes *et al.*, 1971; Wainwright *et al.*, 1976). The elastic and viscous properties of a material can be characterised by storage ( $E'$ ) and loss ( $E''$ ) modulus, respectively. The dynamic modulus ( $E^*$ ) is a complex number which is comprised of real and imaginary components (Hukins *et al.*, 1999). The diagram shown in Figure 2.7 shows an Argand diagram for a complex number and, therefore, suggests a complex number representation for the moduli term such that  $E'$  and  $E''$  are the real and imaginary parts of a complex number  $E^*$ , respectively. Accordingly:

$$E^* = E' + i E'' \quad (2.1)$$

where,  $E^*$  is described as the complex modulus,  $E'$  is the real (or the storage) modulus, and represents the elastic component of viscoelastic behaviour,  $E''$  is the loss modulus (energy dissipation), and represents the viscous component of the viscoelastic behaviour, and “i” is the imaginary number ( $i^2 = -1$ ).

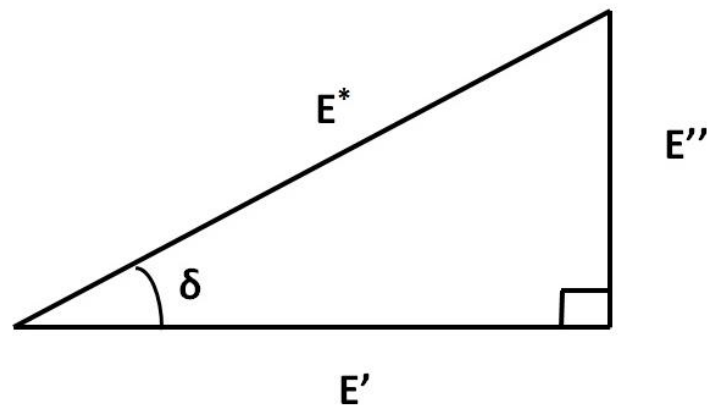


Figure 2.7. Geometric relationship between the terms; storage ( $E'$ ), loss ( $E''$ ), dynamic ( $E^*$ ) modulus and phase angle ( $\delta$ ).

The composition of articular cartilage plays an important role in its mechanical behaviour, with different models used to explain this mechanical behaviour and deformation. In the biphasic model of cartilage, the deformation of cartilage stems from the combination of interactions between the fluid and solid phases. The biphasic model of cartilage is based on the assumption that cartilage is a complex material, essentially a fluid-saturated, fiber-reinforced, porous, permeable composite matrix (Mow & Holmes *et al.*, 1984). The interactions among these extracellular components determine the biomechanical properties of articular cartilage including its viscoelastic response to loads applied at different rates (Shrive & Frank *et al.*, 1999). The biphasic model suggested that when cartilage is deformed, water and collagen fibrils play the viscous and elastic components, respectively. Thus, at lower rates of loading there is more time of water to flow due to the permeability of the cartilage matrix (Oloyede *et al.*, 1992). However, more recent studies (Pearson & Espino *et al.*, 2013; Sadeghi *et al.*, 2015) which have investigated the viscoelastic properties of cartilage at physiological loading rates, demonstrated limitations with this original model. Those studies have shown that as the rate of loading decreases, the loss modulus,  $E''$  (dissipated energy) remained unchanged. However, storage modulus,  $E'$  (stored energy) varied hugely at the same tested loading rates. The biphasic theory also suggests that the load-bearing task of cartilage is a result of internal fluid pressure and an osmotic swelling pressure due to the negatively charged proteoglycans (Ateshian *et al.*, 2009). However, it was reported that this fluid pore pressure takes approximately 15 minutes to reach the maximum level (Fick *et al.*, 2011); therefore, the role of permeability through the cartilage matrix, as the biphasic theory advocates, requires longer loading times than might be associated with physiological loading. Fick *et al.* (2011) measured the rise in pore pressure of cartilage samples using a pressure sensor.

Recent studies (Fulcher *et al.* 2009, Espino *et al.*, 2014; Sadeghi *et al.*, 2015) have investigated changes in cartilage viscoelastic properties with frequencies up to 92 Hz. The suggestion from these studies is that the likelihood of cartilage failure increases with loading frequency. This was suggested, because at higher frequencies the ability of the tissue to store

energy, for elastic recoil, increased. It was suggested that if the energy available for storage exceeded a certain level it might induce damage to the cartilage. Damage caused by increasing the loading frequency has been suggested to be different to the damage caused by increasing load only following comparisons between failure patterns from static loading tests (Fick *et al.*, 2011 & 2012).

An alternative for the biphasic theory is the triphasic theory. In the triphasic theory, negatively-charged proteoglycans in cartilage produce an osmotic pressure which swells the tissue and contribute to its compressive stiffness. However, the main limitation regarding this theory is that it does not fulfil the second law of thermodynamics (Huyghe *et al.*, 2009). This is because free energy of a sample of cartilage subjected to a closed cycle of mechanical and chemical loading is calculated using this theory. Huyghe *et al.* (2009) calculated that the chemical expansion stress term induces a non-physical generation of free energy during each closed cycle of loading and unloading. The value of free energy production was estimated to be 20 % of the elastic energy stored in the sample (Huyghe *et al.*, 2010).

Another alternative to the biphasic and triphasic theory is to treat cartilage as a gel. In the cartilage tissue, viscoelasticity results from the conformational change of macromolecules (Kovach *et al.*, 1996). Moreover, by balancing proteoglycan swelling, the collagen fibrils affect the degree of tissue hydration, contributing to tissue compressive properties (Kovach *et al.*, 1996). In this model, slowly applied loads displace the fluid and frictional drag arising from fluid flow past the GAG chains has been used to explain the remarkably low permeability of the tissue (Kovach *et al.*, 1995 & 1996).

## **2.3 Cartilage loading**

Gait is a term used to describe locomotion achieved through the movement of human limbs, or the way that a person walks (Figure 2.8). Every individual has a unique gait pattern. Additionally,

a person's gait can be greatly affected by an injury or disease process (Hurwitz *et al.*, 2000). The gait cycle can be divided into various phases and periods to determine normal and abnormal gait (Radin *et al.*, 1986a). Gait analysis provides the information useful for the development of prosthesis and aid for the disabled (Sutherland, 1984). The information can also be useful in characterization of the total load transferred through the joints in the body during locomotion (DeFrate *et al.*, 2004). Cartilage is responsible for distributing a great part of the loads developed in the joint during gait, which can be more than five times body weight in the knee (Bergmann *et al.*, 2014).

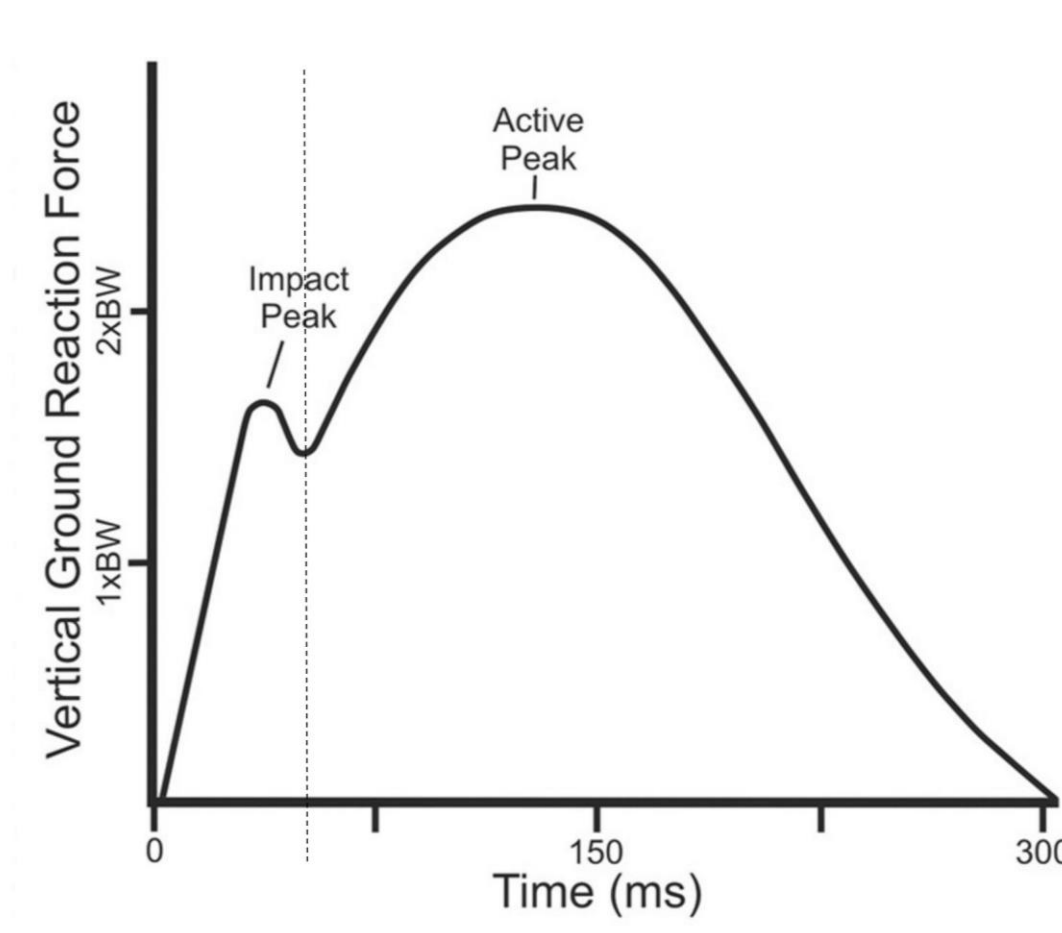


Figure 2.8. The vertical (Y) axis displays the value of the vertical GRF as a function of body weight (BW), and the horizontal (X) axis shows time in milliseconds. The GRF associated with foot contact have been studied and are divided into the following components: anterior-posterior, horizontal, and vertical. Of these, the vertical GRF is the greatest in magnitude. (reproduced with permission from Larson *et al.*, 2012).

HS, also known as initial contact, is a short period which starts at the moment the foot makes contact with the ground (Shultz, 2005). During the normal gait cycle for walking there is a rapid rise in foot-to floor reaction force from zero to a peak load of over body weight during the first 100 ms after HS (Barker *et al.*, 1997; Bergmann *et al.*, 2001) (stage 1 in Figure 2.8). The curve shows how vertical GRF varies from the point of initial contact of the foot with the ground (time 0) to the point at which the foot leaves the ground on toe-off (about 300 ms). For a heel-striking runner there are typically two force peaks (Lieberman *et al.*, 2010). These short rise times include large, nearly instantaneous forces that are transmitted through the body via the skeletal system, leading to impact through the joint. These forces result in the deformation of articular cartilage. Thus, GRFs at HS provide indirect information about internal joint loading. This is because a peak GRF corresponds with the timing of peak loads in joints (Bergmann *et al.*, 2001; Bassey *et al.*, 1997; Park *et al.*, 1999). Therefore, the increase in the loading rate of the GRF (shorter rise times) will correlate to the changes in rise times of the GRF acting on articular cartilage in lower limb joints of the body (Barker *et al.*, 1997).

Cyclic loading with rapid rise times (i.e. impact) at HS have been implicated as factors in degenerative conditions such as OA, cartilage failure, prosthetic joint loosening and stress fractures in the lower limb joints (Dickinson *et al.*, 1985; Folman *et al.*, 1986; Whittle *et al.*, 1999). The GRFs at HS include both high load magnitude and high loading rate components. Previous studies (Barker *et al.*, 1997; Bergmann *et al.*, 2001; Park *et al.*, 1999) have associated the increase in the loading rate of the ground reaction, with the changes in the rise times of the forces acting on the cartilage in the joint that could lead to failure of cartilage. Radin *et al.* (1986b) also suggested that cartilage failure could be induced by shear stresses at the cartilage/bone interface. However, such studies were particularly interested in failure at the cartilage-bone interface, not the articular surface or the propagation of failure through the depth of cartilage specimens or across the area of cartilage specimens.

## 2.4 GRF and HS

The law of conservation of momentum states that momentum (either linear or angular) cannot be generated nor destroyed, but transferred from one object to another. This is demonstrated by the momentum transfer occurring during the impact between two objects, such as the foot, and a stationary one, such as the ground (Whittle *et al.*, 1999). According to Newton's third law, as the heel contacts the ground and exerts a measurable force, so too does the ground exert an equal and opposite force on the heel. The force acting on the heel is defined as the GRF that is transferred through the skeletal system (Folman *et al.*, 1986; Lafortune & Henning *et al.*, 1992). An active individual, running 32 Km a week over 30 years, will expose their skeletal system to approximately 50 million loading cycles, in addition to the million cycles that the lower limb joints undergo during walking in normal daily activity (Dickinson *et al.*, 1985).

GRF with rapid rise times in the range of 1-5 ms of HS (Dickinson *et al.*, 1985; Folman *et al.*, 1986; Simon *et al.*, 1981) are experienced throughout the entire musculoskeletal system, even in the skull (Wosk & Voloshin, 1981). Although large load magnitudes may be experienced during these loading conditions, and are of considerable importance, particularly in areas adjacent to the contact areas, the response of the musculoskeletal system in terms of loading frequency could also be of importance in understanding the effect of initial foot contact on the articular cartilage. This is because during barefoot walking, 18.6 % of the GRFs have a frequency component that occurs between 60-100 Hz (Gilespeie & Dickey *et al.*, 2003). Overall, up to 22.7 % of the impact energy during the 1-5 ms of HS is contained between 60-400 Hz (Gilespeie & Dickey *et al.*, 2003). The entire skeleton is exposed to these forces with rapid rise times during HS (Light *et al.*, 1980). These studies have shown measurable stresses caused by rapid rise times during gait in the skull during HS (Light *et al.*, 1980). Both bone and soft tissues attenuate this signal each displaying certain loading rate specificity (Paul *et al.*, 1978). In rabbits, bone and soft tissue attenuate 18 % of the stresses induced during HS loading at 60 Hz, which increased to 98 % of loading at a frequency of

360 Hz (Paul *et al.*, 1978). Therefore, increasing the loading frequency alone might make the skeletal system prone to injury during cyclic loading.

## **2.5 GRF at RHS rise times during gait and OA**

OA is a degenerative, multifactorial disease (Stockwell *et al.*, 1991). The most recognized symptom of this disease is pain that drives individuals to seek medical attention (Ayis *et al.*, 2009; Dominick *et al.*, 2004). Approximately 27 million US adults and 8.5 million UK adults have clinical OA defined on the basis of symptoms and physical findings (National collaborating centre for chronic conditions, 2008; Lawrence *et al.*, 2008). The significant disability associated with this disease is a great physical burden for affected individuals and an economic burden on the health-care system (Woolf *et al.*, 2003). Although OA is considered to be a disease of the joint (Loeser *et al.*, 2012), articular cartilage is central to the disease and its progression (Creamer *et al.*, 1997). The disease involves a decrease in thickness and volume of the tissue, (Cicuttini *et al.*, 2004; Jones *et al.*, 2004) in addition to an increase in the number and the size of cartilage defects (Ding *et al.*, 2005). This can be observed in both animal and human cartilage (Clark *et al.*, 1991). An important element in the disease is the fracture of cartilage, because once cartilage fractures, it has a limited ability to heal the cracks (Buckwalter *et al.*, 1988; Adams *et al.*, 1997; Mankin *et al.*, 1982).

The most recognized feature of OA is the progressive damage of articular cartilage, resulting in impaired joint motion, severe pain, and disability (Creamer *et al.*, 1997). However, OA can be correlated to factors such as obesity or cartilage metabolism (Sowers *et al.*, 2010). The articular cartilage surface begins to change from a smooth to a rough or fissured appearance in early OA (Chiang *et al.*, 1997). Cyclic compressive loading has been used to subject the surface of cartilage to damage (Weightman *et al.*, 1973; Kerin *et al.*, 2003). OA may represent a reaction to primary mechanical damage to one or more joint tissues, because cartilage failure tends to be

located in the region of high loading (Byers *et al.*, 1970; Murray *et al.*, 2001). Figure 2.9 shows an osteoarthritic patellofemoral groove of a rabbit cartilage with a surface defect.



Figure 2.9. OA of a rabbit (leporine) patellofemoral groove, showing a defect (shown with arrow). (reproduced with permission from CRC Press/Taylor & Francis Group, LLC (Athanasίου, 2013)).

RHS rise times during gait have been implicated in the onset of OA (Radin *et al.*, 1991). Cartilage is typically subjected to loading with a HS rise time of 100 to 150 ms (Shepherd *et al.*, 1997). A subset of the population with HS rise times from 5 to 25 ms has been identified as being linked to the onset of OA (Radin *et al.*, 1986b). The timing of these HS corresponds to frequencies of 3–5 Hz for normal and up to 90 Hz for RHS rise times (Fulcher *et al.*, 2009).

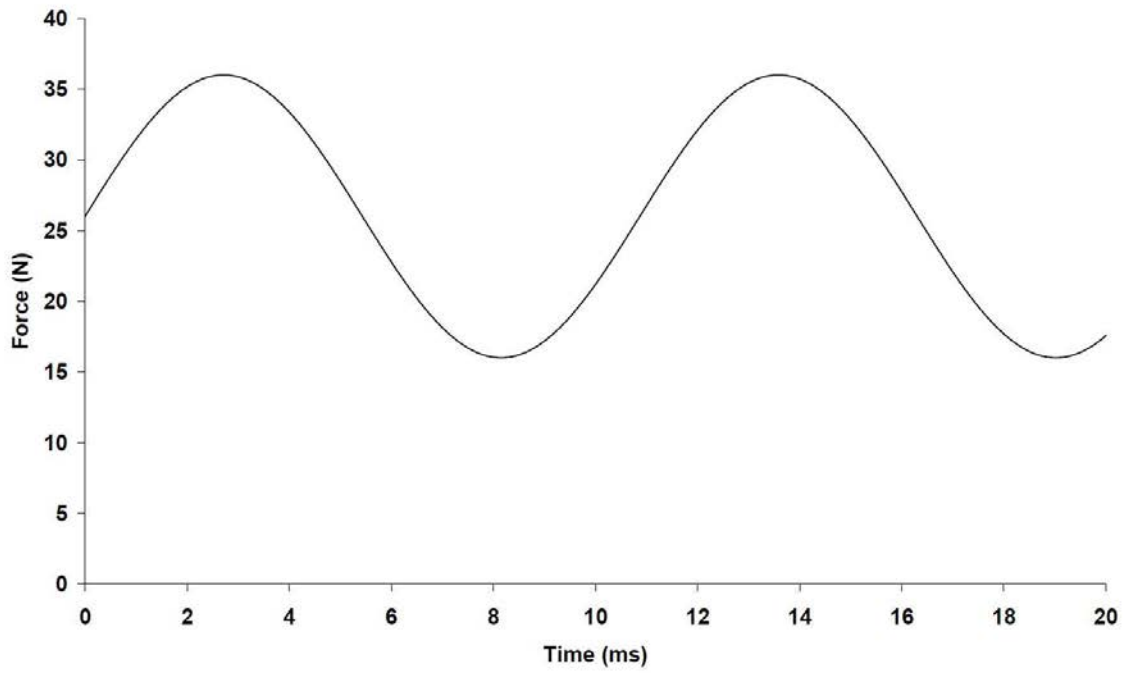
The effect of the application of GRFs with RHS rise times during gait on the failure of articular cartilage can be investigated by subjecting cartilage/cartilage-on-bone specimens to loading with frequencies representative to such rise times, as shown in Figure 2.10. The rise time

of the force is approximated by the time taken from the trough to the peak of the sine wave (Fulcher *et al.*, 2009). That is

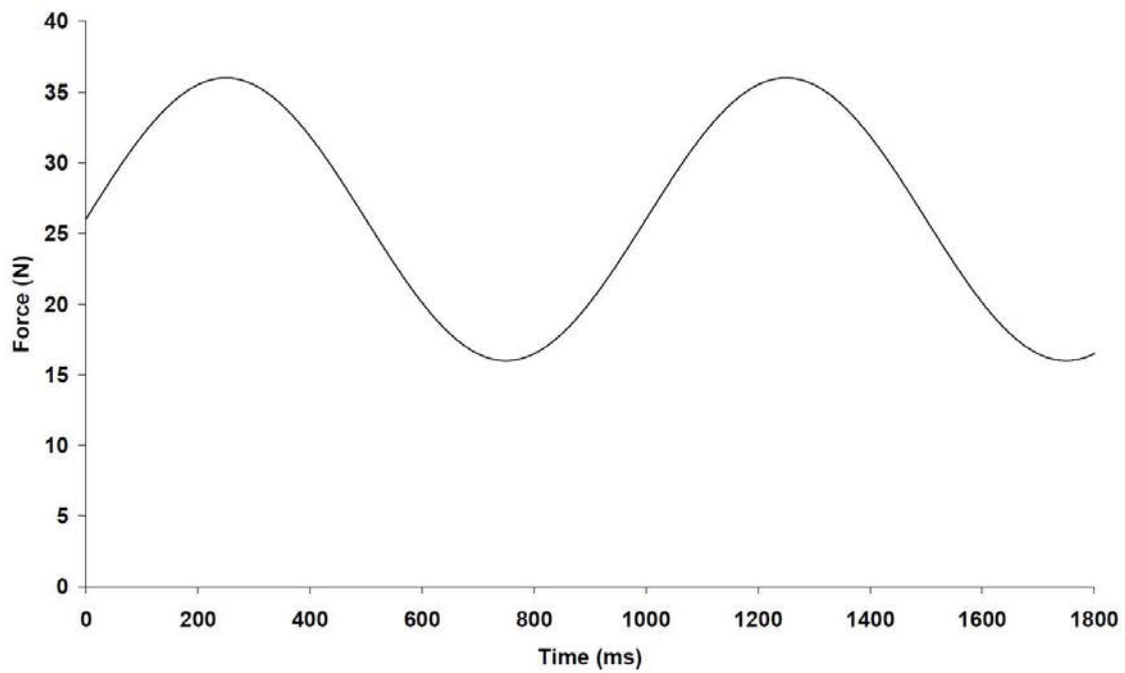
$$t = \frac{1}{2f} \quad (2.1)$$

where  $f$  is the frequency of the sine wave. Thus, a sinusoidally varying force with a frequency of 92 Hz has been estimated as being representative of a rise time of 5.4 ms, and a frequency of 1 Hz as representative of a HS with a rise time of 500 ms (Fulcher *et al.*, 2009). It has been argued that RHS rise times (e.g. 5 ms) lead to impulsive loading (Radin *et al.*, 1991), which might be associated with a predisposition to OA.

Individuals with degenerative joint disease such as OA may have up to a 30 % decrease in the capacity to attenuate stresses generated during RHS rise times through their musculoskeletal system (Voloshin & Wosk *et al.*, 1981). This may have particular importance during HS loading that consists not only of high magnitude stress, but also high frequency (Folman *et al.*, 1986; Simon *et al.*, 1981). These high frequency stresses are only partially attenuated during impact loading (Folman *et al.*, 1986; Simon *et al.*, 1981). Exposure to loads representative of RHS rise times has been shown to have the ability to initiate degenerative joint changes.



A



B

Figure 2.10. Sinusoidally varying force a) at 92 Hz (rise time 5.4 ms); b) at 1 Hz (rise time 500 ms).

Repetitive impulsive loading also provokes OA in the joints of experimental animals (Radin *et al.*, 1978 & 1982). An advantage of this model is that it is more controlled than surgical models; the force applied to the limb is known and can be altered. These models have demonstrated the effect of loading rate on the development of OA. Impulsively applied loads were found to produce OA, while higher loads applied at a lower rate do not. Although using an animal model may not be directly indicative of changes seen in the progression of OA in humans, these findings do suggest the potential for high frequency loading to affect musculoskeletal tissues.

## **2.6 Experimental failure of articular cartilage**

Cartilage injuries can result from impact and repeated loading, and these can occur under a wide range of load magnitudes and frequencies. Because of the viscoelastic nature of articular cartilage, the rates of applied stress, strain, and load must be considered. For example, using a confined compression loading protocol, the dynamic modulus has been shown to increase from 225 to 850 MPa as the load rate was increased from 25 to 1000 MPa/s (Milentijevic & Torzilli 2005). Peak forces during normal physiological loading of knee articular cartilage range from 1.9 to 7.2 times the body weight. For a 70 kg person, this would correspond to ~1400 to 4900 N (Natoli & Athanasiou 2008). Considering the human medial tibial plateau contact area which was measured to be approximately 1,670 mm<sup>2</sup> (Wang & Wluka, 2005). This corresponds to a maximum stress of around 3 MPa. During normal activities, like running the time to peak force is of the order of 30 ms, leading to a stress rate of 1000 MPa/s.

Expressed in terms of stresses on cartilage, if typical stresses in the hip or knee are about 1 – 10 MPa, then stress rates would be expected to be of the order of 10 – 100 MPa/s during walking and could be up to an order of magnitude when running (Basse *et al.*, 1997). Therefore, Aspden

& Jeffery (2002) suggested three criteria for injurious impact loading of cartilage as time to peak load of the order of milliseconds, plus one of the following: (1) stress rate greater than 1000 MPa/s, (2) Strain rate greater than  $500 \text{ s}^{-1}$ , or (3) loading rates in excess of 100 kN/s. Articular cartilage subjected to loads that do not satisfy Aspden's three criteria for impact could cause failure of cartilage using cyclic loading. For example, Repo *et al.* (1977) used a drop tower to apply strain rates of up to  $1000 \text{ s}^{-1}$ . This rate was more representative of events like road traffic accidents rather than impact loads. More recent drop tower studies should be described as impact, in which a mass is allowed to freely fall on cartilage specimens, typical loading times are of the order of 1 ms (Burgin *et al.*, 2001; Jeffrey *et al.*, 1995). The specimens used by Burgin *et al.* (2001) and Jeffrey *et al.* (1995) were 5 mm in diameter, which an area of about  $20 \text{ mm}^2$  and maximum stresses that were in the range of 5-40 MPa. This results in the rates of application of stress of approximately 5000-80,000 MPa/s.

The thresholds of forces and timescale required to produce failure are important in determining the type of injury sustained and for modelling impact and injurious compression experimentally. Mathematical models of impact and injurious compression have been performed (Armstrong *et al.*, 1984), as well as studies of impact undertaken on explants *in vitro* (Jeffrey *et al.*, 1995 & 1997; Milentijevic & Torzilli, 2005), and *in vivo* (Dekel *et al.*, 1978) based on this and other classifications. The difference between impact and injurious compression is that injurious compression occurs over a longer time span. Other comparable studies (Morel *et al.*, 2005; Quinn & Morel *et al.*, 2007) of impact on the cartilage specimens have been predominantly focused on the effect of impact on surface rupture and how it is altered with fluid content, matrix swelling, and the collagen network.

Strain rate has been used in injurious compression and impact studies on cartilage-on-bone specimens. Studies with very slow strain rates of the order of 1 ms ( $0.01 \text{ s}^{-1}$ ) and up to 50 % strain have resulted in no measurable effect on chondrocyte metabolism, while the same strain applied at  $0.1\text{-}1.0 \text{ s}^{-1}$  had a significant decrease in cell viability and biosynthetic response (Kurz *et al.*, 2001).

Using a drop tower to apply impact on cartilage-on-bone specimens, it was noted that, increasing the strain rate from  $1040\text{ s}^{-1}$  to  $1512\text{ s}^{-1}$  caused an increase in the impact energy from 0.5 to 1.96 J, respectively. The impact energies above 1.5 J caused severe surface damage on cartilage-on-bone specimens (Jeffrey *et al.*, 1995). These results indicated that the main mechanism for releasing the excess energy when the strain rate increased could have been the formation of cracks and fissures.

Surface damage on bovine cartilage-on-bone specimens have been created in several conditions in a few studies (Flachsmann *et al.*, 2001 & 2005 & 2006). For example, increasing the level and the rate of the applied compressive stress has been suggested as a factor in the formation of surface damage in cartilage-on-bone specimens (Flachsmann *et al.*, 2006). Open cracks have been created on bovine cartilage-on-bone specimens, loaded through a transparent acrylic indenter under dynamic and static compression. However, cracks were only formed following static compression and not dynamic loading (Flachsmann *et al.*, 2001). The proximity of the intact tissue to a lesion site is also suggested as being an important factor in the development of surface failure in cartilage-on-bone specimens. Tissue adjacent to a lesion site incurred more surface ruptures than healthy cartilage under impact loading (Flachsmann *et al.*, 2005). This proximity has been estimated up to the 1 mm radius of the lesioned site (Flachsmann *et al.*, 2006).

Strength thresholds of bovine cartilage-on-bone specimens have also been evaluated using static compression i.e. creep (the tendency of a material to continually deform under constant stress) using a flat metal indenter, previously (Kerin *et al.*, 1998; Fick *et al.*, 2011 & 2012). The strength threshold of cartilage-on-bone specimens have been reported from the complete fracture of the specimens under the stress of 35.7 MPa (Kerin *et al.*, 1998) or the formation of surface lesions under the stress of 8 MPa (Fick *et al.*, 2011 & 2012). Another similar study (Oloyede *et al.*, 1994a), which cartilage specimens were subjected to static compression, investigated the effect of compression-induced anisotropic permeability of the tissue on such a load bearing condition. The maximum period of creep loading was measured, in a comparable study, during static compression loading of cartilage specimens using strain vs time plots of each test (Oloyede *et al.*, 1994b). While

such methods reveal the effect of a certain loading regime on articular cartilage-on-bone, they predict the long-term response of cartilage during activities such as prolonged standing, and are generally less appropriate for investigating activities involving dynamic loading such as walking or running (Hayes & Bodline *et al.*, 1978). Dynamic activity may involve loading with frequency components of up to 100 Hz (Folman *et al.*, 1986; Hayes & Bodline, 1978; Light & McLellan, 1977; Simon *et al.*, 1981).

### 2.6.1 Dynamic testing

Dynamic testing of articular cartilage has been limited to the investigation of the dependence of loading velocity on the stiffness of cartilage using a combination of impact and dynamic testing (Oloyede *et al.*, 1992) or the effect of altered strain rate by loading cartilage specimens in unconfined compression (Radin *et al.*, 1970). Oloyede *et al.* (1992) used a conventional materials testing machine to apply slow strain rates ( $5 \times 10^{-5} - 5 \times 10^{-2} \text{ s}^{-1}$ ) and a free-swinging pendulum for impact strain rates ( $1000 \text{ s}^{-1}$ ). The compressive stiffness of the cartilage (modulus) increased with strain rate, however, the modulus reached a maximum of  $\sim 40 \text{ MPa}$  for strain rates  $\geq 5 \times 10^{-2} \text{ s}^{-1}$ . Radin *et al.* (1970) loaded bovine cartilage (without the underlying bone) at slow (0.1-16 %/s) and fast (up to 670 %/s) strain rates, and found that the compressive stiffness increased from 20 to 50 MPa with increasing strain rate (0.5 – 35 %/s).

Studies that have induced cartilage failure on the articular surface under dynamic conditions, have used loading frequencies representative of normal gait activities e.g. 1 Hz over a long period of time (Weightman *et al.*, 1979; Kerin *et al.*, 2003). However, in these studies the frequency of loading did not exceed 1 Hz. The ability of specific loading frequencies to alter tissue behaviour may indicate loading frequency as an important factor affecting the articular cartilage to measurable GRFs corresponding to frequencies as high as 100 Hz (Folman *et al.*, 1986; Light & McLellan *et al.*, 1977; Simon *et al.*, 1981). McCormack & Mansour (1989) reported that, after

loading articular cartilage with a nominal compressive stress that ranged from 0.6-1.5 MPa over 64,800 cycles, no changes in the tensile strength occurred. However, when the number of cycles continued up to 97,200 cycles, a significant decrease in values of maximum tensile stress was found. McCormack & Mansour (1989) demonstrated that following cyclic loading, cartilage was prone to failure under tension. How cartilage tissue responds to the application of physiological stresses at frequencies (e.g. 100 Hz) representative of RHS, in terms of the induced failure has yet to be fully investigated under different types of loading.

Most studies of cartilage failure are based directly on the evaluating the ultimate stress or strain values of cartilage/cartilage-on-bone specimens. An alternative is to use parameters that more directly represent the propagation of an initial crack in cartilage specimens. Chin-Purcell *et al.* (1996) have evaluated the fracture parameters of cartilage specimens with an initial crack using fracture toughness methods. These methods were based on measurements of fracture energy dissipated per unit of crack extension. A tear test was also evaluated by Chin-Purcell *et al.* (1996) to ensure the cracks propagated through the cartilage specimens. The tear test introduced fracture parameters similar to fracture toughness methods. Previous studies have produced cartilage failure in tension (Sasazarki *et al.*, 2006). This was done by applying large cyclic strains i.e. 30 %, compared to physiologically relevant strains *in vivo*, until the complete rupture of cartilage specimens is achieved. Maximum physiological cartilage strains have been measured to be approximately 12 % (Chan *et al.*, 2016). In comparable studies (Stoke *et al.*, 2003 & 2007), crack growth was investigated through the depth of cartilage specimens. Propagation across cartilage is relevant as shown by Fick, (2013) who found that loading was distributed to adjacent areas under compression. This indicates that crack propagation could occur across the area of cartilage not only through the depth. Propagation of an initial crack seems more likely, across a cartilage specimen area rather than through the depth of it. This is because of the transitional variations of the tissue through the depth of the cartilage specimen. For instance, previous studies have shown that the

superficial layer of cartilage tissue is more resistant to crack growth than the deeper layers (Roth *et al.*, 1980; Chin-Purcell *et al.*, 1996).

## **2.7 Chapter summary**

Articular cartilage is a highly specialized connective tissue that covers the end of long bones in synovial joints. Cartilage can become damaged under cyclic mechanical loading during locomotion. Rise times during gait have been implicated in the onset of OA. These rise times are representative of frequencies as high as 100 Hz. Most studies in the literature regarding the failure of articular cartilage are limited to studies on the formation of cartilage damage using single impact, cyclic loading or studies that have investigated crack propagation in cartilage via measuring fracture toughness techniques. However, the role of loading frequency in the initiation and progression of cartilage has not been fully investigated. Therefore, this thesis was aimed to determine the influence of loading frequency on the failure of articular cartilage. The next chapter investigates the difference in the surface failure of articular cartilage at various loading frequencies.

### **3. Effect of the variation of loading frequency on surface failure of articular cartilage-on-bone**

#### **3.1 Introduction**

Articular cartilage can become damaged when subjected to repetitive mechanical loading (Weightman *et al.*, 1973; Kerin *et al.*, 2003; Zimmerman *et al.*, 1988). However, the mechanism by which the surface of cartilage becomes damaged under loading frequencies associated with normal, above normal and RHS rise time is unknown. In this chapter, experimental damage of the articular cartilage surface was produced by applying five sinusoidally varying compressive force ranges over three magnitudes of loading frequency. The aim of this chapter was to distinguish between the effect of force ranges and frequency on the surface failure of cartilage-on-bone specimens.

Compressive loading is a major component of normal mechanical function within synovial joints. Cartilage prevents high contact stresses which could ultimately damage the bone in a joint (Buckwalter *et al.*, 2003). Cartilage needs, therefore, to be able to deform in order to increase the total surface area for contact, thereby reducing the overall stress (Kerin *et al.*, 2003).

This chapter describes the surface failure of cartilage-on-bone specimens at different frequencies. Section 3.2 describes the materials and methods used to induce failure onto the surface of cartilage-on-bone specimens, the preliminary testing and the details of the methods used for the analysis of cartilage surface damage. Section 3.3 details the results. Section 3.4 discusses the significance of the results found and Section 3.5 provides the overall conclusions.

## 3.2 Material and methods

### 3.2.1 General methods

Fresh bovine shoulders, from animals less than 30 months old, were obtained from a supplier [REDACTED]. Bovine articular cartilage was used because it is an established model for human articular cartilage (Taylor *et al.*, 2011) and the frequency-dependent viscoelastic trends of bovine articular cartilage have been shown to be consistent with those of human articular cartilage; this includes a similar frequency dependency and high-frequency plateau of the viscoelastic trends (Temple *et al.*, 2016). Furthermore, the uniform surface of the bovine humeral head reduces thickness variability of the specimen samples, which is beneficial for quantitative experiments (Clements *et al.*, 2001). On arrival in the laboratory they were wrapped in tissue paper and soaked in Ringer's solution. The bovine shoulders were then sealed in plastic bags, stored in a freezer at -40°C until they were required for testing (Kerin *et al.*, 2003; Fulcher *et al.*, 2009). Freeze-thaw treatment has not been found to alter the mechanical properties of articular cartilage (Szarko *et al.*, 2010; Kiefer *et al.*, 1989; Swann *et al.*, 1988) or bone (Seldin *et al.*, 1966). Prior to testing, the specimens were thawed at room temperature for approximately 2 hours (Fulcher *et al.*, 2009; Espino *et al.*, 2014). Two 50 × 50 mm cartilage-on-bone specimens were obtained from the humeral head of a shoulder joint (Figure 3.1). Typically, specimens had a total thickness of 20 mm (cartilage and subchondral bone) to allow sufficient bone for secure fixation in the test rig (Fulcher *et al.*, 2009; Sadeghi *et al.*, 2015) (Figure 3.2). The specimens were secured into a custom-made test rig using acrylic cement (WHW plastics, Hull, UK). Each specimen was then bathed in Ringer's solution at room temperature throughout the whole test, as in previous studies (Kerin *et al.*, 2003; Fulcher *et al.*, 2009).

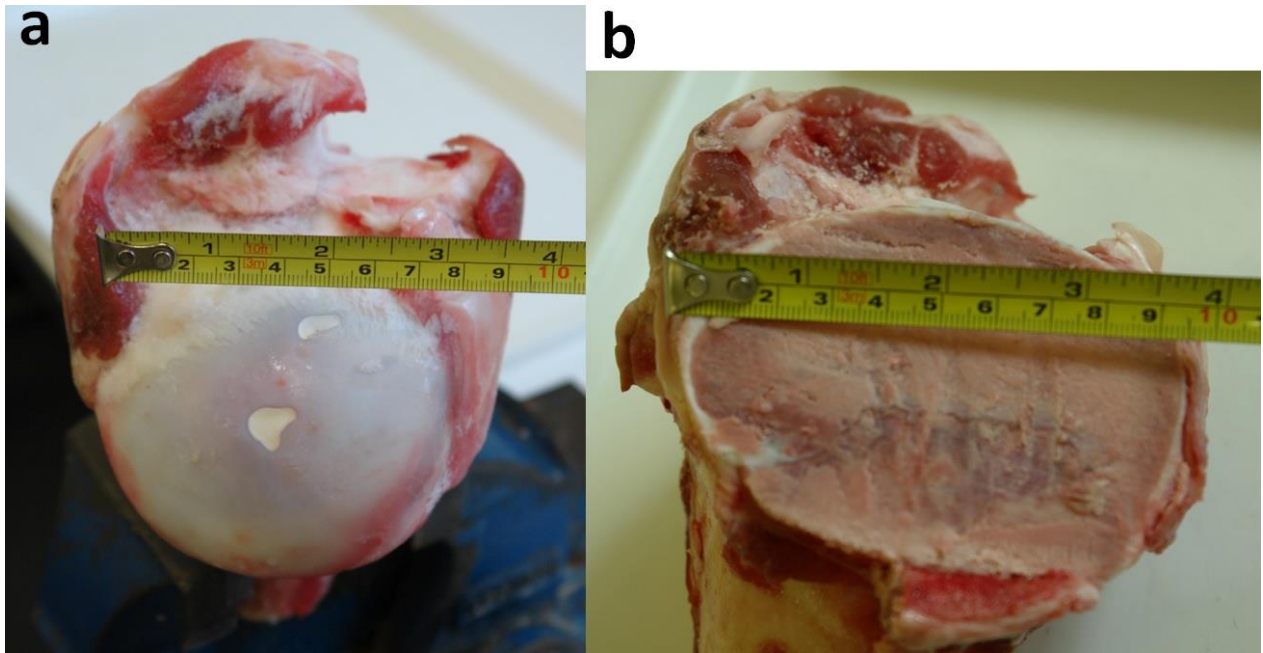


Figure 3.1. Dissection. (a) Bovine shoulder joint (b) humeral head removed from the shoulder joint.

India ink has been used extensively to show clearly the loss of smooth cartilage surface integrity in the literature (Meachim *et al.*, 1972 & 1974). In this thesis India ink (Loxley Art Materials, Sheffield, UK) was used to confirm that each cartilage surface was initially free from defects (Figure 3.3).

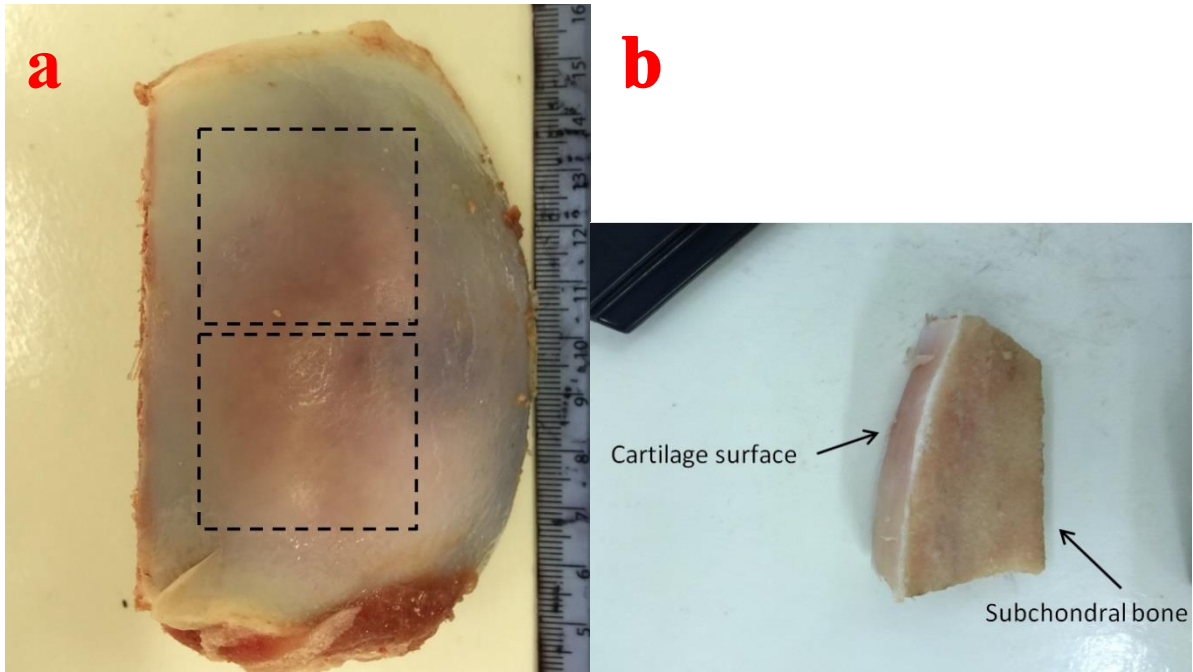


Figure 3.2. Cartilage samples. (a) Two  $50 \times 50$  mm areas were selected from the central region of the humeral head after its removal from the shoulder joint (b) side view of a cartilage-on-bone specimen obtained from the humeral head using a hacksaw. Cartilage-on-bone specimens were selected from the central flat surface of the humeral head. Flattest regions were selected for testing only. The scale bar is in mm.



Figure 3.3. India ink. (a) A sample image taken from the cartilage surface of a cartilage-on-bone specimen. This image shows the glistening nature of the cartilage surface. (b) India ink was applied on the cartilage surface. (c) Any damage on the cartilage surface (shown with arrows) is visible after the India ink was rinsed off the surface. Damaged areas are highlighted as cracks and fissures on the cartilage surface and were not used for testing.

Large scale damage was not observed on the surface of any specimen before mechanical testing; this was expected because since the joints were not osteoarthritic (Espino *et al.*, 2014; Meachim *et al.*, 1974).

### 3.2.2 Preliminary experiments

To evaluate the typical forces that cartilage-on-bone can experience before signs of damage appear on the cartilage surface, three sites on a cartilage-on-bone specimen were selected for performing compression tests using a metal indenter. The indenter had a 5.2 mm diameter flat circular face with a 0.5 mm radius bevel in order to avoid high stresses around its edge. A Bose ElectroForce ELF3200 material testing machine, operated under the control of WinTest software (Bose corporation, Minnesota, USA; now, TA instruments, New Castle, DE, USA) was used to perform compression tests on cartilage-on-bone specimens (Figure 3.4 and 3.5). A preload of 0.5 N was applied on the cartilage surface to ensure that the cartilage surface was in contact with the indenter.

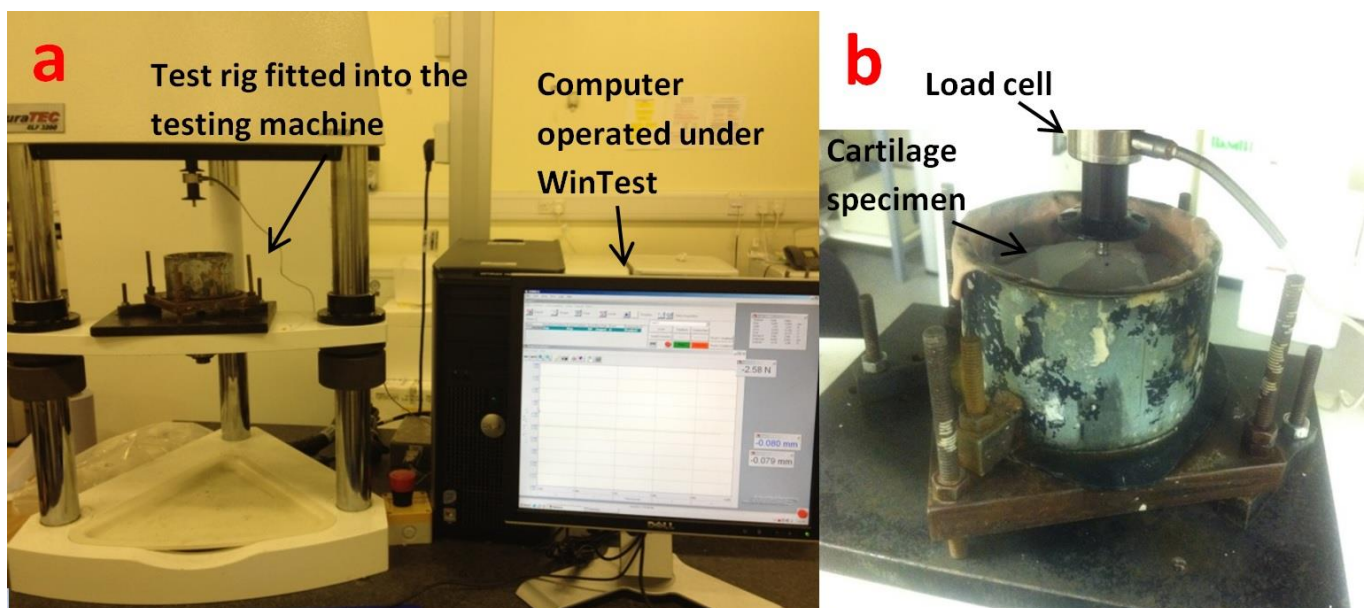


Figure 3.4. Mechanical testing machine. (a) Bose ELF 3200 testing machine (b) test rig fitted into the testing machine with cartilage-on-bone specimen bathed into Ringer's solution secured using acrylic cement.

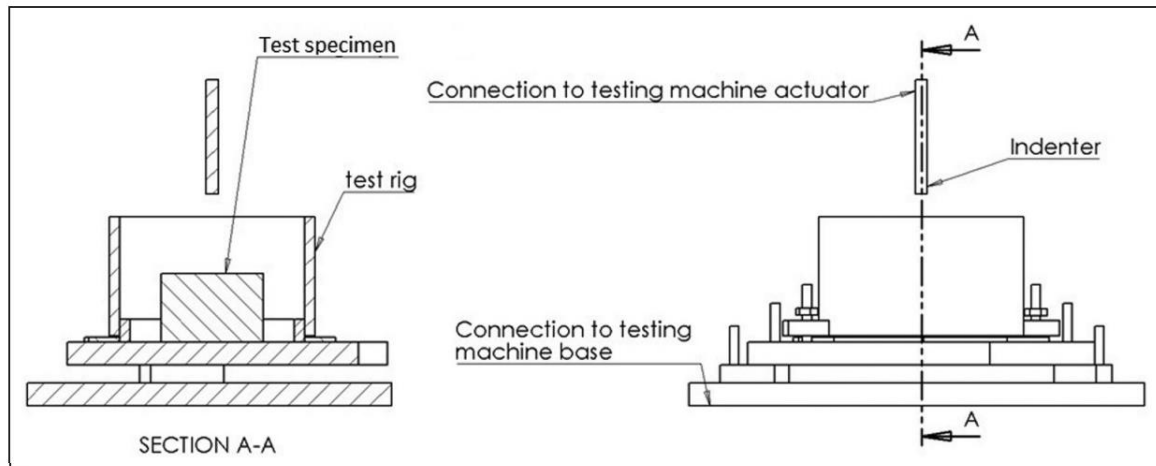


Figure 3.5. Diagram of the experimental set-up used during the testing procedure.

The actuator of the testing machine was set to lower, at a rate of 0.05 mm/s. Load and displacement were recorded throughout the test. Testing continued up to a maximum force of 150 N. Failure was indicated by a change in the direction of the load-displacement graph and further by applying India ink on the cartilage surface following the test. Samples were bathed in Ringer's solution during testing to prevent specimen dehydration (Kerin *et al.*, 2003; Fulcher *et al.*, 2009). Maximum stresses induced on the cartilage surface by the indenter were calculated from

$$\sigma = \frac{F}{A} \quad (3.1)$$

where  $F$  is the maximum force and  $A$  is the cross-sectional end face area.

Figure 3.6 shows a typical force against displacement graph of a cartilage-on-bone specimen under compression. Stress at the point of failure of the cartilage-on-bone specimens was  $1.94 \pm 0.33$  MPa (mean  $\pm$  SD) calculated from equation 3.1. This corresponded to a maximum force of  $125.6 \pm 19$  N, which occurred at a maximum displacement of  $0.6 \pm 0.18$  mm. Figure 3.7 shows the cartilage-on-bone specimen after India ink has been used on the cartilage surface. Cartilage testing sites show surface damage in the form of cracks and fissures.

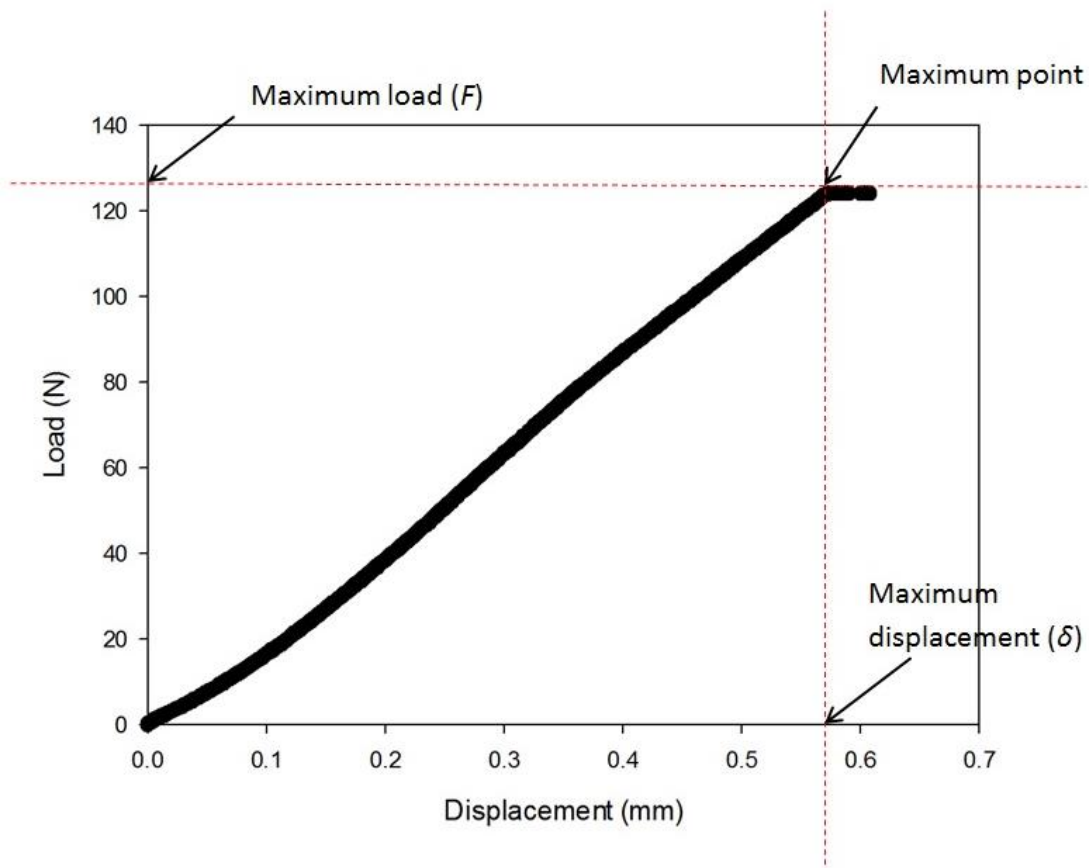


Figure 3.6. Load against displacement of a cartilage-on-bone specimen subjected to compression. The cartilage surface was damaged at a load ( $F$ ) of 123 N corresponding to the failure displacement ( $\delta$ ) of 0.58 mm.



Figure 3.7. Three sites were chosen on a cartilage-on-bone specimen to perform compression tests. The cartilage surface damage was highlighted with the aid of India ink. Cracks appeared on the cartilage surface following testing. Black circles inserted in the image are 5.2 mm in diameter, the same diameter as the indenter. Scale bar (red bar at the bottom right) ~ 1 cm.

In order to see whether surface cracks could be induced on the cartilage surface by cyclic compressive loading, three sites were chosen on three different cartilage-on-bone specimens. Previous work has shown that cracks occur in the cartilage surface following cyclic compressive testing using a metal indenter, resembling minimal fibrillation, and not in the subchondral bone (Adams *et al.*, 1998; Kerin *et al.*, 1998). Three sinusoidally varying maximum compressive forces of 60, 90 and 120 N were used for testing. Cyclic testing was performed by using the same equipment as described in section 3.2.2. The lowest maximum force of 60 N was chosen as approximately 50 % of the maximum force (125 N) measured in section 3.2.2. This maximum force was considered suitable because previous work has shown that damage does not propagate in fibrocartilage at less than 40 % of its own failure stress (Green *et al.*, 1993). This percentage was also used in studies of crack propagation in cartilage-on-bone specimens (Kerin *et al.*, 2003; Adams *et al.*, 1998). The highest maximum force of 120 N was chosen as 97 % of the mean failure force measured in section 3.2.2. For the sinusoidally varying force tests the ratio of maximum to

minimum force was 10. Therefore, three sinusoidally varying force ranges of 6-60, 9-90 and 12-120 N were used. These force ranges were applied at loading frequencies of 1, 10 and 100 Hz on the three chosen testing sites on each cartilage-on-bone specimen. A preload of 0.5 N was applied to the cartilage surface of the specimens to ensure that the indenter was in contact with the cartilage surface.

An image taken from each three cartilage-on-bone specimens at the three used loading ranges is shown in Figure 3.8. From qualitative observations damage appeared on the cartilage surfaces as cracks following the application of India ink. From qualitative observations, higher frequencies caused more damage on the testing sites. The next section provides the details of the approaches that was attempted to quantify cartilage surface cracks.

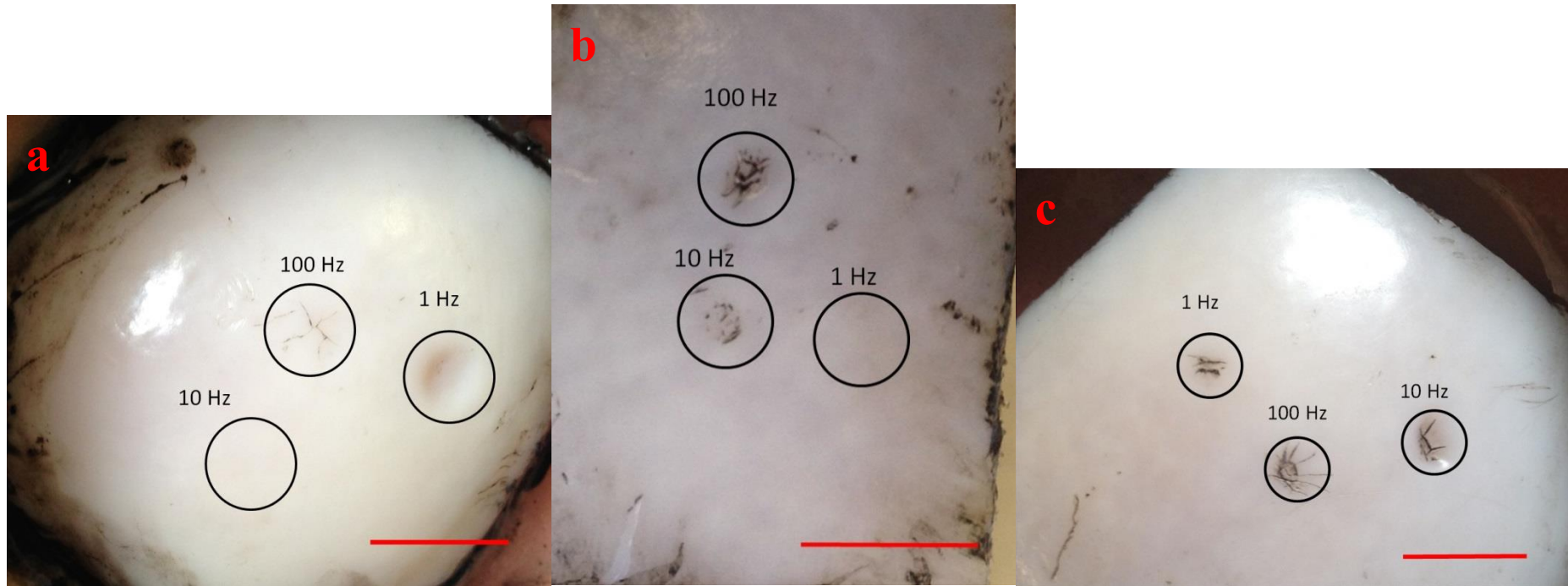


Figure 3.8. Images taken from the cartilage surface of three cartilage-on-bone specimens. The black circles show the loaded region. Loading ranges included were (a) 6-60 N, (b) 9-90 N and (c) 12-120 N. The increase in crack length with increasing maximum load can be observed from left to right. India ink was applied to the cartilage surface to easily distinguish the surface cracks. Scale bar (red bar at the bottom right) ~ 1 cm.

### **3.2.3 Analysis of cartilage surface damage**

This section provides the details of the alternative methods that were assessed in order to quantify cartilage surface cracks using Image-J (version 1.48, Rasband, W.S., U. S. National Institutes of Health, Bethesda, Maryland, USA) software. Figure 3.8-c was used as a sample image in this section. Different strategies such as maximum crack length, area of damage and total crack length at each testing site were considered in order to quantify the cartilage surface damage. The method which provided the most realistic representation of the cartilage surface damage was ultimately chosen in order to analyse the images from the final cyclic tests.

Initially images were imported into Image-J. Images were calibrated by using a scale bar within the field of view. The “Line selection tool” was used to draw a selection line of known length, along a 10 mm line which was drawn on the scale bar (Figure 3.9).



Figure 3.9. Drawing a 10 mm line on the scale bar manually.

From visual observations of the damaged area at each image, the longest crack on each testing site was selected (Figure 3.11). Maximum crack lengths were measured to be 2.12, 1.82 and 3.16 mm at loading frequencies of 1, 10 and 100 Hz, respectively (Figure 3.11). This method had the advantage of representing the increase in the damage for Figure 3.11. However, this method had limitations which could impact upon the final conclusions. For example, it might not provide a good representation of the data when the cracks with the maximum length were difficult to identify in the damaged region (Figure 3.8 – b). Thus, an attempt was made to measure the area of damage at each testing site and compare them at each test frequency.

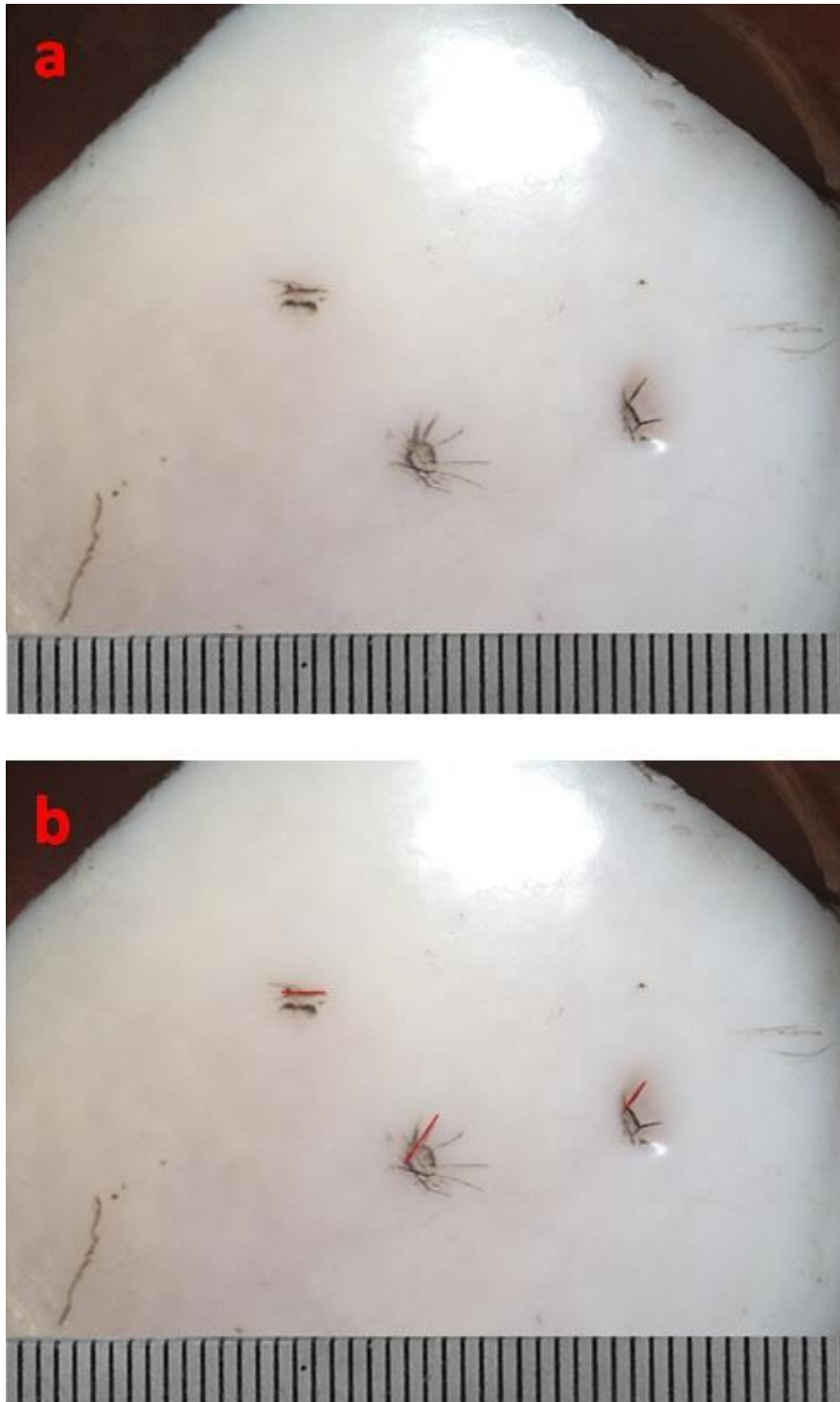


Figure 3.10. Maximum crack length. (a) Figure 3.8-c (b)The maximum crack length at each testing site was selected from visual observations. In this image, maximum crack lengths were highlighted using red lines.

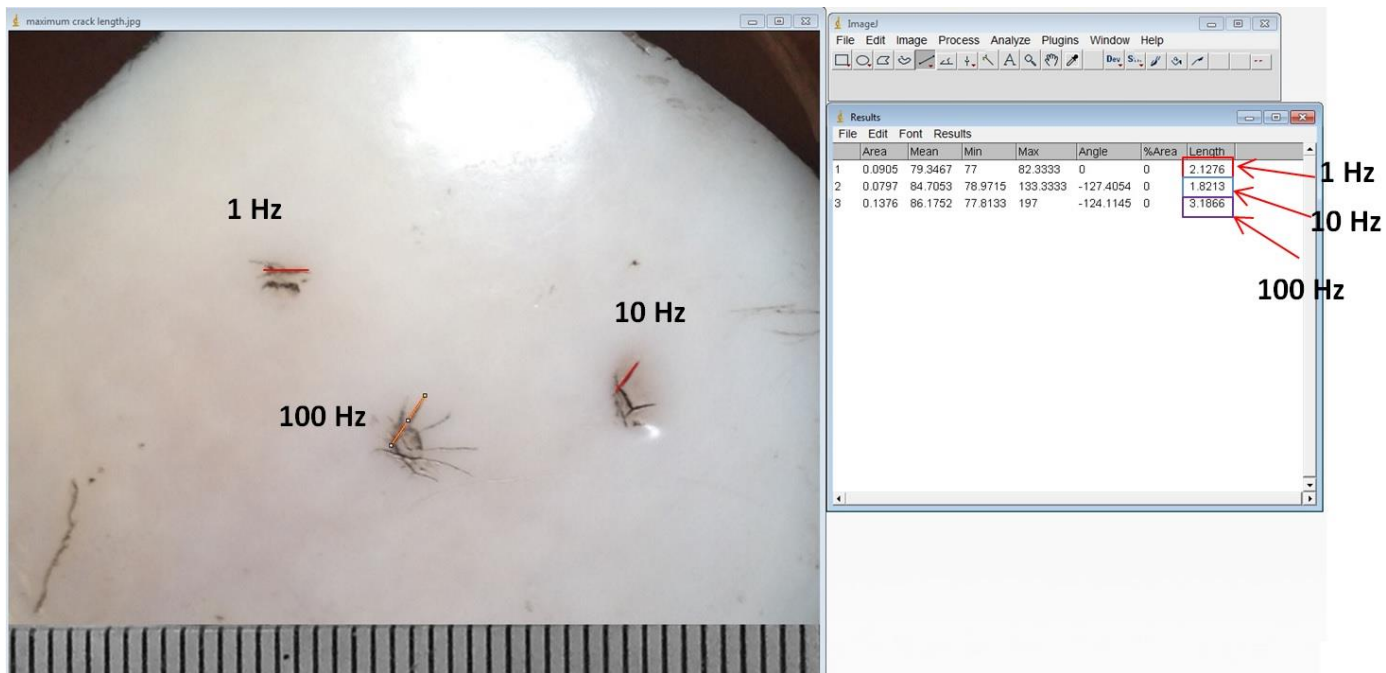


Figure 3.11. The length of the maximum cracks was measured.

To measure the area of damage following loading, images were converted to grayscale by using “8-bit” resolution (Figure 3.12). This action converts each pixel’s colour information into a grayscale brightness measurement. In an 8-bit grayscale image there are 255 intensity graduations which can be assigned to a pixel. A pixel with an intensity of 0 is black, a pixel with a value of 255 is white, everything in between is a shade of gray. A threshold was then applied to the image. Thresholding works best on grayscale images. Thresholding works by separating pixels which fall within a desired range of intensity values from those which do not, (also known as ‘segmentation’).



Figure 3.12. An example of a gray-scale image. Images were converted into 8-bit grayscale before the application of threshold.

The image was adjusted so that the white, low value pixels that represent damage turn white, but those that represented the cartilage area without damage remained unchanged. Dragging the sliders selects different regions within the grayscale; pixels in the image which fall in the selected range are highlighted as white. Figure 3.13 shows the image after the application of the threshold. A threshold of 116 was applied to the image by the software's default. Figure 3.14-a shows the image with the threshold of 116. Since most of the crack branches adjacent to the damaged region at the frequency of 100 Hz did not appear as white lines, the threshold was increased to 156. However, when the threshold was increased the areas between the cracks also turned white. This could lead to the overestimation of the data (Figure 3.14-b).

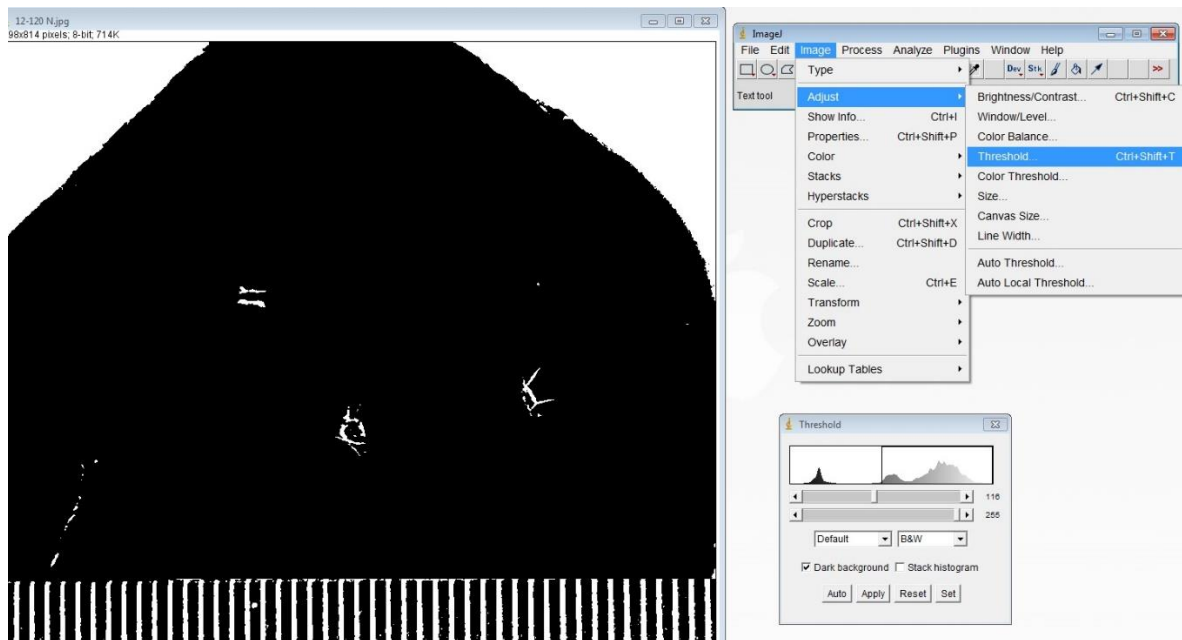


Figure 3.13. A threshold was applied to the image to enable quantitative evaluation of the damage induced.

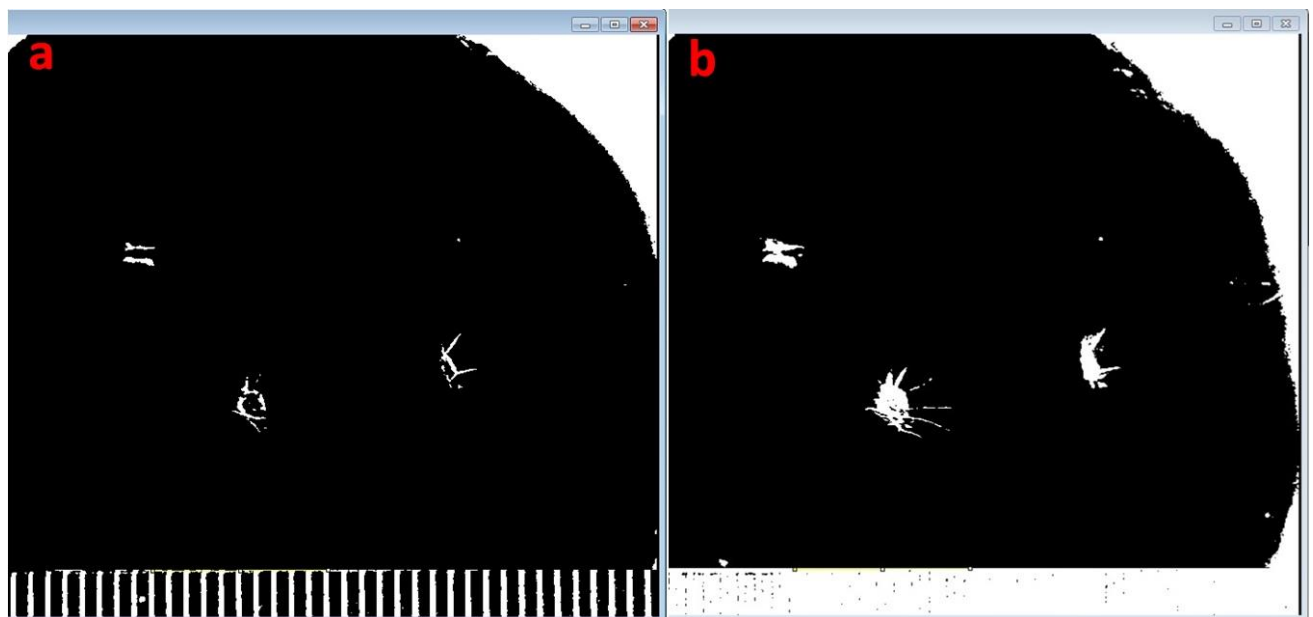


Figure 3.14. Threshold was increased from 116 (a) to 156 (b).

A threshold of 116 was chosen as an example to quantify the damaged areas. A rectangular area of cartilage surface was selected which included the damaged (white) area at each testing site (Figure 3.15). Image-J measured the area of 'white' within the rectangle independent of the dimensions of the rectangle, while the 'black' area was ignored. The area of damage was calculated to be 3.21, 4.78 and 4.79 mm<sup>2</sup> at frequencies of 1, 10 and 100 Hz, respectively (Figure 3.16). Using an objective (user-independent) method would be useful in order to quantify the damaged areas at each testing site.

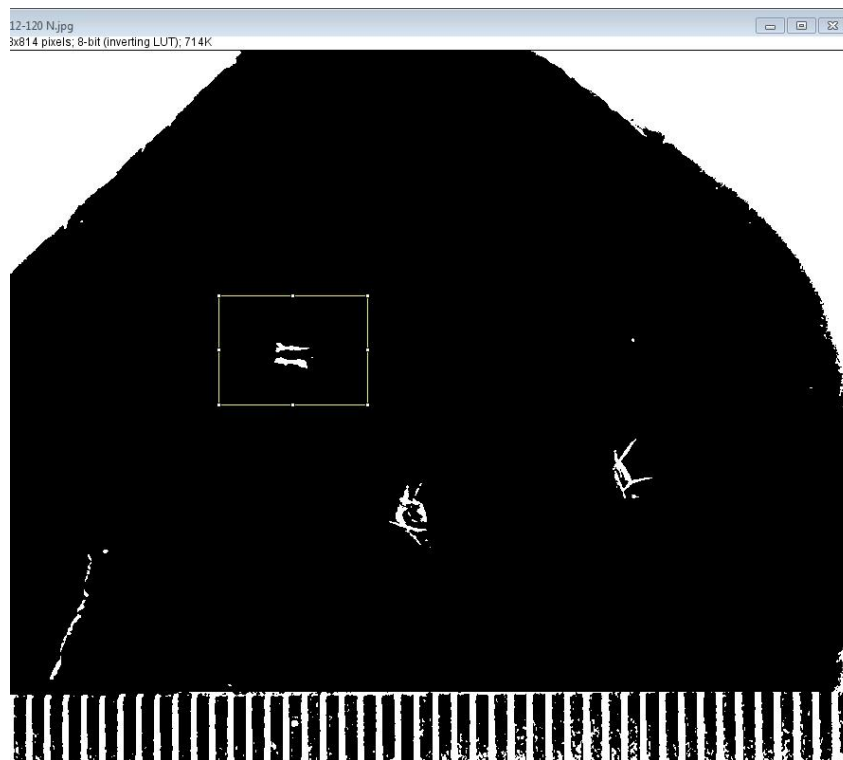


Figure 3.15. The area of damage was identified at each individual test site as shown by the rectangular box.

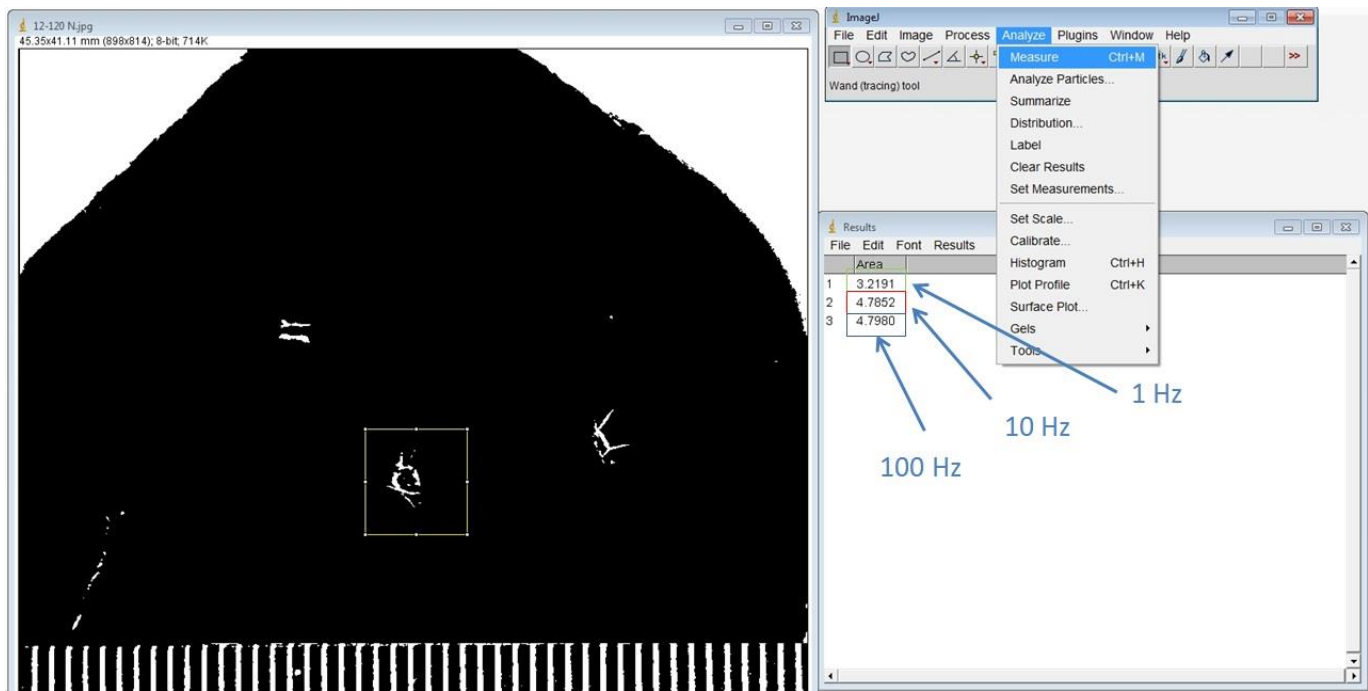


Figure 3.16. The white areas represent damage with the area of damage identified objectively.

The method of objectively measuring the area of damage for each test-site overcame the limitations of the method of only measuring the longest crack, but still contained limitations which would limit any conclusions drawn. Firstly, it did not provide a good representation of the data because the damaged region at the frequency of 100 Hz is larger compared to 10 Hz as can be observed from Figure 3.8-c. However, the calculated area is 4.78 and 4.79 mm<sup>2</sup> at frequencies of 10 and 100 Hz, respectively. Secondly, in some images there are areas around the damaged region that are black but they should be considered as damage. This could lead to overestimation of the data. Thus, a method was necessary which accounted for the full crack-length without overestimating area damage at the lower testing frequencies.

An attempt was made to quantify the full length of crack on the cartilage surface at each frequency separately. Each individual crack line was measured and subsequently a total crack length was calculated by adding the measured crack length for a given testing site. Figure 3.17-a shows the cartilage surface containing cracks. Figure 3.17-b shows red lines highlighting the

measured crack lengths. Lines were drawn along the cartilage surface cracks following calibration and the lengths of the cracks were measured. Crack lengths were added together for each frequency (Figure 3.18).

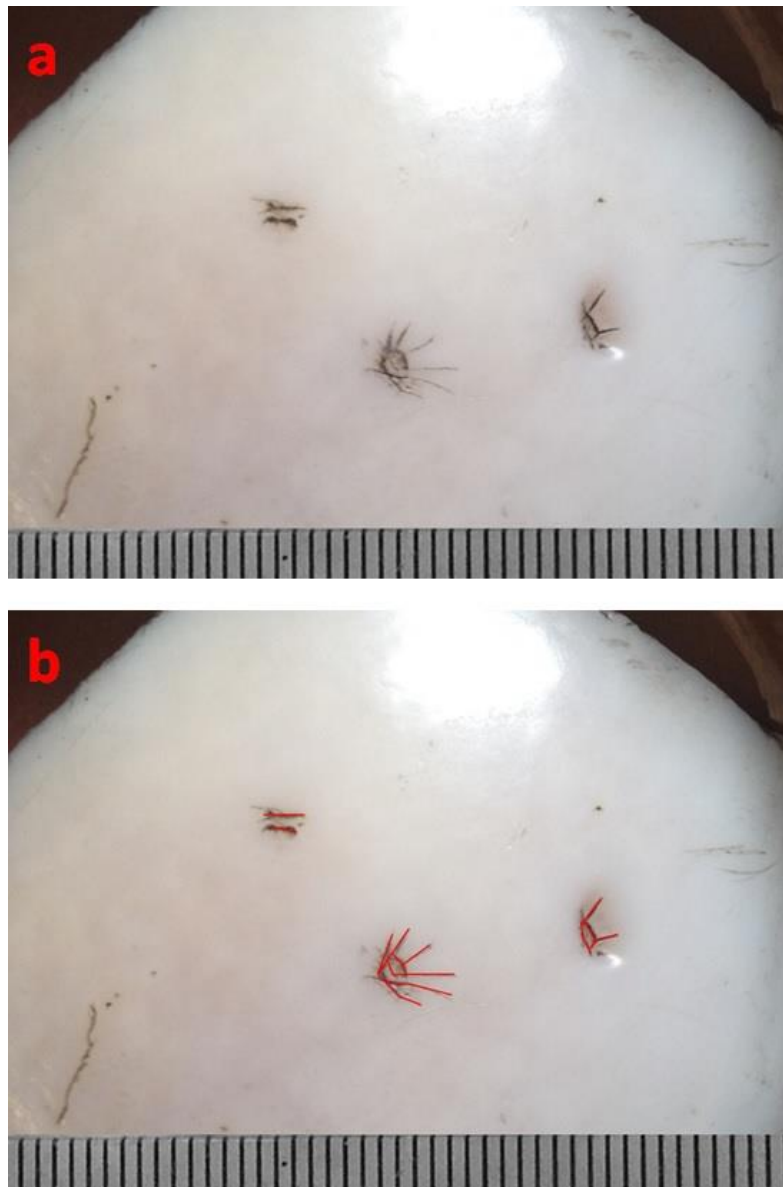


Figure 3.17. Total crack length (a) Cartilage surface cracks highlighted with the aid of India ink. (b) Red lines were drawn along the surface cracks to highlight damaged areas.

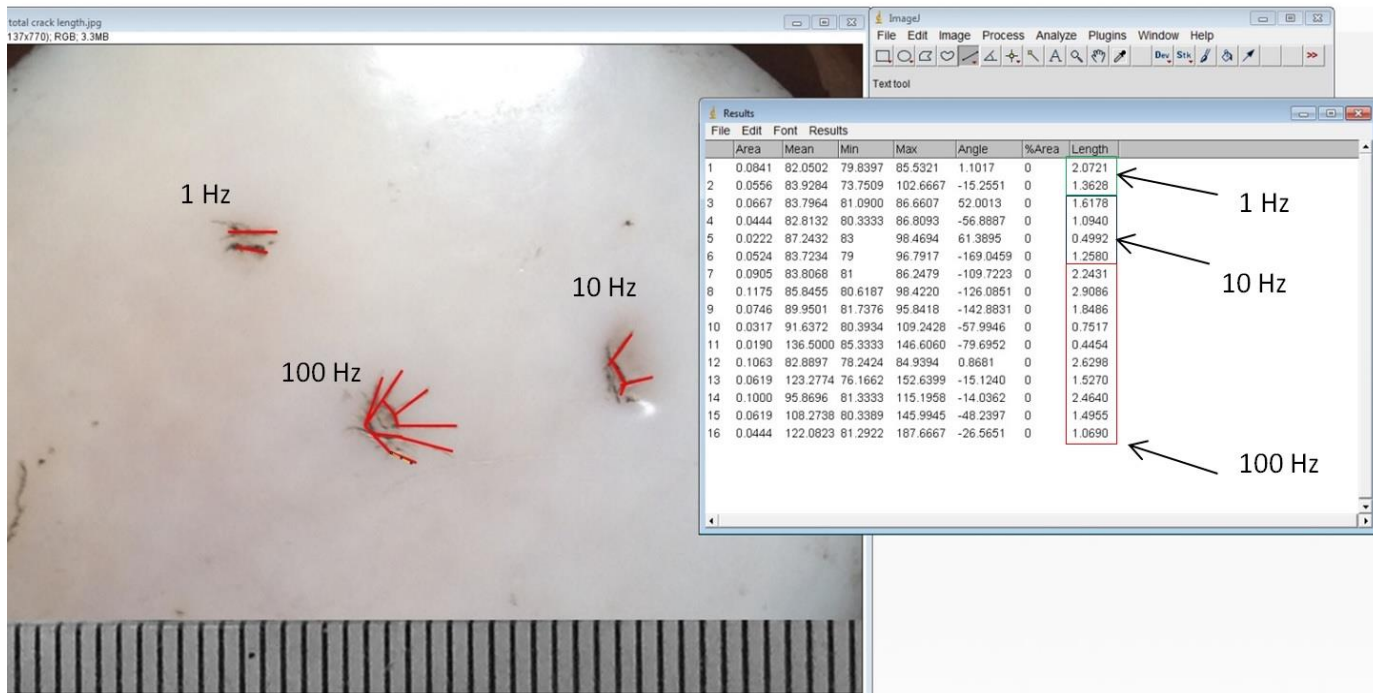


Figure 3.18. The individual length of each crack was measured manually (in mm).

Total crack length was calculated to be 3.43, 4.44 and 17.28 mm at frequencies of 1, 10 and 100 Hz. This method was chosen for the calculation from the images as it represented the increase in the surface failure of cartilage with increasing frequency. Total crack length was measured from the images acquired from the cartilage-on-bone specimens in the final tests that as covered in the subsequent sections. The disadvantage of using this method was that this method was not automated. However, it matched the results which best matched the observed failure. Each total crack length measurement was repeated twice to ensure the repeatability of such method.

### 3.3 Cyclic experiments

An experimental protocol was developed to investigate the role of frequency of loading on damage to the articular cartilage surface using the equipment described in section 3.2.2. Damage

was created using a sinusoidally varying compressive load with a solid cylindrical indenter used in section 3.2.2. A total of 40 specimens were obtained from 20 bovine shoulder joints; it is unknown if any of the joints were from the same animal, so in the calculations of the 95% confidence intervals it was assumed that the joints came from 10 animals to avoid any possibility of dependant observations (Ranstam *et al.*, 2012). Three sites, free from pre-existing lesions, were chosen for testing on each tissue sample over three magnitudes of loading frequency (i.e. one frequency per test site). Therefore, a total of 120 distinct test sites were analysed for crack measurements. Each test consisted of the cartilage tissue samples being loaded for 10,000 cycles (Zimmerman *et al.*, 1988) for each loading frequency individually. The number of cycles was kept constant for all tests over all three magnitudes of frequency, in order to be able to observe the change in damage when only frequency was altered. Surface effects may extend up to 1 mm from the loaded site in healthy cartilage (Fick *et al.*, 2013); therefore, an average distance of 5 mm was kept between the test sites. Five sinusoidally varying compressive force ranges were used for testing: 6-60 N, 9-90 N, 10-100 N, 12-120 N and 16-160 N. The maximum used forces started from 50 % (60 N) up to 128 % (160 N) of the maximum force measured in section 3.2.2. These forces were chosen to ensure that a transition from no-damage to damage was achieved following cyclic tests. The maximum applied loads induced a nominal compressive stress of 2.8 MPa, 4.2 MPa, 4.7 MPa, 5.6 MPa and 7.5 MPa, respectively, as calculated using equation 3.1. Eight samples were tested for each loading range at 1 Hz, 10 Hz and 100 Hz. The loading ranges were chosen to determine in which loading range and frequency the surface damage was initiated and how it changes with load or frequency. These values were chosen based on preliminary tests and the stresses induced by the maximum load.

The mean total crack length against the three frequencies (1 Hz, 10 Hz and 100 Hz) was analysed for all load ranges using Sigma Plot (Version 11.0, Systat Software Inc., London, UK). 95% confidence intervals were calculated with the  $n$  values (i.e. number of independent observations) shown in Figure 3.19, so that independent observations could be assumed (Ranstam *et al.*, 2012). The 95 % confidence intervals were also generated using Sigma Plot. The relationship

between total crack length against maximum load was analysed to determine the variation of crack length when the maximum load range was altered. A polynomial or linear regression was used to fit a curve or line to the data. A  $p$  value  $< 0.05$  indicated that the curve or line fit was significant.

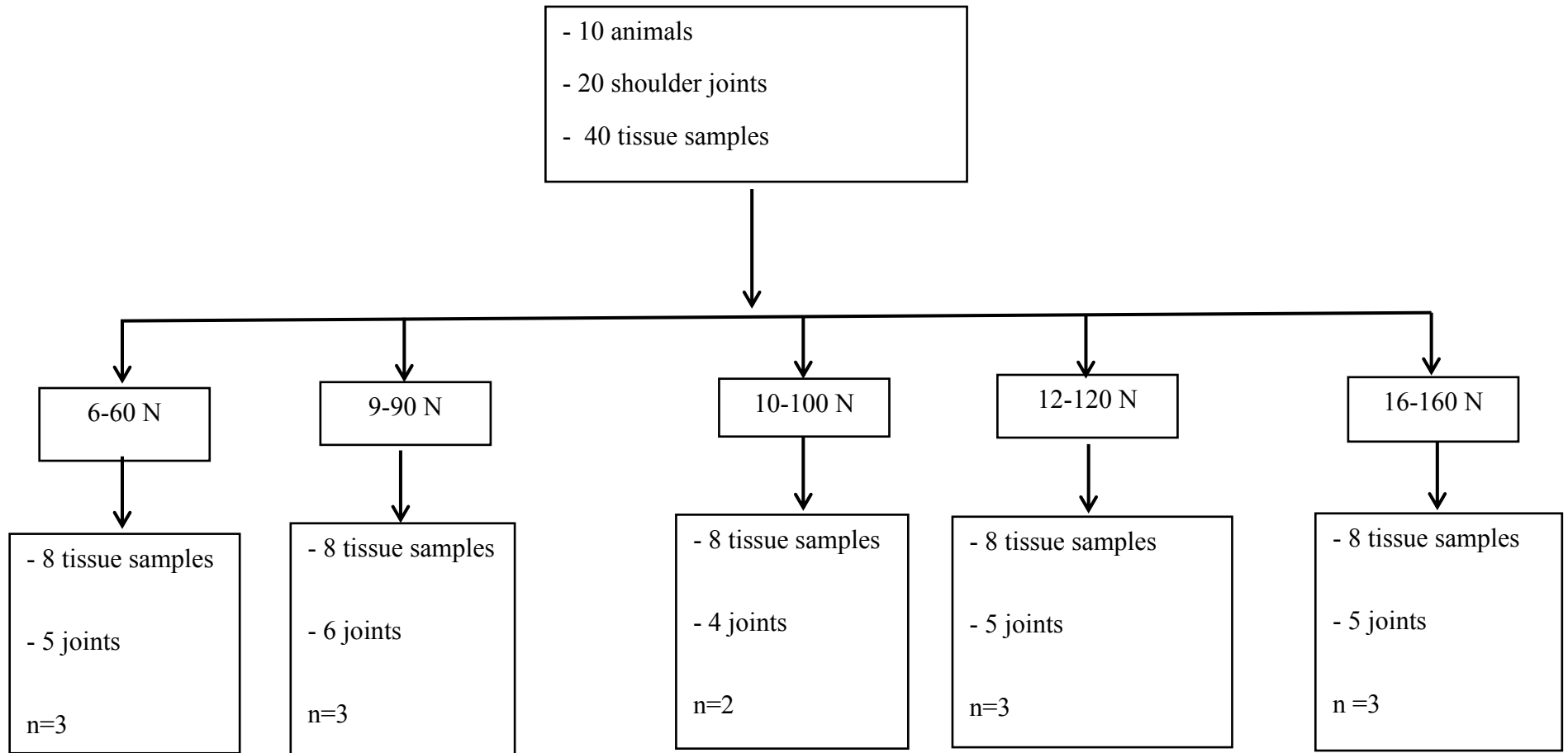


Figure 3.19. Number of independent observations ( $n$ ) used for calculating the 95% confidence intervals in Figures 3.25 and 3.26. Each load range was tested at three loading frequencies on distinct test sites (120 tests).

### **3.4 Cyclic experiment results**

A sample image taken from five cartilage samples at the five loading ranges is provided in Figure 3.20. At lower loading frequencies, such as 1 Hz and 10 Hz, cracks and fissures on the surface of articular cartilage following cyclic tests appeared to be single or parallel lines. However, at 100 Hz, the loaded region contained a greater number of branches. Cracks also increased in length with frequency for all samples, except for the lowest loading range of 6-60 N where there were no cracks at 1 or 10 Hz. There also appeared to be more crack branches at higher frequencies from qualitative observations (Figure 3.20).

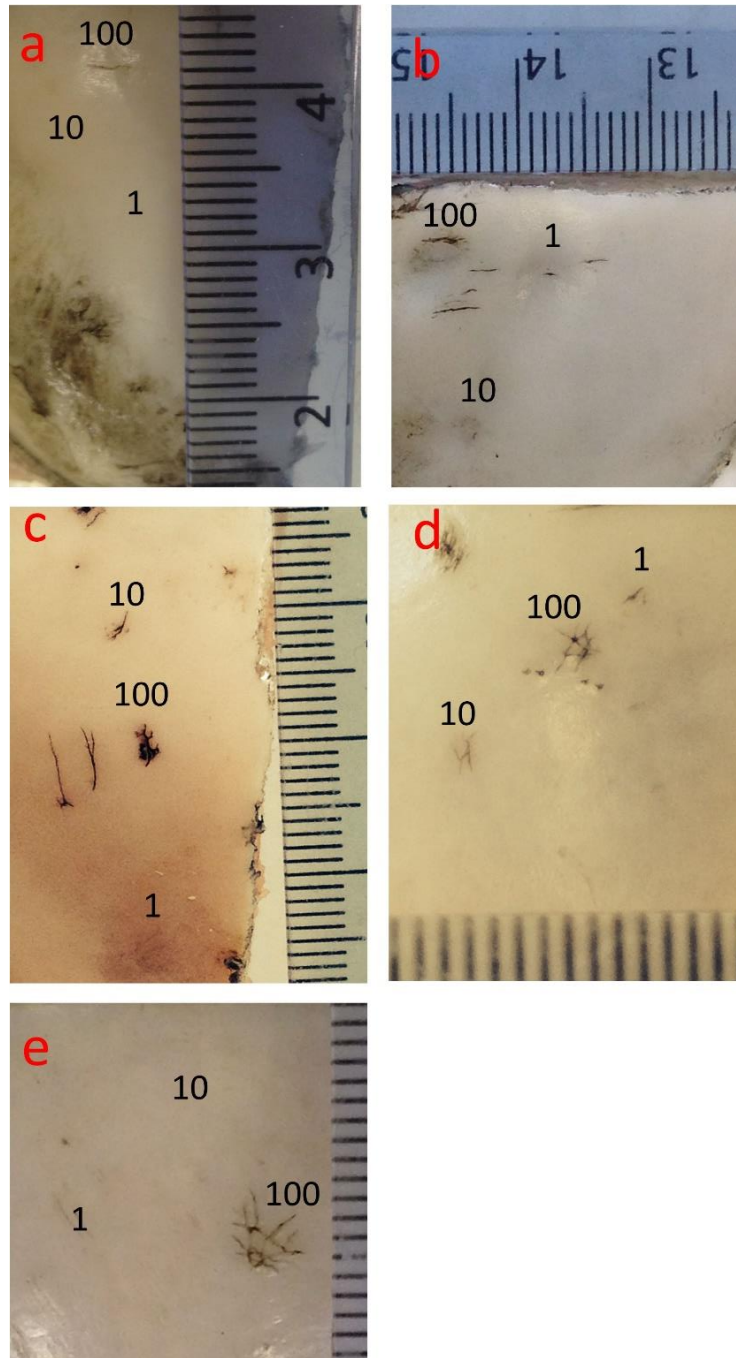


Figure 3.20. Representative images taken from cartilage samples following cyclic loading. Loading ranges included were (a) 6-60 N, (b) 9-90 N, (c) 10-100 N, (d) 12-120 N and (e) 16-160 N. The formation and increase in crack length can be generally observed with increasing load and frequencies of 1, 10 and 100 Hz. India ink was applied to the cartilage surface to easily distinguish the surface cracks. A scale bar is included in every image in order to measure the surface features.

The crack length was found to increase with loading frequency. This was the case for individual tissue samples (Figure 3.21) and also when the mean values from 8 tissues samples were used (Figure 3.22). Figure 3.22, shows the mean total crack length against frequency of 1, 10 and 100 Hz over five load ranges. The first signs of failure were observed in the loading range of 6-60 N (maximum peak nominal stress of 2.8 MPa) at 100 Hz. Maximum damage was observed in the loading range of 16-160 N (maximum peak nominal stress of 7.5 MPa) at 100 Hz. Signs of damage at a loading frequency of 1 Hz and 10 Hz were first observed in 10-100 N (maximum peak nominal stress of 4.7 MPa) and 9-90 N (maximum peak nominal stress of 4.23 MPa), respectively.

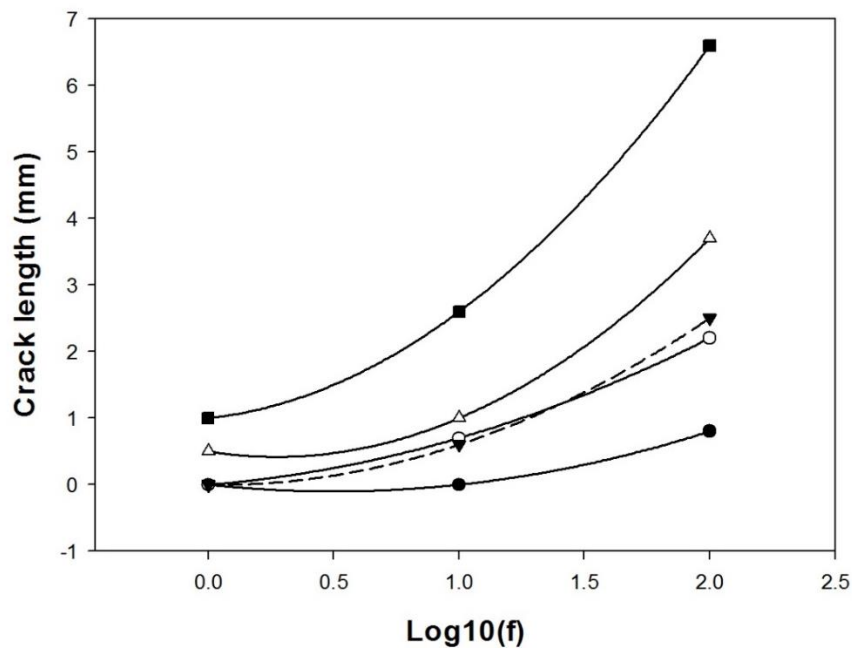


Figure 3.21. Total crack length plotted against the logarithm (with base 10) of the loading frequency for testing on one tissue sample. Three selective data points have been chosen from load ranges of 6-60 N (●), 9-90 N (○), 10-100 N (▼), 12-120 N (△) and 16-160 N (■).

The crack length increased significantly ( $p < 0.05$ ) with increasing loading frequency for all loading ranges. Second order polynomial curves (equation 3.2) were found to fit the data well for all sites tested in the form

$$c = A(\log_{10}(f))^2 + B(\log_{10}(f)) + D \quad \text{for } f \geq 1 \quad (3.2)$$

where  $c$  is the mean total crack length,  $f$  represents frequency and  $A$ ,  $B$  and  $D$  are constants. (Table 3.1).

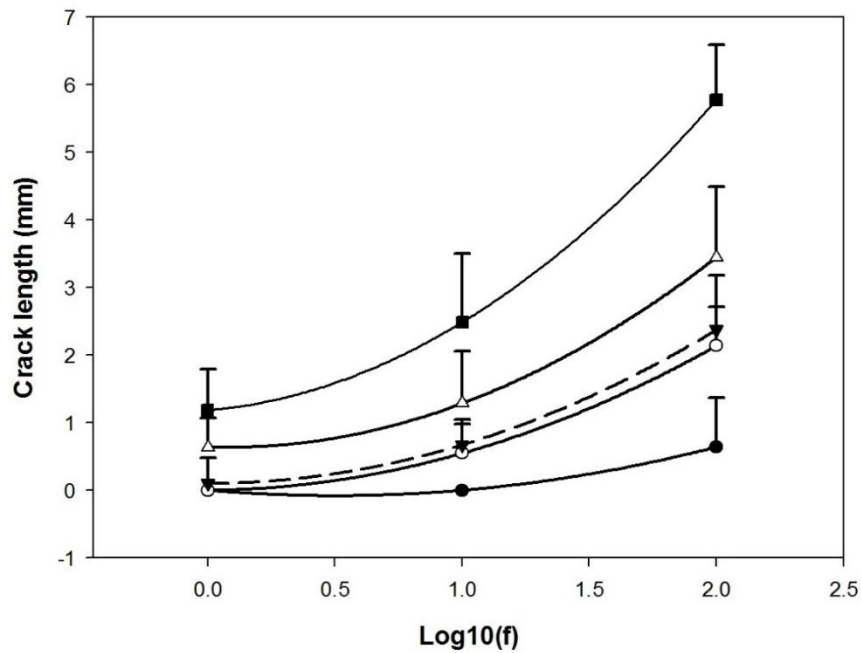


Figure 3.22. Mean total crack length plotted against the logarithm (with base 10) of the loading frequency for the load ranges of 6-60 N (●), 9-90 N (○), 10-100 N (▼), 12-120 N (△) and 16-160 N (■). Second order polynomials (see equation 3.1) fitted the data well. Error bars represent 95% confidence intervals, for clarity only positive error bars have been included. When error bars are not visible they are smaller than the symbols used to represent the data point.

**Table 3.1**

Details of the constants from the mean total crack length against frequency curve fits (Figure 3.22).

Load range (N)	Total crack length ( <i>c</i> ) curve fit				
	A	B	D	$R^2$	P-Value
6-60	-0.32	0.32	0	1	< 0.0001
9-90	0.03	0.51	0	1	< 0.0001
10-100	0.12	0.56	0.1	1	< 0.0001
12-120	-0.1	0.75	0.63	1	< 0.0001
16-160	0.3	0.99	1.18	1	< 0.0001

The total crack length is described by lines of the quadratic form for each load range. They are characterized by constants *A*, *B* and *D*.  $R^2$  is the squared correlation coefficient and shows how well the line fits the data points. If  $p < 0.05$  it indicates that the correlation is statistically significant.

The crack length increased with increasing the maximum load (Figure 3.23). Mean total crack length increased to 1.1, 2.4 and 5.1 mm at loading frequencies of 1, 10 and 100 Hz, respectively. A linear relationship was found to fit the experimental data in the form:

$$c = EL + G \quad \text{for } 60 \leq L \leq 160 \quad (3.3)$$

where  $c$  is the mean total crack length,  $L$  is the maximum load and  $E$  and  $G$  are constants. Mean values of the constants  $E$  and  $G$  were  $0.02 \text{ mm.N}^{-1}$  (SD  $0.019 \text{ mmN}^{-1}$ , range  $0.013\text{--}0.051 \text{ mm.N}^{-1}$ ) and  $-1.74 \text{ mm}$  (SD  $0.77 \text{ mm}$ , range  $-2.54 - -1 \text{ mm}$ ), respectively.

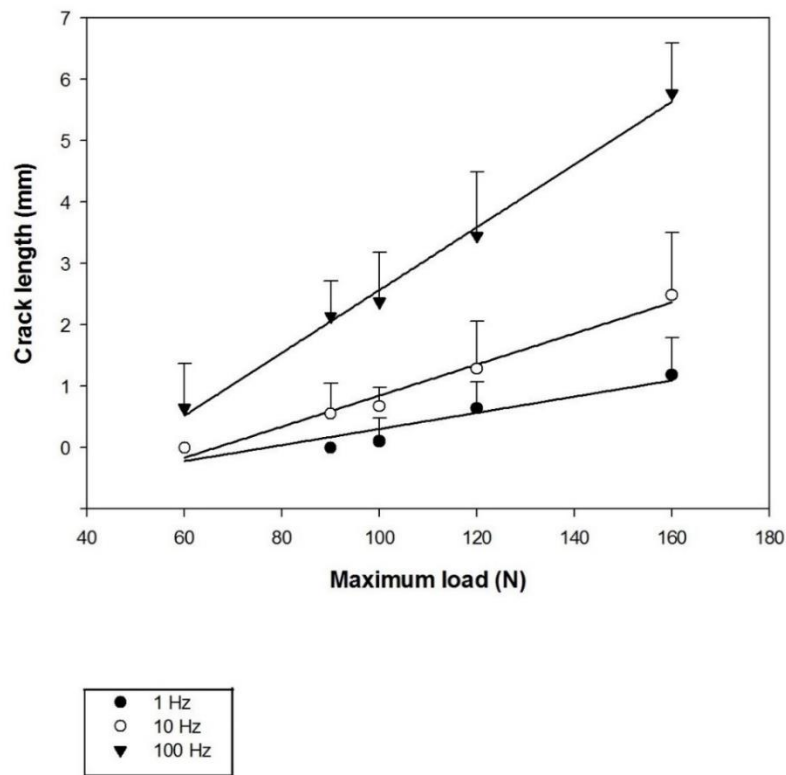


Figure 3.23. Mean total crack length plotted against the maximum load for loading frequencies of 1 Hz (●), 10 Hz (○) and 100 Hz (▼). Each point in this graph represents the mean crack length of 8 measurements. The crack length is described by linear curve fits (see equation 3.2).  $P$ -value for all lines were  $p < 0.05$  which indicates that lines are statistically significant.  $R^2$  is the squared correlation coefficients and shows how well the lines fit the data point.  $R^2$  value for loading frequencies of 1, 10 and 100 Hz are 0.87, 0.97 and 0.99, respectively. Uncertainty of estimates is presented in the form of 95% confidence intervals for clarity only positive error bars have been included. When error bars are not visible it is because they are smaller than the symbols used to represent the data point.

### 3.5 Discussion

The results from this chapter show that surface cracks can form purely by mechanical means, and this progression is frequency dependant. This chapter has investigated the dependency of surface damage on loading frequency. Frequencies of 1, 10 and 100 Hz were used as they correspond to normal gait, above healthy gait HS and similar to traumatic HS rates, respectively (Fulcher *et al.*, 2009). The results show that repetitive mechanical loading of articular cartilage causes damage in the form of crack and fissures to its surface. Crack length was found to increase with increasing loading frequency; this increase was also found to be greater at higher maximum loads. An increase in cartilage damage with increasing the loading frequency was predicted in previous studies (Fulcher *et al.*, 2009; Sadeghi *et al.*, 2015; Pearson & Espino, 2013). This prediction was made because of the change in viscoelastic properties of articular cartilage with frequency. At frequencies of up to 92 Hz, there was an increase in storage to loss modulus, i.e. the ability of the material to store energy rather than dissipate it increased (Fulcher *et al.*, 2009). The main mechanism for releasing the excess energy was suggested to be by the formation of cracks. The proposed mechanism was consistent with increased cartilage failure which occurs with increasing energy during impact loading *in vitro* (Jeffrey *et al.*, 2006; Verteramo *et al.*, 2007).

Increase in the length of cracks and fissures during mechanical cyclic loading have been reported in previous studies, but only up to frequencies of 0.1 Hz (Weightman *et al.*, 1973) or 0.5 Hz (Kerin *et al.*, 2003) and 1 Hz (Radin *et al.*, 1984). In the current study damage was created on cartilage samples by applying 10,000 cycles over five load ranges with peak stresses from 2.8 to 7.5 MPa. The change in damage was observed when frequency alone was altered. Ewers *et al.* (2001) who investigated the propagation of damage in rabbit cartilage after blunt impact *in vivo* also reported that the total length of fissures increased during the first 4 months following impact tests.

Articular cartilage is subjected to various ranges of peak stresses under light to moderate activities which typically range from 1 to 6 MPa (Ahmed *et al.*, 1983; Brown *et al.*, 1983). Peak stress amplitudes, under more vigorous activities in natural joints have been estimated up to 12 MPa (Mathews *et al.*, 1977) or even 18 MPa (Hodge *et al.*, 1989). The maximum peak stresses used in this study were from 2.8 to 7.5 MPa, which is similar to peak stresses acting on cartilage during light to moderate activities.

It has been suggested that rapid rise times during heel strike could be implicated in the onset of OA (Radin *et al.*, 1991). Repetitive mechanical loading can create fissures in the surface of cartilage (Weightman *et al.*, 1973). Significant increase in crack length with frequency in peak stresses which resembles peak stresses acting on cartilage during light and moderate activities shows the important role of loading frequency in the initiation and propagation of damage on the surface of articular cartilage in this study. Other studies (Fulcher *et al.*, 2009; Espino *et al.*, 2014; Pearson *et al.*, 2013) have reported that the ability of cartilage to store and dissipate energy is altered with loading frequency. This may change the stress transfer to the underlying bone which leads to bone stiffening and ultimately failure of articular cartilage (Espino *et al.*, 2014). However, energy transfer between cartilage and subchondral bone has not been investigated in this study.

The effect of increasing the loading frequency was investigated in a comparable study (Tomatsu *et al.*, 1992) when shear force was used to create fractures on the surface of articular cartilage experimentally. Results from this study showed that with increasing the speed of the applied load (increasing the frequency), surface cracks appeared on the surface of cartilage whereas low speed loads with the same energy, did not create cracks on the surface of cartilage.

The effect of slowly applied loads and suddenly applied loads on articular cartilage was suggested to differ considerably in previous studies (Tomatsu *et al.*, 1992; Buckwalter *et al.*, 2003; Kafka *et al.*, 2002; Mow *et al.*, 1988). This was associated with the deformation of cartilage under different loading frequencies with displacement of water inside and outside of the collagen network. These studies assumed cartilage as a biphasic material composed of a solid matrix phase

(20% of the total mass by weight) and an interstitial fluid phase (80%) (Kafka *et al.*, 2002). It is not clear why the cartilage surface shows sign of cracking following cyclic tests, a behaviour mostly seen in brittle materials (Silyn-Roberts *et al.*, 1990; Kelly *et al.*, 1996). However, using a theoretical model (Armstrong *et al.*, 1986), it has been shown that increasing the loading frequency, also increases the flow of interstitial fluid inside the cartilage tissue. This fluid flow in and out of the collagen matrix is eventually inhibited together at higher frequencies; therefore cartilage acts as a brittle, largely incompressible elastic solid. The biphasic mechanism was explained by assuming the solid matrix, to be a porous, permeable elastic solid and the interstitial fluid to be movable within the tissue (Lu *et al.*, 2008). Both phases were modelled to be intrinsically incompressible and the diffusive drag forces between the two phases resulted in the viscoelastic behaviour of the tissue (Mow *et al.*, 1980; Martin *et al.*, 2002). However, this mechanism was not supported, when viscoelastic properties of cartilage were measured up to 10 Hz (Sadeghi *et al.*, 2015) or 90 Hz (Fulcher *et al.*, 2009) as almost no variation was observed in loss modulus/stiffness with the loading frequency. This might be due to the constraining effect of the underlying bone (Sadeghi *et al.*, 2015; Aspden *et al.*, 1990). The underlying bone has previously been predicted to prevent an increase in loss modulus (Edelsten *et al.*, 2010).

Fluid flow is not the only possible mechanism which is involved in cartilage deformation and ultimately failure. Another alternative is to treat cartilage as a hydrated gel (Kovach *et al.*, 1995 & 1996), undergoing glass transition (transition from a soft to a glass like material), under high loading frequencies. This has been discussed in several studies (Fulcher *et al.*, 2009; Hukins *et al.*, 1985; Meakin *et al.*, 2003) because of the existence of hydrated proteoglycans in the cartilage matrix which act as a natural hydrogel under deformation. This is consistent with increased injury observed with increased stiffness under increased loading frequencies (Tomatsu *et al.*, 1992).

Articular cartilage is a composite material in which collagen fibrils provide tensile reinforcement. The alignment of collagen is different in every layer of cartilage (Aspden *et al.*, 1990 & 1981; Hukins *et al.*, 1985). One of the mechanisms which has been suggested as being

involved in crack growth under repetitive loading on the cartilage surface is the tension developed in the superficial layer of the cartilage surface (10-20 % of cartilage thickness) (Korhonen *et al.*, 2002a). The propagation of a pre-existing notch through the depth of cartilage specimens is the subject of chapter 5 of this thesis.

The indentation technique used in this chapter ensured that the loaded cartilage was supported naturally by adjacent cartilage and subchondral bone. Lateral support from adjacent cartilage greatly affects cartilage deformation (Korhonen *et al.*, 2002b), and the natural support provided in the present experiment lies in-between the two extreme conditions of “confined” and “unconfined” compression which are often used to test mathematical theories (DiSilvestro & Suh, 2001). A limitation of this technique could be that relative hardness of the metal indenter, compared to cartilage, would tend to concentrate stress around its edge. However, the effect of this artefact appears to have been invalidated by the smoothly bevelled edges of the indenter. This is because the results from this chapter showed that most cracks occurred, and propagated, near the centre of the loaded area. Additionally, indentation loading does not require complex specimen preparation required by experiments such as confined compression where exact radial dimensions are needed to ensure both biomechanical sensitivity and to reduce sample variability.

Another limitation of using a metal indenter to apply high cyclic loads on the cartilage surface could be that it is not realistic when compared to real deformation of two compressed cartilage surfaces in the joint. However, a stiff metal indenter remains flat under high load, but considerations of symmetry suggest that two similarly soft cartilage surfaces would also remain flat in their region of contact. When two joints are pressed together, cartilage would deform under load to increase its contact area and decrease the contact stress. As two cartilage surfaces contact each other, the edges surrounding the area of contact ‘bulge’ due to water under the contact area being displaced laterally as compressive deformation proceeds (Shrive & Frank, 1999). Using an indenter with a radius substantially smaller than the cartilage sample also allowed this natural ‘bulging’ to occur at the contact boundary. Indentation technique also compresses the articulating surface, allowing articular

cartilage to remain on the subchondral bone during loading more closely approximated by *in vivo* loading conditions (Lu *et al.*, 2004; Mow *et al.*, 1980).

### **3.6 Chapter summary**

It can be concluded from this chapter that surface damage to cartilage following sinusoidal loading increased with frequency throughout all load ranges investigated. Cracks appeared on the surface of articular cartilage in lower load ranges (below a maximum peak stress of 4.7 MPa) only at loading frequencies which are associated with RHS and above healthy gait HS rise times, 100 Hz and 10 Hz, respectively. However, cracks appeared at all loading frequencies in higher maximum load ranges (above maximum peak stress of 4.7 MPa). Variation of damage with different loading frequencies has implications in the early stages of OA. The next chapter deals with the effect of loading frequency on failure of cartilage-on-bone specimens under bending. In the next chapter an investigation was undertaken to determine if the variation of loading frequency affects the failure of cartilage-on-bone specimens during cyclic bending tests.

## **4. Fatigue strength of bovine articular cartilage-on-bone under bending: the effect of loading frequency**

### **4.1 Introduction**

Chapter 3 investigated the effect of loading frequency on damage to articular cartilage, demonstrating that at frequencies representative of RHS rise times (100 Hz), damage was more extensive than at lower frequencies (1 Hz). The overall aim of this current chapter was to determine whether failure of cartilage-on-bone during bending was also frequency dependent. Different bending methods were initially performed on cartilage-on-bone specimens in order to decide on the most appropriate test method to investigate frequency-dependent failure.

Previous studies (Stockwell *et al.*, 1991) have suggested that vigorous physical activities such as frequent bending and lifting are risk factors for OA. Such an association implies that mechanical fatigue could also be a factor in the development/progression of the disease. Freeman *et al.* (1972) suggested that a fatigue mechanism might be associated in the progression of OA. Weightman *et al.* (1976 & 1975), Kempson *et al.* (1991) and Simon *et al.* (1989) have studied compressive, tensile and shear fatigue effects on articular cartilage, respectively. All of these studies have provided data, which demonstrate the progression of damage within cartilage under cyclic mechanical loading. Freeman *et al.*, (1972) was one of the earliest studies to suggest that repeated cyclic loading could lead to the fatigue failure in the cartilage surface layer. As described elsewhere (Byers *et al.*, 1977; Maroudas *et al.*, 1977), disruption of the cartilage surface appear with fissuring, resulting in fibrillation of the cartilage surface. Cartilage surface fissures penetrating into the cartilage depth could lead to further roughening of the joint surface, which has been observed in osteoarthritic joints. The earliest changes in osteoarthritic joints were reported to involve an increase in joint volume followed by an increase in cartilage volume (Cicutini *et al.*, 2004).

Implication of RHS during gait in the onset of OA is in addition to the link between cartilage failure and mechanical overload of a joint during vigorous physical activities such as

heavy manual labour (Cooper *et al.*, 1994). A previous study (Baltzopoulos *et al.*, 1995) has also found evidence suggesting that high internal compressive joint forces by leg muscles during activities which involve deep knee bending maybe a risk factor in osteoarthritis. Therefore, large internal joint forces, applied at frequencies associated with RHS rise times might further predispose cartilage to damage during bending, however, this is not currently known. Previous studies (Radin *et al.*, 1973 & 1978; Dekel *et al.*, 1978) have suggested that the frequency of loading of a joint might be important with respect to the possibility of damage to articular cartilage.

## 4.2. Material and Methods

### 4.2.1 General Methods

Ten humeral heads from bovine shoulder joints were obtained from an established supplier [REDACTED]. Joints were from skeletally mature cows which were approximately 24 months old. Humeral heads were dissected from areas free from defect using methods explained in section 3.2.2.

Rectangular shaped samples, measuring approximately 36 mm × 8 mm along their surface and 4 mm in depth, were cut from the joints (Figure 4.1). Cartilage-on-bone samples were obtained from the central region of the humeral head. Samples were selected from this location because it has a flat surface and is in the centre of the contact region of the joint. Articular cartilage located in this position has been shown to undergo maximum deformation in the humeral head (Canal *et al.*, 2008). An aluminium test rig was designed and manufactured to hold the sample and apply the loads in a three-point bend configuration (Figure 4.2-a). The main advantage of a three-point bending test is the ease of the specimen preparation and testing. However, this method has also some disadvantages; the results of the testing method are sensitive to specimen and loading geometry. The designed test rig could also be altered to hold the specimen under four-point bending

with the outer supports, which were used to apply the loading when held 20 mm apart. The inner supports of the rig that held the specimen were 10 mm apart (Figure 4.2-b). This testing configuration is very similar to the three-point bending test. The main difference is the addition of a fourth loading support that could induce maximum stress along a larger portion of the beam, as opposed to concentrating stress to only the material under the central bearing in three-point bending (ASTM-D7774).

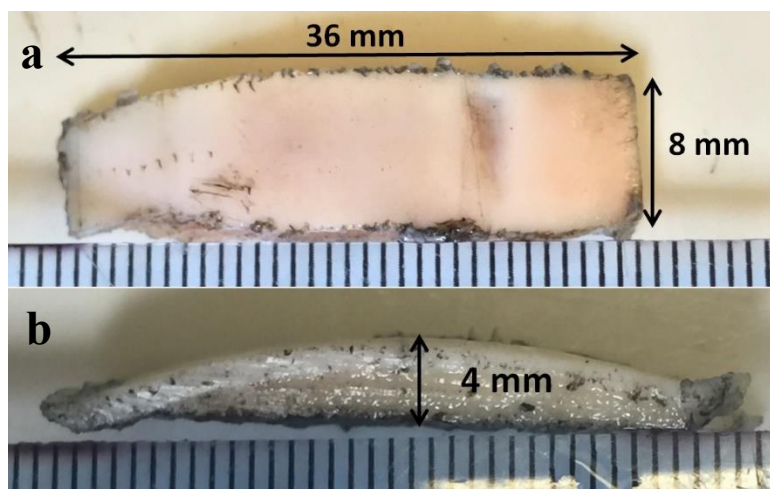


Figure 4.1. Cartilage-on-bone specimen (a) Sample image of the top view of a cartilage-on-bone specimen used to perform bending tests (b) side view of the same specimen showing the depth of the specimen. The scale bar is in mm.

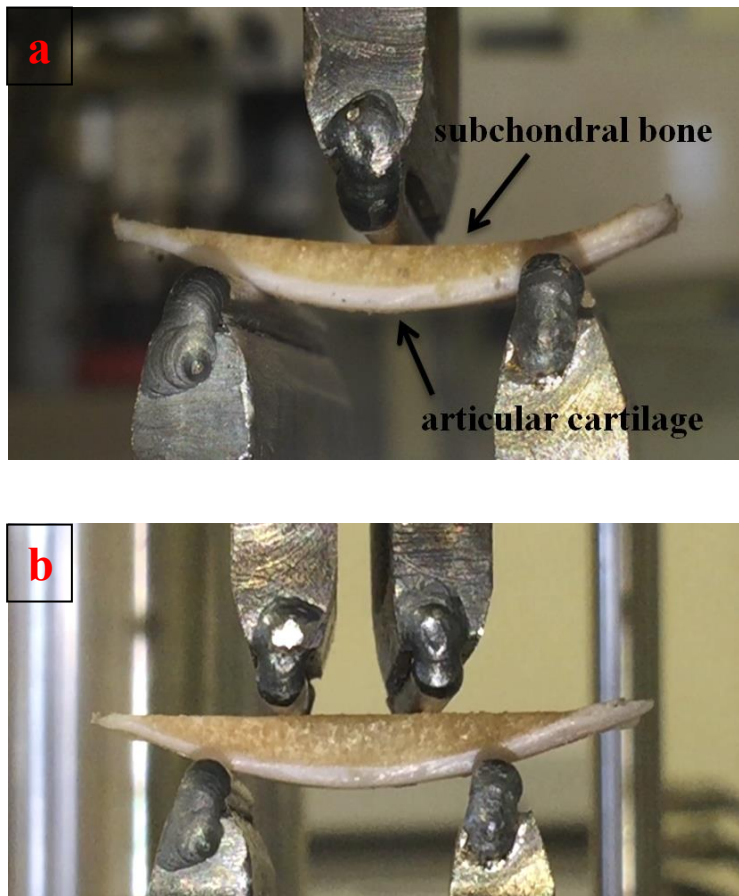


Figure 4.2. Bending test configurations. (a) Three-point bend and (b) four-point bend test rig with a cartilage-on-bone specimen in the starting test position. The distances between the inner and outer supports of the four-point bending test were 10 and 20 mm, respectively.

The lower test rig consisted of two supports (20 mm apart) that attached to the base of the testing machine. The contact radii of the loading supports were 1.5 mm, consistent with a previous study of bone (Draper *et al.*, 2003). The upper test rig, attached to the actuator of the testing machine, comprised a bar with a 1.5 mm radius at the contacting end. The specimen was placed on the supports so that the lower supports were in contact with cartilage and the upper roller, which was used to apply the load, was in contact with the subchondral bone (Figure 4.2). The length of the specimens varied between 32 and 36 mm, providing overhangs of between 6 and 8 mm on each side of a sample when subjected to three-point bend (Draper *et al.*, 2003).

## 4.2.2 Preliminary experiments

To evaluate typical loads that a cartilage-on-bone specimen experience under three-point bend, six cartilage-on-bone specimens were subjected to a three-point bend ramp test, using a Bose ElectroForce ELF3300 materials testing machine (Bose corporation, Minnesota, USA; now, TA instruments, New Castle, DE, USA), operated under the control of WinTest 4.1 software (Figure 4.3). The actuator of the material testing machine was set to lower at a rate of 0.05 mm/s consistent with a rate used by Mente *et al.* (1994). Load and displacement were recorded throughout the test. Testing continued up to a maximum displacement of 4.5 mm (the maximum thickness of cartilage-on-bone specimens was 4 mm). Samples were under saline irrigation during testing to prevent dehydration. The flexural stress of each specimen was calculated from

$$\sigma_{max} = \frac{3PL}{2bh^2} \quad (4.1)$$

where  $P$  is the maximum force,  $L$  is the length,  $b$  is the width and  $h$  is the depth of test samples (ASTM-D7774). The failure of cartilage-on-bone specimens was defined as a complete fracture of the cartilage and the underlying bone.

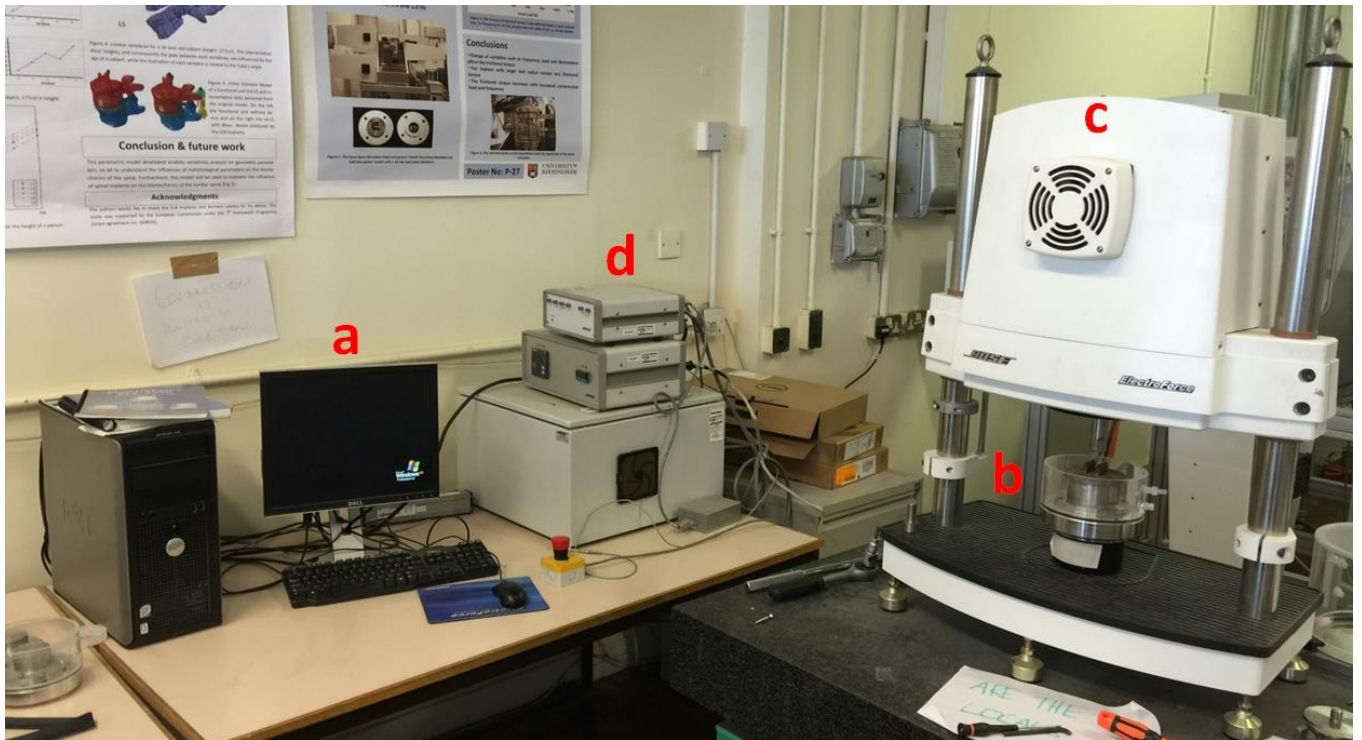


Figure 4.3. Bose ELF3300 material testing machine. (a) Computer (b) Bending test rig fitted into the testing machine (c) Machine (d) Power tower.

All six specimens failed before reaching the displacement limit of 4.5 mm. Figure 4.4 shows a typical load against displacement curve of cartilage-on-bone specimens subjected to three-point bending. The flexural strength of specimens subjected to three-point bending was  $29.6 \pm 8.0$  MPa (mean  $\pm$  SD) which was calculated from equation 4.1, corresponding to a failure force of  $126.1 \pm 34.3$  N, which occurred at a failure displacement of  $3.6 \pm 1.9$  mm.

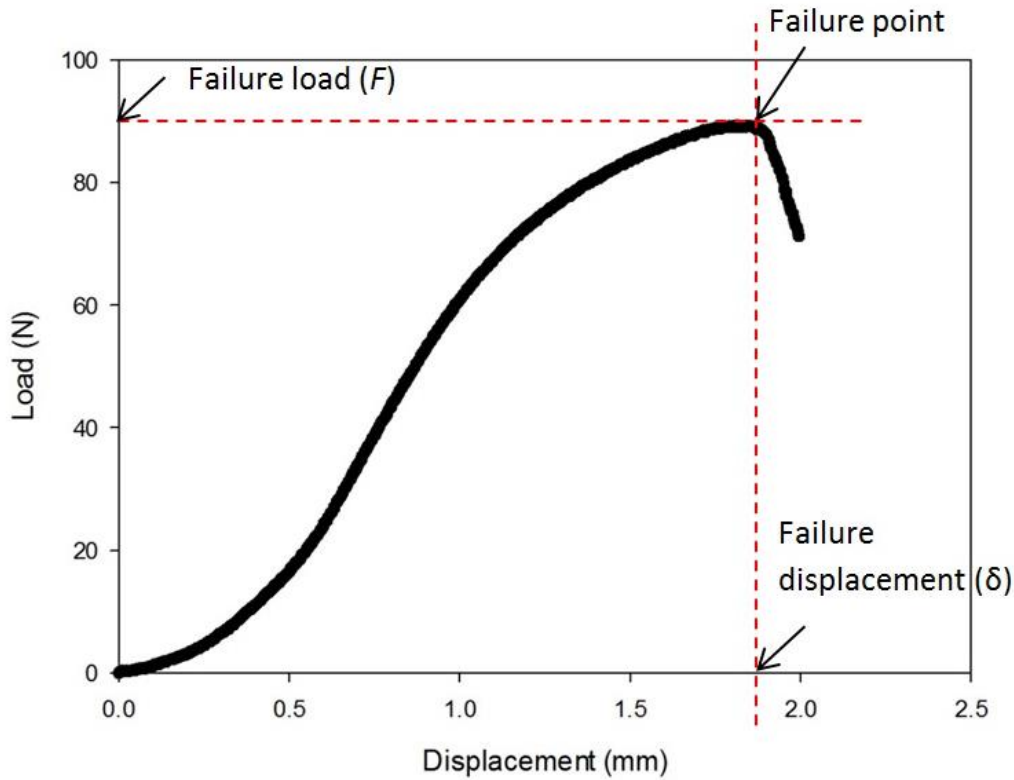


Figure 4.4. Load against displacement of a cartilage-on-bone specimen under three-point bending. Failure occurred at a load ( $F$ ) of 89 N corresponding to a failure displacement ( $\delta$ ) of 1.85 mm.

To evaluate typical forces that cartilage on-bone experience under four-point bending, three specimens were prepared with the dimensions detailed in section 4.2.1. Cartilage-on-bone specimens were tested under four-point bending. The flexural stresses for each test were calculated from:

$$\sigma_{max} = \frac{3PL}{4bh^2} \quad (4.2)$$

where  $P$  is the maximum force,  $L$  is the length,  $b$  is the width and  $h$  is the depth of test samples (ASTM-D7774).

Figure 4.5 shows a typical force against displacement graph under four-point bending. The flexural strength of the specimens was  $50.6 \pm 14.4$  MPa (mean  $\pm$  SD) calculated from equation 4.2. This corresponded to a failure force of  $270 \pm 77.2$  N, which occurred at a failure displacement of  $3.9 \pm 1.3$  mm.

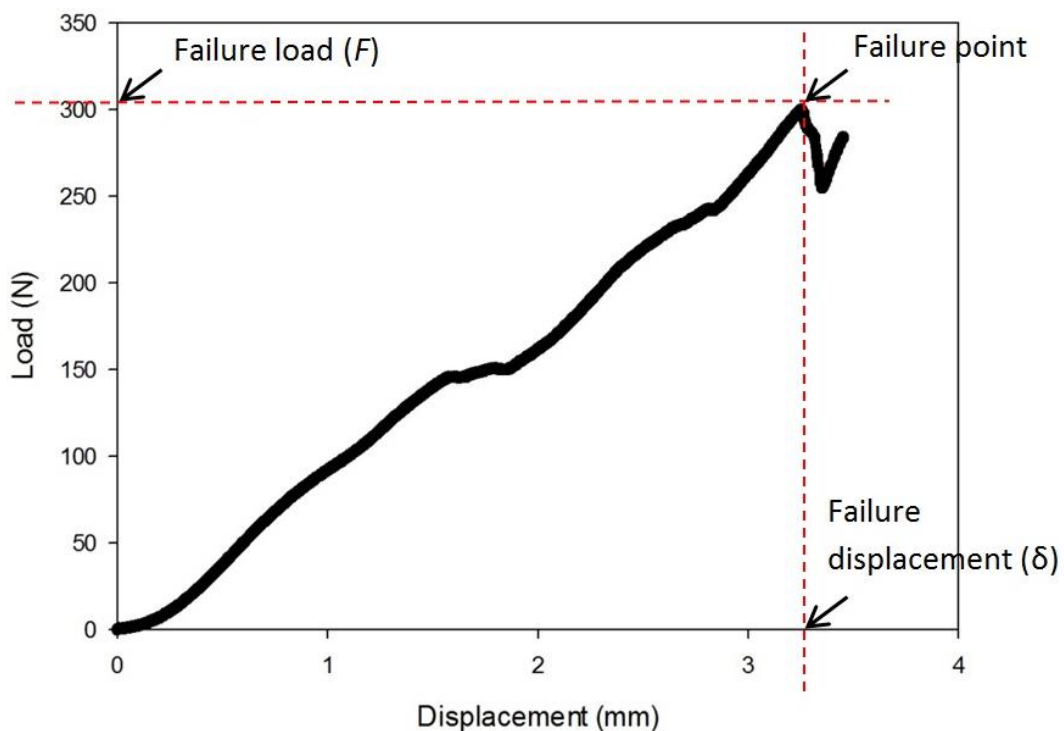


Figure 4.5. Load against displacement of a cartilage-on-bone specimen under four-point bending. Failure occurred at the load ( $F$ ) of 304 N corresponding to the failure displacement ( $\delta$ ) of 3.24 mm.

The failure force was  $126.1 \pm 34.3$  N in specimens subjected to three-point bend tests. However, this value was around double ( $270 \pm 77.2$  N) for specimens tested under four-point bend tests. From qualitative observations after the three-point bending tests, failure occurred at the centre of the

cartilage-on-bone specimens (Figure 4.6-a). However, failure mostly occurred at the point of the outer contact of the specimens subjected to four-point bending (Figure 4.6-b).

Three-point bending constrains failure to occur at the central contact and, therefore, it is not possible to separate the stress causing failure from the stress concentration due to the test rig contact. Four-point bending, however, has a region of uniform stress distribution between the inner contacts. The failure point usually lies anywhere along this region and away from the immediate region of the contacts. However, failure occurred at the point of contact in four-point bending tests. This means that stresses were not distributed evenly between the two support contacts. Therefore, the three-point bending configuration was chosen in order to perform further cyclic tests.

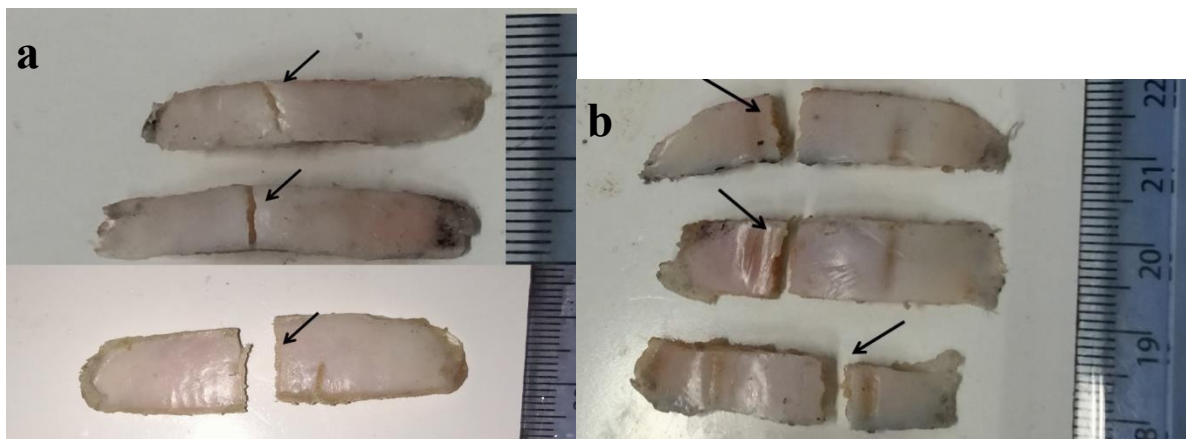


Figure 4.6. Images taken from six cartilage-on-bone specimens after failure under bending. (a) Failure occurred at the centre of the specimens tested in a three-point bending configuration. (b) Failure occurred at the point of the outer contacts for specimens tested in four-point bending suggesting that stress is concentrated at these points.

All cyclic tests were performed with the same three-point bending test rig, as described in section 4.2.1. The aim of these tests was to determine whether the growth of an initial crack could be measured over a specific number of cycles. An initial crack of 0.5 mm depth was introduced into the middle of the cartilage surface of the specimens (Figure 4.7). Briefly, 0.5 mm of the tip of a scalpel blade (Swann-Morton, Sheffield, UK) was marked with a water resistant marker (Fischer

Scientific, UK). The blade was pushed into the middle of the cartilage surface of the specimen up to the marked point.



Figure 4.7. An initial crack of 0.5 mm depth was cut into the centre of the cartilage-on-bone specimen.

Specimens were subjected to a sinusoidally varying force in the range of 7-70 N at a frequency of 10 Hz. The maximum force (70 N) was chosen as 55% of the mean failure force ( $126.1 \pm 34.3$  N) measured from the ramp three-point bend tests explained in section 4.2.4. A frequency of 10 Hz was chosen since crack growth is more likely to occur at this frequency than at 1 Hz, because the reduced rate of loading has been found to lead to reduced failure in chapter 3, or traumatic loading frequencies (50 and 100 Hz), because the progression might be too quick to measure reliably. Figure 4.8 shows three specimens after their failure. One of the specimens fractured on the first application of load. The remaining specimens failed after 4,000 loading cycles. Tests were stopped every 1,000 cycles to observe whether the initial crack had grown. India ink was applied to the specimens and the pre-existing crack was measured using a Vernier caliper (Fisher Scientific, Leicestershire, UK) and photographed using a DSC-R1 Cyber-shot© digital camera (10MP, 5 x Optical Zoom) 2.0" (Sony Corporation, 6-7-35 Kitashinagawa, Shinagawa-ku, Tokyo, Japan). No consistent growth of the initial cracks was observed (Figure 4.9). Furthermore, failure eventually occurred not within the region of the pre-existing crack (Figure 4.8). Fracture in the specimens that failed, occurred rapidly rather than through the slow propagation of a crack.

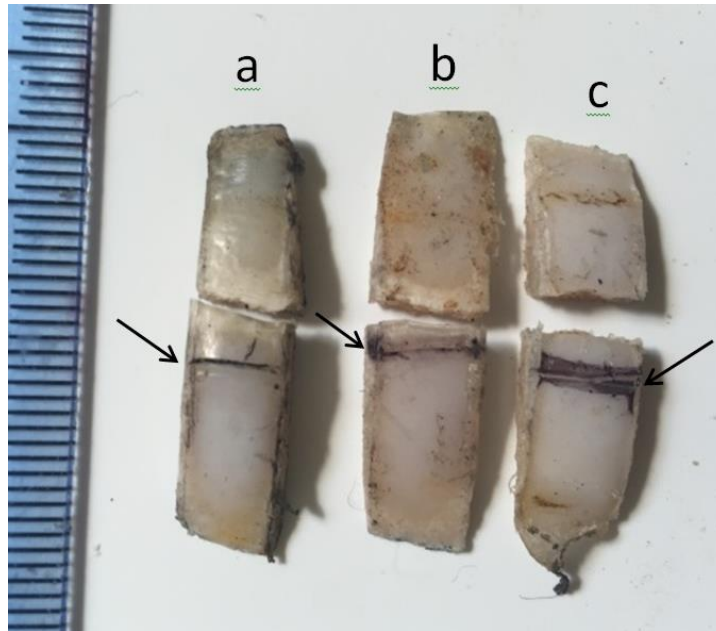


Figure 4.8. Three specimens subjected to sinusoidally varying forces of 7-70 N at 10 Hz. Specimen (a) fractured after the first application of load. Specimens (b) and (c) fractured at 4,715 and 5,242 cycles, respectively. However, the point at which the specimens fractured was not where the pre-existing crack was introduced (marked with arrows).

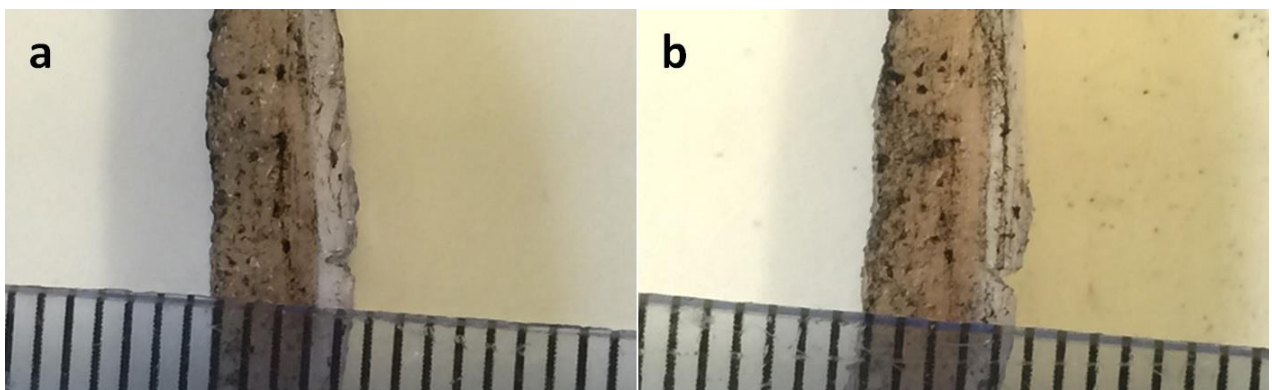


Figure 4.9. Sample images taken from cartilage-on-bone (specimen c from figure 4.7). (a) specimen at the starting position (b) specimen after the application of 5,000 loading cycles. A pre-existing crack showing minimal growth after the application of 5,000 loading cycles. The scale bar is in mm.

Three different three-point bending tests were conducted to see if an initial crack could grow. An initial crack of 1 mm was introduced into the centre of three cartilage-on-bone specimens.

This method was used to determine if crack growth could be achieved. Specimens were subjected to a force range of 7-70 N at a frequency of 10 Hz. It appeared that increasing the initial crack from 0.5 to 1 mm concentrated the stresses which may have led to failure. This was concluded as two of the specimens fractured at the centre, where the initial crack was introduced (Figure 4.10). However, one of the specimens reached run-out. No consistent growth of the initial cracks was observed (Figure 4.11). Therefore, it was decided that the fatigue strength of the specimens was to be measured using the number of cycles to failure, where failure is defined as the complete fracture of cartilage and the underlying bone. The typical thickness of bovine humeral articular cartilage varies from 0.8 to 1.6 mm (Toyras *et al.*, 2001). Therefore, a 1 mm pre-existing crack included most of the cartilage thickness, which leaves a minimal cartilage thickness for the crack to grow through.

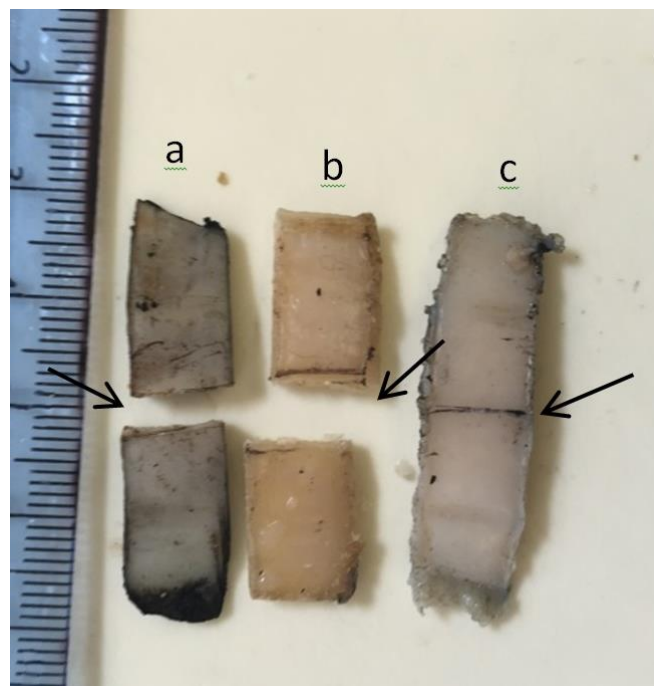


Figure 4.10. Initial crack was introduced at the centre of each specimen. Two of the cartilage-on-bone specimens fractured at 2,102 (a) and 3,454 (b) of loading cycles. However, one of the specimens reached run-out (c). The scale bar is in mm.

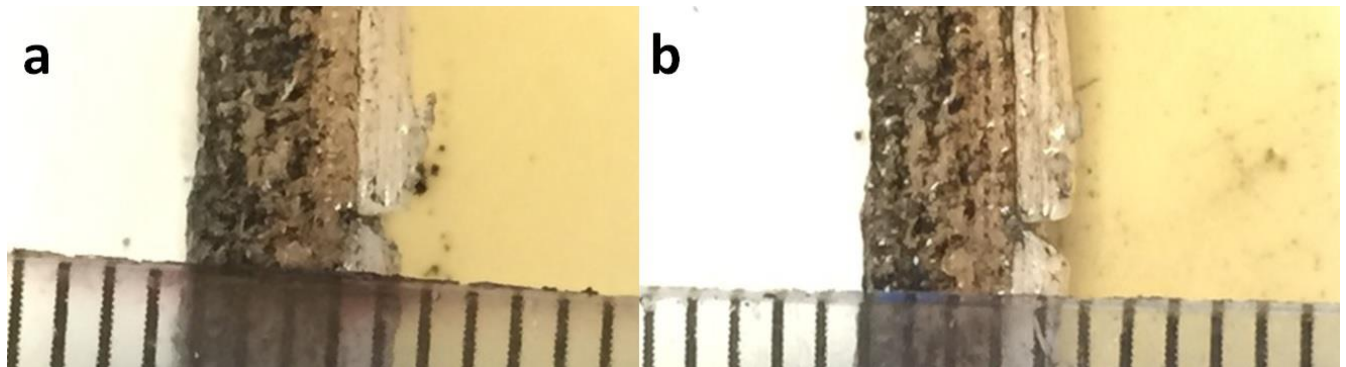


Figure 4.11. Sample images taken from cartilage-on-bone specimen (b) from figure 4.9. (a) specimen at the starting position (b) specimen after the application of 5,000 loading cycles. A pre-existing crack showing minimal growth after the application of 5,000 loading cycles. The scale bar is in mm.

Three preliminary cyclic three-point bend tests were performed on cartilage-on-bone specimens at a loading frequency of 10 Hz. Testing continued until 10,000 loading cycles had been completed or the specimen had failed. Three sinusoidally varying force ranges were used for testing on three separate cartilage-on-bone specimens. The maximum force started from 70 N (55 % of the mean static yield force) (Figure 4.12) and increased by 30 N, up to the maximum force of 130 N. Therefore, specimens were subjected to three sinusoidally varying force ranges of 7-70, 10-100 and 13-130 N. The ratio of maximum to minimum force ranges was kept as 10 (Xin *et al.*, 2013).

Figure 4.13 shows three cartilage-on-bone specimens after fracture. The number of cycles to failure was found to be 1,490, 110 and 239 at force ranges of 7-70, 10-100 and 13-130 N, respectively. All three cartilage-on-bone specimens failed at the force ranges used for testing. Therefore, it was decided that for the final cyclic tests the maximum force would start at 40 N (30 % of mean static failure force), and increase in steps of 30 N up to the maximum force of 130 N (103 % of the mean static failure force) in order to have a wider range of data for the final testing.

The starting maximum force was chosen to be 30 N lower than the minimum forces used in section 4.3.8 to determine whether failure could occur in the specimen during the 10,000 loading cycles or run-out was going to be reached. These force ranges were applied at gait and above gait relevant frequencies of 1 and 10 Hz, respectively, up to frequencies of 50 and 100 Hz to understand the effect of frequency on fatigue strength of cartilage-on-bone samples.

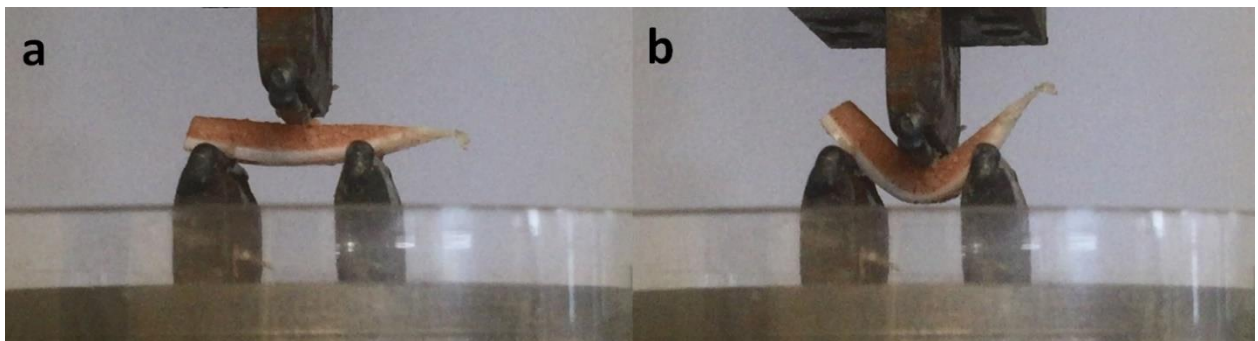


Figure 4.12. Cyclic three-point bending. (a) Cartilage-on-bone specimen at the starting position for three-point bending (b) Specimen deflecting under cyclic three-point bending subjected to a force range of 7-70 N at a frequency of 10 Hz.

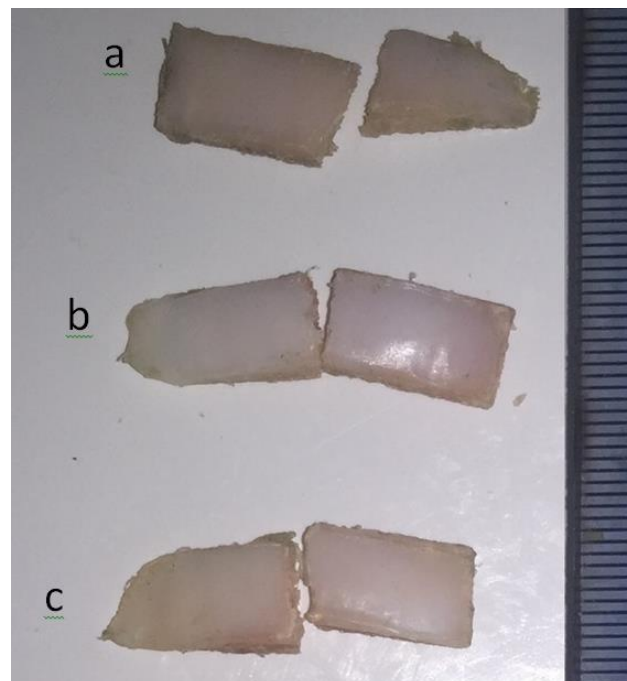


Figure 4.13. Fractured cartilage-on-bone specimens. (a) Cartilage-on-bone specimen subjected to three sinusoidally varying force ranges of 7-70, (b) 10-100 and (c) 13-130 N after their fracture. The scale bar is in mm.

### 4.3. Cyclic three-point bend testing

The final cyclic three-point bending tests involved the application of 10,000 cycles of sinusoidally varying compressive force at loading frequencies of 1, 10, 50 and 100 Hz (Sadeghi *et al.*, 2015; Fulcher *et al.*, 2009). A loading frequency of 50 Hz was used to have a wider range of data on fatigue strength of the specimen samples, compared with the frequency ranges used in chapters 3. A wider range of data was considered important for this particular set of tests because of the effect of bone on the data. Bone could affect the results since cyclic loading was applied from bone to cartilage.

A total of 120 cartilage-on-bone samples, obtained from 10 bovine humeral heads, were subjected to the cyclic three-point bend tests. Ten sinusoidally varying compressive force ranges were used for testing. The sinusoidal force ranges started at 4-40 N with the maximum force increased by 10 N up to a force range of 13-130 N; the ratio of maximum to minimum force was 10. The associated peak stresses ( $\sigma_{max}$ ) of the selected peak loads ( $P$ ) during cyclic three-point bending tests were calculated from equation 4.1. Therefore, specimens experienced a range of maximum flexural stresses of 15 to 50 MPa. Each test was repeated on three separate specimens. A different specimen was used for every test. Testing continued until complete fracture of the specimen or run out of 10,000 cycles. If a specimen reached 10,000 cycles and it did not fail, it was considered to have reached run-out.

After testing, specimens were immersed in Ringer's solution for 30 minutes, to ensure that the cartilage returned to its original thickness (Barker *et al.*, 2001). India ink was then applied on the cartilage surface. A visual inspection of individual specimens was undertaken and the cartilage surface was examined. Each specimen was then photographed using a DSC-R1 Cyber-shot© digital camera (10MP, 5 x Optical Zoom) 2.0" (Sony Corporation, 6-7-35 Kitashinagawa, Shinagawa-ku, Tokyo, Japan).

#### 4.4. Cyclic three-point bend results

Figure 4.14 shows the results of the cyclic three-point bend tests of cartilage-on-bone specimen samples in which the maximum force applied was plotted against the number of cycles to failure. Each data point represents one cartilage-on-bone specimen. The number of cycles to failure decreased with increasing maximum force for all frequencies tested. This relationship can be described using individual logarithmic curve fits in the form:

$$S = A(\ln(N)) + B \quad (4.3)$$

where  $S$  is maximum force,  $N$  is number of cycles to failure and  $A$  and  $B$  are constants.

The number of cycles to failure decreased significantly ( $p < 0.001$ ) with the increasing maximum force at loading frequencies of 10 and 50 Hz. The correlation was not significant ( $p \geq 0.05$ ) at 1 or 100 Hz. The corresponding  $p$  and  $R^2$  values are provided in Table 4.1.

From the specimens that were subjected to three-point bend tests at a loading frequency of 1 Hz, 20 out of 30 specimens reached run-out of 10,000 cycles (67%; Figure 4.14-a). The number of specimens that reached run-out at a loading frequency of 10 Hz was 8 out of 30 (27%; Figure 4.14-b). However, none of the samples reached run-out at loading frequencies of 50 or 100 Hz (Figures 4.14-c and 4.14-d). The numbers of cycles to failure were in the ranges of 5 to 217 and 6 to 374 at frequencies of 50 and 100 Hz, respectively.

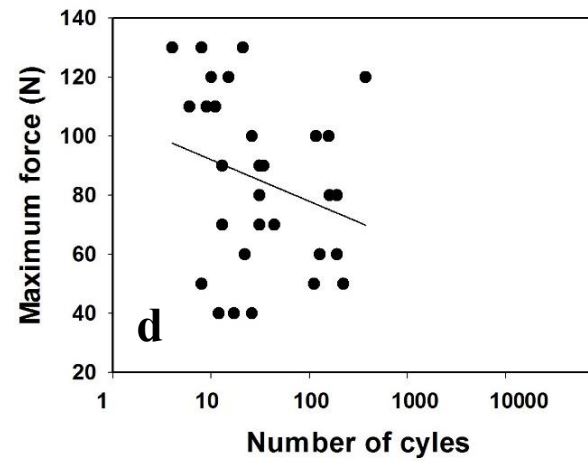
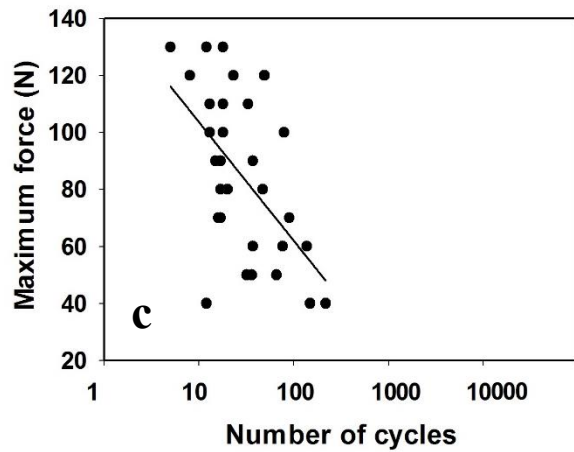
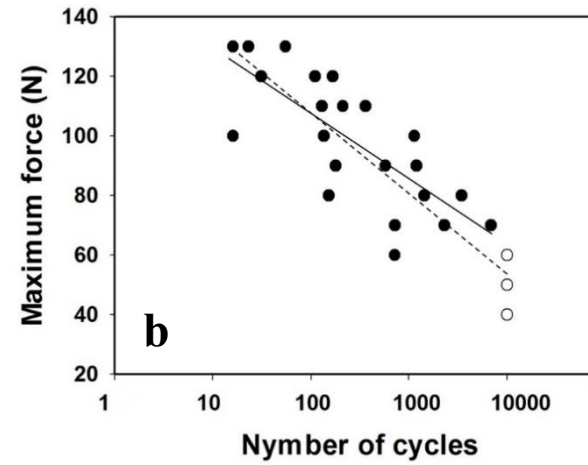
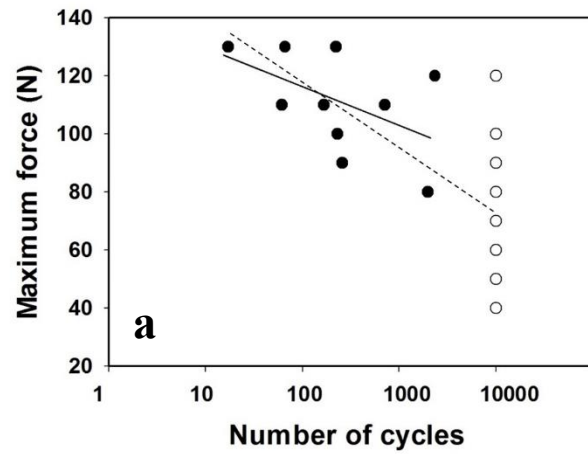


Figure 4.14. Maximum force plotted against the number of cycles to failure, with the number of cycles on a logarithmic scale (base 10) at loading frequencies of 1 Hz (a), 10 Hz (b), 50 Hz (c) and 100 Hz (d). Specimens that failed were plotted with (●) and specimens that reached run-out were plotted with (○). Details of the regression curves are included in Table 1. Solid curve fits indicate best curve fit for specimens that failed before 10,000 cycles were completed. Dashed curve fits also include the specimens that reached run-out.

Table 4.1. Constants from the curve fit correlations of Figure 4.14.

Curve fit	Loading frequency (Hz)	A (SE)	B (SE)	<i>P</i>	<i>R</i> <sup>2</sup>
(a)	1	-5.6 (3.4)	142 (19.0)	0.12	0.25
(a) <sup>*</sup>	1	-9.5 (2.0)	160 (17.2)	<0.001	0.42
(b)	10	-9.6 (1.8)	152 (10.5)	<0.001	0.77
(b) <sup>*</sup>	10	-12 (1.4)	162 (8.0)	<0.0001	0.80
(c)	50	-20 (4.6)	150 (14.5)	<0.001	0.52
(d)	100	-6 (4.2)	106 (15.6)	0.24	0.04

SE is the standard error of the coefficients *A* and *B*. *R*<sup>2</sup> is a squared correlation coefficient and defines how well the lines fit the data points. Asterisks (\*) above the curve fit names are for the details of regression curves including specimen samples that reached run-out at loading frequencies of 1 Hz (a) and 10 Hz (b). These curve fits were included as dashed lines in Figure 4.14.

Figure 4.15 shows a bar graph of the number of cycles against loading frequency. The decrease in the number of cycles when the loading frequency increased from gait relevant frequencies (1 and 10 Hz) to frequencies representative of RHS (50 and 100 Hz), can be observed clearly in this figure. The decrease in the number of cycles with increasing frequency can be observed in Figure 4.14 as loading frequency increased from 1 and 10 Hz to 50 and 100 Hz. The dependence of the maximum force on the number of cycles to failure is also clear at the frequencies of 10 and 50 Hz.

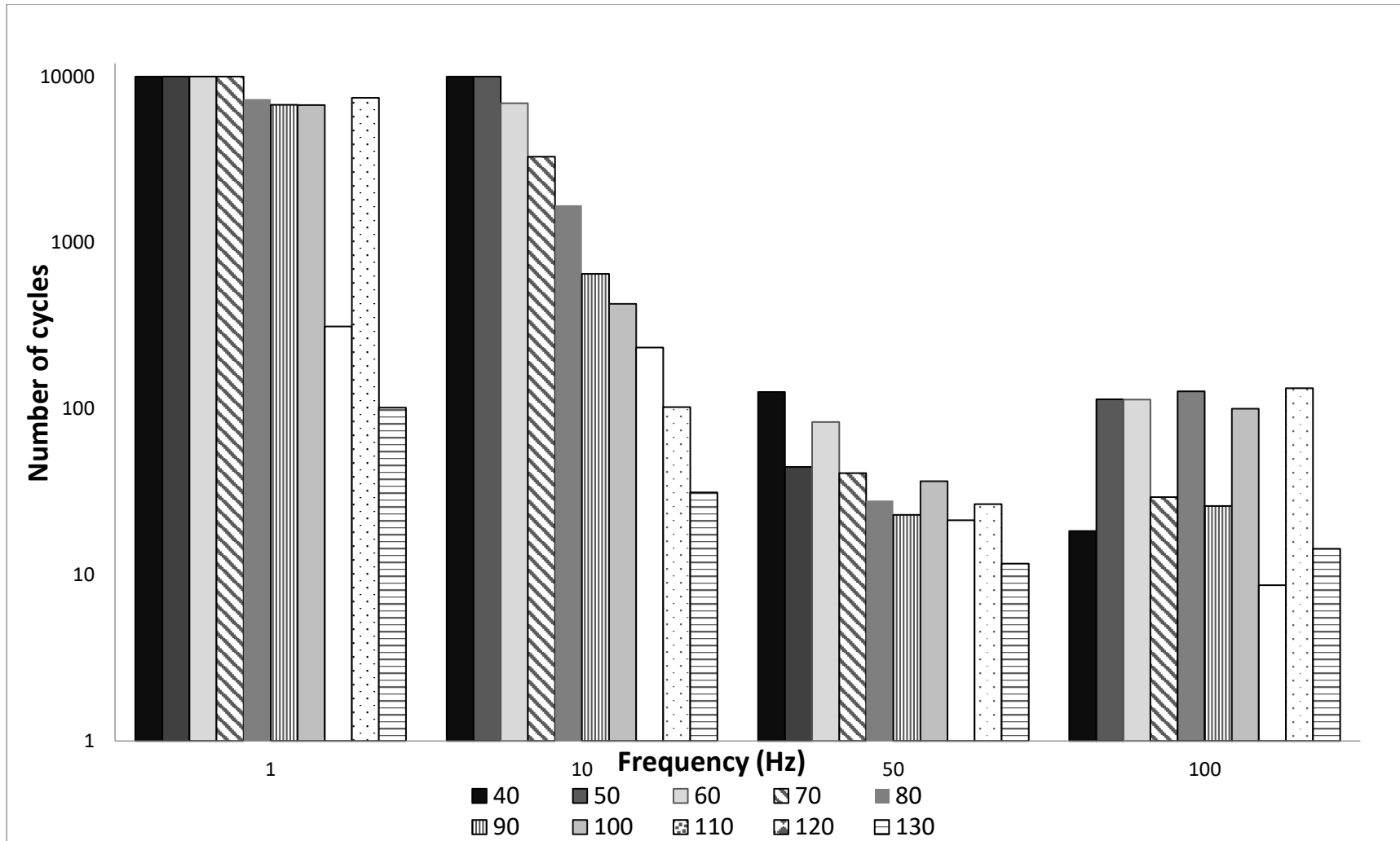


Figure 4.15. Mean number of cycles plotted against loading frequency, with the number of cycles on a logarithmic scale (base 10). Specimens that have reached run-out are included in the analysis of this plot as 10,000.

Images of two samples that reached run-out, which had been loaded between 6–60 N (maximum flexural stress of 23 MPa) at loading frequencies of 1 and 10 Hz are shown in Figures 4.16-a and Figure 4.16-b, respectively. Through qualitative assessments after each test, it was observed that four out of eight of the specimens, which reached run-out at a loading frequency of 10 Hz, had surface cracks at the centre of the specimens. However, no signs of damage were observed for specimens, which completed run-out, at a loading frequency of 1 Hz (Figure 4.16-a).



Figure 4.16. Cartilage surface crack observed on specimens that reached run-out at loading frequencies of 1 Hz and 10 Hz (a) Top view of the selected specimens after run-out was reached at a loading frequency of 1 Hz and (b) 10 Hz. Both specimens in these images were loaded between 6-60 N.

## 4.5. Discussion

This chapter has used sinusoidally varying compressive cyclic force to produce failure in cartilage-on-bone specimens under three-point bend tests. The number of cycles to failure decreased with increasing maximum force. The fatigue curves were statistically significant for loading frequencies of 10 and 50 Hz, however, this relationship was not found to be significant at loading frequencies of 1 and 100 Hz. Increasing the loading frequency resulted in increased failure for a given load. It

was found that 67% of the specimen samples reached run-out at a frequency of 1 Hz, 27% at 10 Hz, but 0% at frequencies of 50 and 100 Hz.

The effect of loading frequency on fatigue strength under bending has previously been carried out on bone only. An *in vitro* study of bovine cortical bone (Lafferty *et al.*, 1979) found that increasing the frequency of loading from 2 to 125 Hz decreased the number of cycles required to produce fracture by a factor of three to four. The suggestion was that the acceleration of fatigue strength tests with increasing loading frequency is a result of increased strain rate. Another similar study (Lafferty *et al.*, 1978) reported that the effect of loading frequency on bending fatigue strength of bone below 30 Hz is negligible. Loading frequencies above 30 Hz resulted in a shorter fatigue life. This is consistent with the present study where cartilage-on-bone specimen samples subjected to three-point bending decreased in the number of cycles to failure when frequency increased. The variation in the number of cycles to failure when frequency increased from 10 to 50 Hz is in agreement with Lafferty *et al.* (1978 & 1979).

The variation in the number of cycles to failure with increasing loading frequency from physiological (1 and 10 Hz) to loading frequencies representative of RHS (50 and 100 Hz), could correspond to before/after the glass transition in cartilage (Fulcher *et al.*, 2009). Articular cartilage has been shown to behave as a viscoelastic material from below gait relevant frequencies such as 0.01 to 1 Hz (Sadeghi *et al.*, 2015) up to a loading frequency of 92 Hz which is representative of RHS (Fulcher *et al.*, 2009). Fulcher *et al.* (2009) showed that storage modulus increased with increasing frequency, but it was asymptotic above 20 Hz, attributed to a glass transition, while the loss modulus remained constant. However, to date, there are no data available on the variation of mechanical properties of bone with increasing loading frequency. Therefore, it is difficult to distinguish between the effect of frequency on bone and cartilage as related to failure. However, previous studies (Lafferty *et al.*, 1978 & 1979) demonstrated that the resilience of bone decreased at frequencies above 30 Hz. Furthermore, the increased tendency of cartilage to fail above the

loading frequency of 20 Hz is also consistent with findings of this study that showed increasing the loading frequency may predispose both bone and cartilage to fracture.

Results from this study showed that increasing the loading frequency towards frequencies representative of RHS (50 and 100 Hz) resulted in more specimen failures. This is in agreement with a study on bovine cartilage under impact testing *in vitro* showing that when high rate impact was applied on the surface of cartilage-on-bone explants this caused severe damage to the tissue (Jeffrey *et al.*, 1995). Burgin *et al.* (2008) also showed that increased energy of deformation (per unit volume) occurred in cartilage with increased stress and strain rates.

This current study found that 10,000 loading cycles at a frequency of 10 Hz with an induced stress of 23 MPa caused cracks on half of the cartilage surfaces of specimen samples that reached 'run-out'. However, the same peak load and number of cycles at 1 Hz did not create any cracks. This observation is consistent with previous findings that following 10,000 cycles of compressive stress in the range of between ~ 3 and 7.5 MPa, through an indenter, produced surface cracks on cartilage in chapter 3. It should be noted that both this chapter and chapter 3 tested cartilage-on-bone. The physical behaviour of cartilage when on and off-bone was suggested to be different (Summers *et al.*, 2008) because of the restraining effects of the underlying bone to cartilage (Aspden *et al.*, 1990; Edelsten *et al.*, 2010). The cartilage-bone interface has been reported to predispose cartilage-on-bone specimen samples to the formation of cracks (Minns *et al.*, 1979). This interface is characterized by fibrils approximately perpendicular to the articular surface (Aspden *et al.*, 1981). Repetitive shear stresses developed at the cartilage-bone interface have been suggested to produce cracks and splits similar to that observed in osteoarthritic cartilage (Byers *et al.*, 1974) particularly under impulsive loading (Radin *et al.*, 1984 & 1978).

In this study, the number of cycles required to cause cartilage failure decreased with increasing maximum force. This is consistent with tensile fatigue failure for off-bone cartilage during cyclic loading (Kempson *et al.*, 1982 & 1991). Kempson *et al.* (1982) extrapolated from their data that 30 year-old patellar cartilage should not fail *in vivo* until the age of 200 years. The

results from Kempson *et al.* (1982 & 1991) showed that increasing the frequency used for cyclic loading lowered the tensile strength of cartilage. The same conclusion has been stated when tensile fatigue failure of cartilage, leading to the prediction of advancing failure with age under tensile loading (Weightman *et al.*, 1976 & 1978). Weightman *et al.* (1973) observed changes on the surface of the femoral head (identified using India ink) which occurred after 90,000 compression cycles. Another study of cartilage-on-bone also revealed that cyclic loading disrupts the specimen and the severity of the damage increased with increasing load and the number of cycles (Zimmerman *et al.*, 1988).

Flexural stresses of cyclic three-point bend tests in this study were calculated, using equation 4.1, to be in the range 15 to 50 MPa. Stresses used in this study are comparable to a previous cyclic compressive study of cartilage-on-bone specimen samples (Kerin *et al.*, 1998), which reported that the mean fracture strength of bovine articular cartilage was 35.7 MPa. Cyclic tensile loading studies, instead, have found experimental damage to occur in human cartilage with the number of cycles up to 1.5 million and stresses in the range of 1–3 MPa (Bellucci *et al.*, 2001) or 97,200 cycles under stresses that averaged 3.2 MPa *in vitro* (McCormack *et al.*, 1998). The difference in the results could be explained by the fact that the strength measured in flexure is usually higher than the strength measured in tension (Turner *et al.*, 1983; Bellucci *et al.*, 2001). Lower failure stresses for cartilage have also been reported in the lower region of 8 MPa under static compressive loading (Fick *et al.*, 2011 & 2012); however, failure was defined as merely large cracks on the surface of the cartilage not failure of the full cartilage depth and its underlying subchondral bone.

Articular cartilage damage, in the form of fissures and fragments, has been observed clinically (Kennedy *et al.*, 1966) and it is similar to those produced experimentally by single and repetitive impact loads (Johnson-Nurse *et al.*, 1985). A threshold of 15-25 MPa was reported to cause subchondral bone fracture and surface fissures on the cartilage surface (Torzilli *et al.*, 1999). None of these studies have assessed the influence of the loading frequency of impacts on the failure

stresses reported. Other single impact studies (Borelli *et al.*, 1997; Flachsmann *et al.*, 1995) have reported the fracture threshold stress of cartilage-on-bone specimens to be 50 MPa, consistent with the largest maximum stress used in this study.

There are known limitations with the three-point bending test of cartilage on-bone tissue samples such as variation in beam thickness (Mente *et al.*, 1994), although it was assumed that cartilage-on-bone specimens used in this study were homogeneous, linear-elastic and isotropic (Hargrave-Thomas *et al.*, 2015). Bone volume has been found to affect the failure of beam shaped specimens which are similar to the dimensions of tissue samples in this study (Bigley *et al.*, 2008). That is another reason that cartilage-on-bone samples were only chosen from a central region and were dissected next to each other in order to keep the bone volume the same as described in chapter 3. Another limitation of this study was the stress concentration due to the contact associated with three-point bending configuration (Draper *et al.*, 2003). However, the aim of this chapter was to produce and compare the failure in cartilage-on-bone specimens at different frequencies and not to measure or identify the stresses that cause failure. Discontinuity in stiffness through the depth of cartilage-on-bone specimens could also be considered as a limitation under three-point bending. This is because the underlying bone is much stiffer than the articular cartilage layer (Mente *et al.*, 1994). There is also an increasing material stiffening from the calcified cartilage to the superficial zone of the cartilage layer (Hargrave-Thomas *et al.*, 2015) that could affect the failure of cartilage-on-bone specimens under bending. However, the aim of this chapter was not to investigate the effect of different variations of cartilage-on-bone specimens on the failure such specimens, but to investigate the difference in the failure of cartilage-on-bone specimens at different frequencies.

Crack growth through the depth of cartilage-on-bone specimens has previously been observed in a single edge notch test under tension to investigate thickness effects in cartilage (Adams *et al.*, 2003). However, Adams *et al.* (2003) used a rate of 0.2 mm/s which would correspond to a loading frequency of below 1 Hz; furthermore, this study measured fracture toughness from bone to cartilage. Results from this chapter demonstrated that growth of an initial

crack could not be measured over a specific number of cycles under three-point bending as failure occurs instantly. However, there might be other strategies to measure crack growth in articular cartilage at different frequencies of loading. Crack growth through cartilage off-bone at different frequencies is presented in the next chapter.

#### **4.6. Chapter summary**

During bending the number of cycles to failure decreased with increased maximum force at all loading frequencies. Independent of load, the number of cycles to failure under bending decreased when the loading frequency increased from normal and above gait (1 and 10 Hz) to loading frequencies representative of RHS rise times (50 and 100 Hz). Furthermore, the proportion of specimen samples reaching run-out of 10,000 cycles under three-point bending decreased from 67% and 27% at physiological loading frequencies of 1 and 10 Hz, respectively, to 0% at 50 and 100 Hz. Therefore, an increased loading frequency predisposes articular cartilage on-bone to damage during bending. The next chapter investigates the propagation of an initial crack in cartilage specimens at different frequencies.

## **5. The effect of frequency on crack growth in articular cartilage under tension**

### **5.1 Introduction**

In this chapter cyclic tensile strains were used to induce crack propagation in cartilage specimens. The aim of this chapter was to determine the effect of the variation of loading frequencies associated with gait (1 Hz), above gait (10 Hz) and frequencies which can be used to represent RHS rise times (100 Hz) on crack growth in bovine articular cartilage specimens.

Most tensile testing of cartilage mechanical failure has been undertaken through quantifying the tensile strength of cartilage tissue (Akizuki *et al.*, 1986; Kempson *et al.*, 1980) or uniaxial tensile testing of cartilage samples (Roberts *et al.*, 1986; Schmidt *et al.*, 1990). These studies have reported that the ability of cartilage to resist failure decreases under cyclic loading. Furthermore, cartilage fails by crack formation and fibrillation (Clark *et al.*, 1997; Lewis *et al.*, 2001). Qualitative measurements of the crack growth in slices of cartilage samples have introduced the concept of cartilage fracture as an important process in the degeneration of cartilage (Broom *et al.*, 1984 & 1986). Previous studies (Chin-Purcell *et al.*, 1996; Stok *et al.*, 2003) have also suggested methods to measure the fracture toughness of cartilage. These studies came to the conclusion that cartilage failure *in vivo* involves the progressive growth of defects.

## 5.2 Material and methods

### 5.2.1 General methods

Ten bovine shoulder joints, aged between 18 and 24 months, were obtained from [REDACTED]. Humeral heads were dissected using the methods described in section 3.2.1. Four rectangular 40 × 20 mm specimens, which comprised of both bone and cartilage, were cut using a saw from the central load-bearing region of each humeral head (Canal *et al.*, 2008) (Figure 5.1-a). The underlying bone was approximately 60 mm in thickness and was used to grip the specimens to obtain the cartilage slices for testing (Figure 5.1-b, Figure 5.1-c).

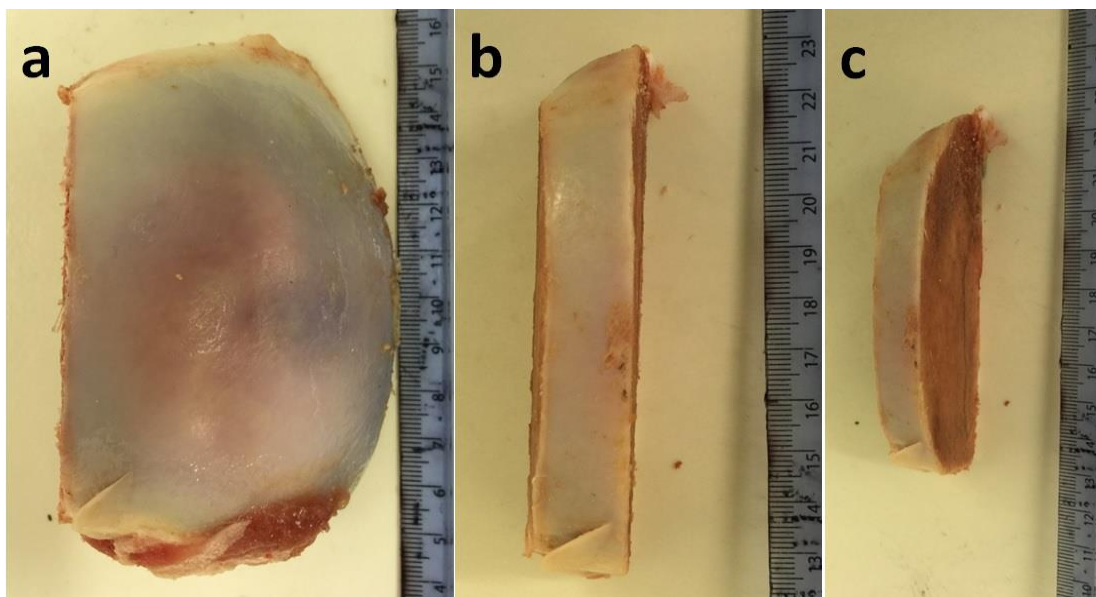


Figure 5.1. Cartilage-on-bone slices (a) Sample image taken from the top view of humeral head removed from the shoulder joint (b) the rectangular cartilage-on-bone specimens obtained from the central region of the humeral head (c) side view of the cartilage-on-bone specimen. Scale bar units are in mm.

A mandoline slicer (Mastrad inc., Paris, France) with a 1 mm gap was used to remove cartilage slices while it was still attached to the bone (Figure 5.2-a) (Adams *et al.*, 2004). Cartilage specimens had a maximum of 1 mm depth from the articulating surface towards the bone (Figure

5.2-b). In total 40 test specimens, consisting only of cartilage, were obtained from ten humeral heads.

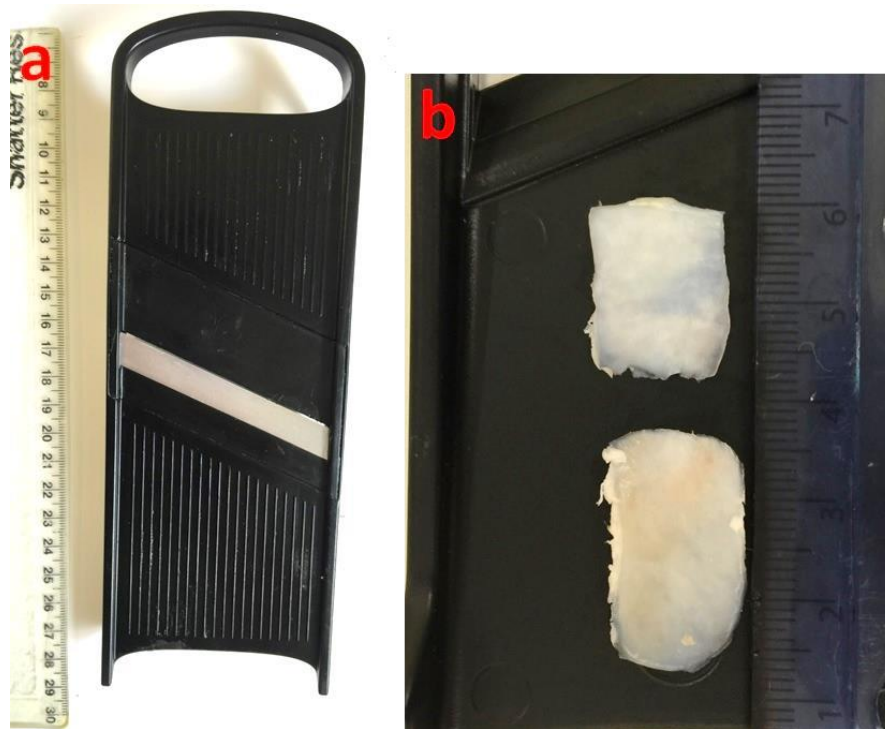


Figure 5.2. Cartilage specimen preparation. a) Mandoline slicer used to remove cartilage sheets from cartilage-on-bone specimens from Figure 5.1. b) Sample image taken from two cartilage specimens with 1 mm depth from the articular surface.

The final cartilage specimens for testing were then produced with dimensions of  $20 \times 10$  mm using a 15 blade medical scalpel (Swann-Morton, Sheffield, UK). A digital Vernier calliper (Fisher Scientific, Leicestershire, UK) was used to measure and highlight an area of  $10 \times 10$  mm and a 2.26 mm crack was cut into the middle of the specimen using a scalpel blade (Figure 5.3-a, 5.3-b).

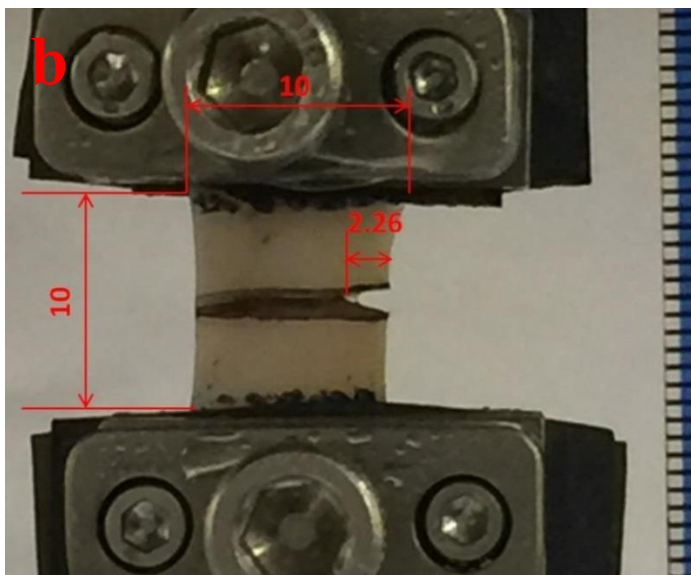
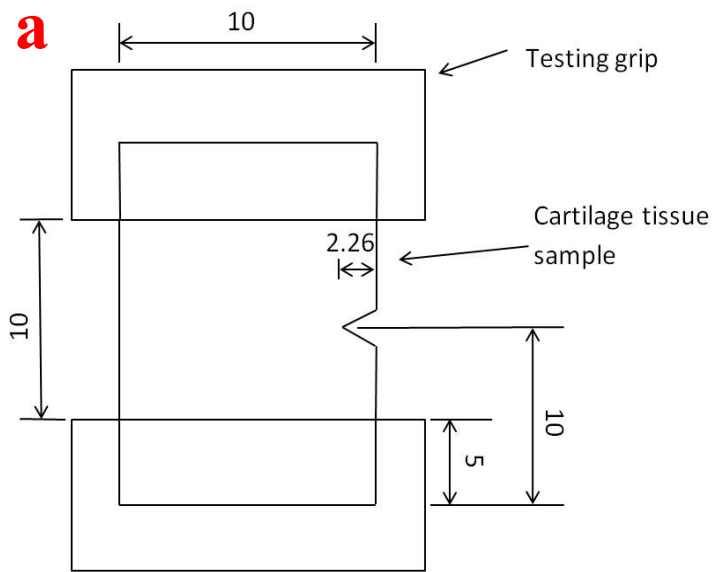


Figure 5.3. Tensile testing configuration. (a) Dimensions of the cartilage specimen (b) Cartilage specimen placed in grips, ready for testing. All units are in mm.

Testing was performed using a Bose ElectroForce 3200 testing machine (Bose corporation, Minnesota, USA; now, TA instruments, New Castle, DE, USA) running WinTest 4.1 Software (Figure 5.4-a). Two custom-made grips were attached to the testing machine. Emery paper (120 grit) was fixed to the grips (McCormack *et al.*, 1998) and the cartilage specimen was secured by

The effect of frequency on crack growth in articular cartilage under tension

the tightening of screws (Figure 5.4-b). A preload of 0.2 N was applied to the tissue specimen to prevent rotation about their length. The length of the crack was based on the work of McCormack *et al.* (1998), where the initial crack length was 22.6 % of the specimen width.

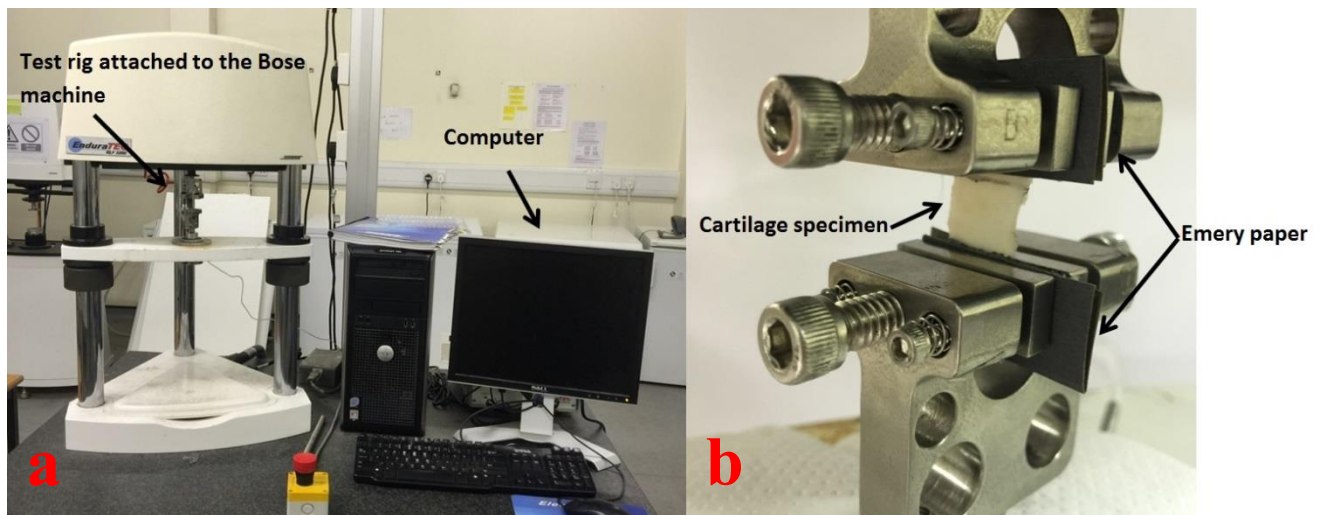


Figure 5.4. Cartilage testing in tension (a) Bose ELF 3200 testing machine used to test cartilage specimens in tension (b) Cartilage specimen secured in the testing grips with the aid of emery paper.

## 5.2.2 Preliminary tensile experiments

To evaluate the forces during the extension of the initial crack in a cartilage specimen four ramp tests were conducted on four separate cartilage specimens with dimensions described in section 5.3.1. The actuator of the testing machine was set to apply a tensile strain at a rate of 0.02 mm/s. Testing continued until a maximum displacement of 5 mm had been applied (the length of the cartilage specimen between the grips was 10 mm) not until the specimen failed. Load and displacement were recorded throughout the tests.

Figure 5.5 shows a graph of force against displacement of one of tested cartilage specimens. Out of the four specimens tested, the results of one were rejected as failure in the specimen occurred near the testing grips. The maximum force of the three remaining cartilage specimens was  $22.6 \pm 8.6$  N (mean  $\pm$  SD) corresponding to a maximum displacement of  $4.1 \pm 1.5$  mm. The 2.26 mm initial crack in cartilage specimens grew to  $3.4 \pm 0.6$  mm.

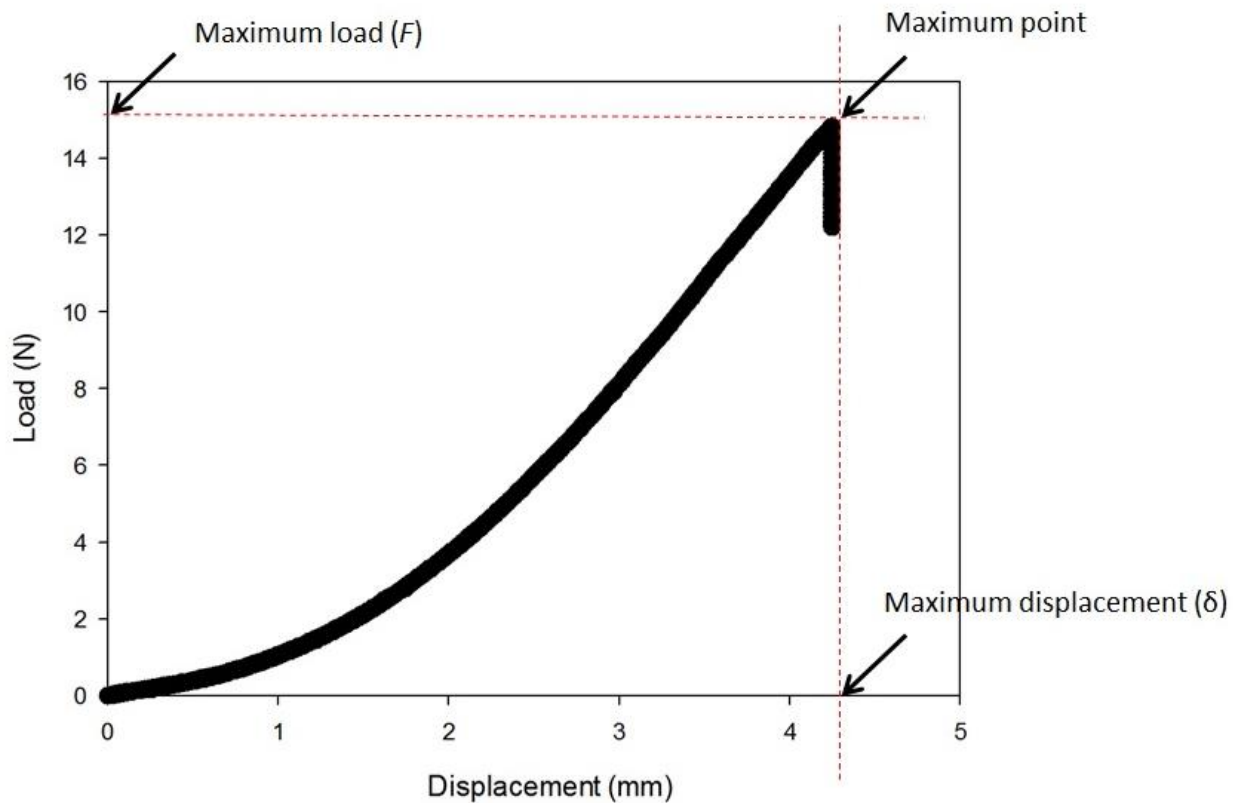


Figure 5.5 Load against displacement of a cartilage specimen under tension. Failure occurred at the load ( $F$ ) of 14.8 N corresponding to the failure displacement ( $\delta$ ) of 4.3 mm. The initial crack in this cartilage specimen extended from 2.26 mm to 2.39 mm during this ramp test.

In order to determine whether crack growth could be achieved under cyclic tensile strains, the actuator of the testing machine was set to move in displacement control to apply a sinusoidally varying tensile strain to the cartilage specimen. After clamping the cartilage specimen in the grips the height of the specimen was 10 mm. A minimum and a maximum displacement of 1 and 2 mm was applied, respectively. Hence applying a minimum strain of 10 % and a maximum of 20 % of the specimen length. The maximum displacement was chosen as 50% of the mean maximum displacement (4.1 mm) measured in section 5.2.3 consistent with the range used by Leslie *et al.* (2008). Testing was undertaken at frequencies of 1, 10 and 100 Hz, which involved applying 10,000 cycles at each frequency on three separate cartilage specimen. As a sinusoidally varying tensile strain was applied to the cartilage specimen the force acting through the specimen (which was also

approximately sinusoidal) was measured. If slippage had occurred, there would have been a drop in the peak force, but this did not happen.

Figure 5.6 shows three cartilage specimens after being subjected to 10,000 sinusoidal cycles of loading. The initial 2.26 mm crack grew up to 3.5, 4.5 and 4 mm at frequencies of 1, 10 and 100 Hz, respectively. These results from this section indicated that the initial crack could grow when subjected to cyclic strains and this growth varies at different frequencies. In the following section of this chapter investigation focused on whether the growth of an initial crack in cartilage specimens could be measured over a specific number of cycles. The effect of cyclic testing was more evident in the specimen tested at a frequency of 1 Hz.

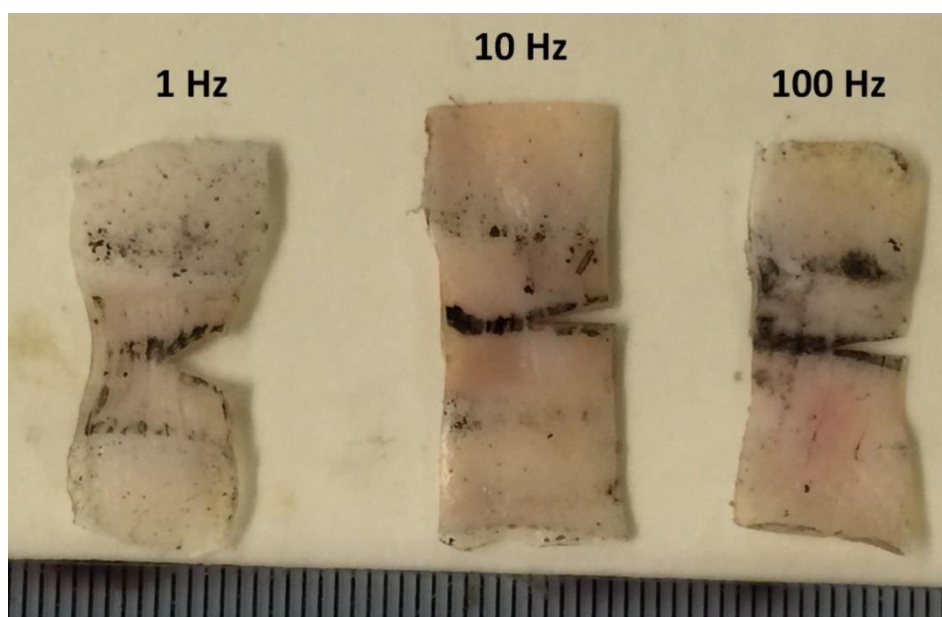


Figure 5.6 Cartilage specimens after being subjected to 10,000 cycles of continuous tensile strain. 2.26 mm initial crack extended up to 3.1, 4.2 and 4 mm at loading frequencies of 1, 10 and 100 Hz, respectively.

### 5.2.3 Crack growth experiments

The actuator of the testing machine applied a sinusoidally varying tensile strain to the tissue specimen with a minimum of 10 % and a maximum of 20 % of the specimen length (10 mm) for 10,000 cycles. A block command function was used, to initially displace specimens to 15% of their gauge length; specimens were then held in this position for 5 seconds while an image was acquired. Images were taken using an Apple iPhone 6 Plus (Apple Inc, California, USA) operated under iOS 8 with Sony Exmor RS camera (8 megapixels, 1.5 focus pixels). A scale-bar was included in each image, positioned in the field of view. Images were acquired at 0, 20, 50, 100, 500, 1,000, 5,000 and 10,000 cycles. Specimens were tested at 1 Hz, 10 Hz or 100 Hz; these test frequencies correspond to normal, above normal and up to RHS rise times, respectively (Fulcher *et al.*, 2009). For the calculation of 95 % confidence intervals, the number of independent observations ( $n$ ) was taken as 10 for each loading frequency. Specimens obtained from different animals have been assumed to produce independent observations. (Ranstam *et al.*, 2012) as described in chapter 3. To prevent dehydration, the tissue specimens were irrigated with Ringer's solution every 600 cycles. Therefore, 480 image analysis measurements were obtained in total. Regression analysis was undertaken using SigmaPlot (version 13.0, SYSTAT, San Jose, CA, USA). The curve fit relationship was considered significant if  $p < 0.05$ .

## 5.2.4 Crack growth analysis

Images were analysed using Image J software (version 1.5, Rasband, W.S., U. S. National Institutes of Health, Bethesda, Maryland, USA). For each image, measurements were calibrated using the methods described in section 3.2.2. Lines were drawn manually along the crack length ( $c$ ) and the side without the pre-existing crack relative to its horizontal position ( $h$ ) for each image (Figure 5.7). The software was then used to measure the crack length (in mm) while the resolution of the software was 0.1 mm using the methods as described in section 3.3.7. The crack growth ( $\delta c$ ) was calculated from:

$$\delta c = c - c_0 \quad (5.1)$$

where  $c$  is the total crack length and  $c_0$  is the originally inserted crack length.

The necking growth ( $\delta h$ ) was calculated from:

$$\delta h = h - h_0 \quad (5.2)$$

where  $h$  is the necking and  $h_0$  is the initial deformation of the side without pre-existing crack relative to its horizontal position. The crack length and necking measurements were obtained from each image.

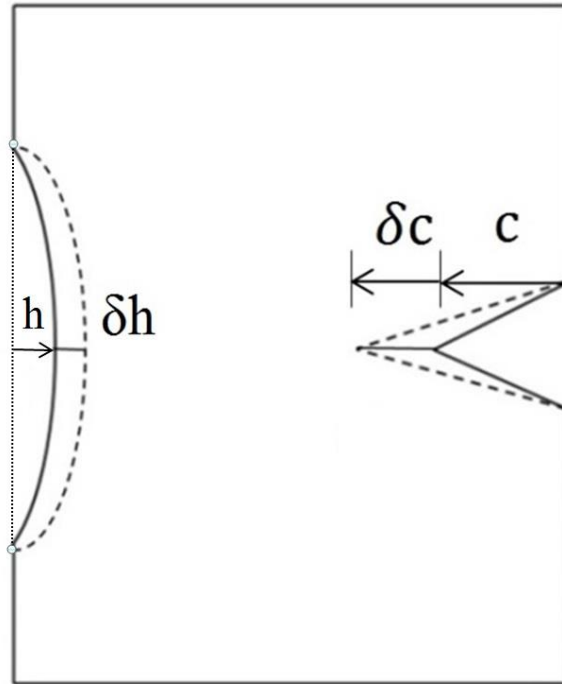


Figure 5.7. Schematic of the cartilage specimen. Crack growth ( $\delta c$ ) and necking ( $\delta h$ ) were measured for each image acquired from cartilage specimens at several stoppages during cyclic testing.

### 5.2.5 Crack growth experiment results

Images from three cartilage specimens, tested at 1, 10 and 100 Hz, with varying number of cycles are shown in Figure 5.8 and it can be observed that higher frequency strains caused a greater crack growth.

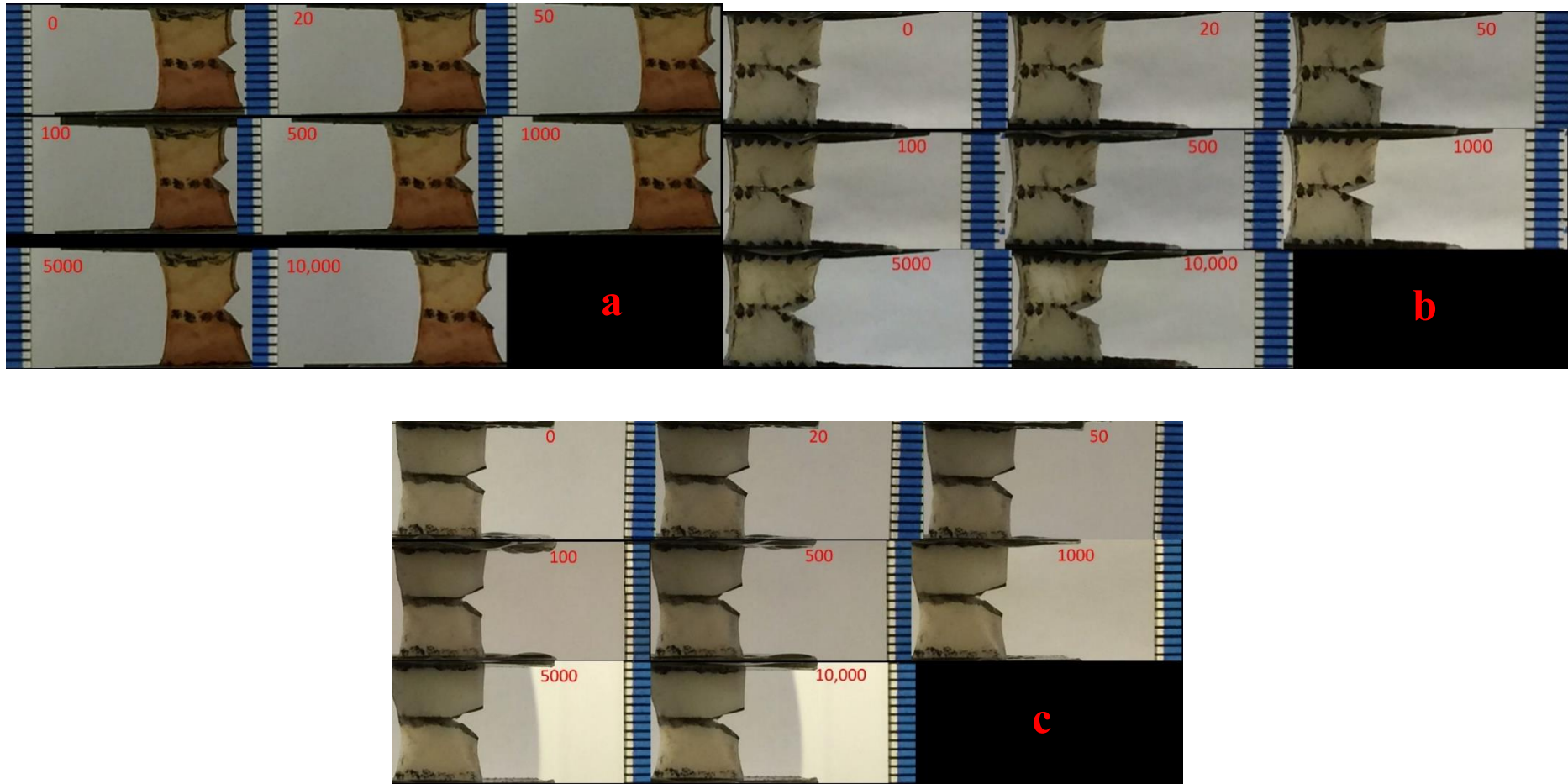


Figure 5.8 Specimen images taken at 0, 20, 50, 100, 500, 1,000, 5,000 and 10,000 cycle. Each specimen was subjected to a maximum strain of 20 % undertaken at loading frequencies of a) 1 Hz, b) 10 Hz and c) 100 Hz. Increasing the loading frequency caused a higher crack growth in cartilage specimens.

Crack growth rate was found to increase with an increasing number of loading cycles for individual cartilage specimens (Figure 5.9). This was also the case when the mean crack growth of 10 specimens (per frequency) was plotted against the number of cycles (Figure 5.10). Figure 5.10 shows that mean crack growth rate increased significantly ( $p < 0.05$ ) with increasing number of cycles for all tested loading frequencies. Crack growth values at a frequency of 100 Hz were always larger compared to the crack growth at a frequency of 1 or 10 Hz. The trends for the crack growth ( $\delta c$ ) against number of cycles ( $N$ ) were described by the logarithmic curve fit

$$\delta c = A(\ln(N)) + B \quad (5.3)$$

where  $A$  and  $B$  are constants and  $N$  is number of cycles (Table 5.1). Gradients of the curve fits were found to increase from 0.08 to 0.14 mm at frequencies of 1 and 100 Hz, respectively.

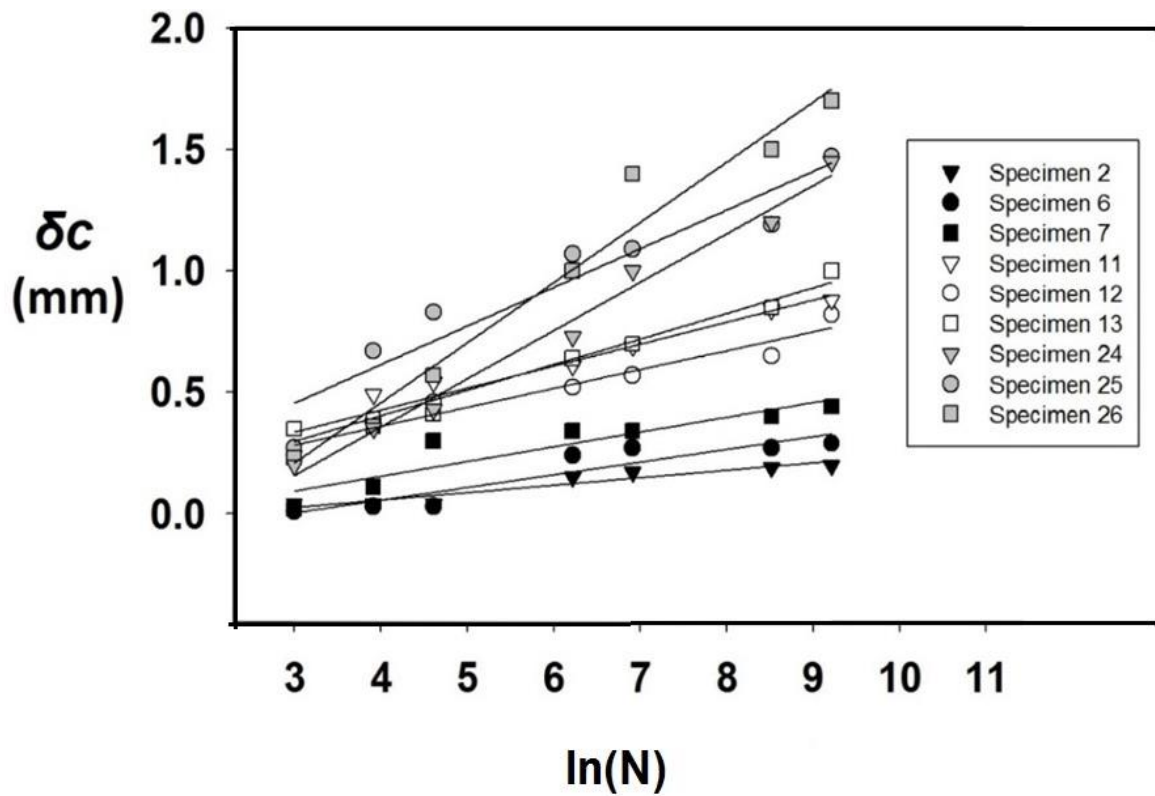


Figure 5.9. Individual specimen crack growth ( $\delta c$ ) plotted against the natural logarithm of number of cycles ( $N$ ) at the three tested frequencies. Three specimens were selected from each loading frequency. Cartilage specimens 2, 6 and 7 were tested at a frequency of 1 Hz (in black) specimens 11, 12 and 13 at 10 Hz (in white) and specimens 24, 25 and 26 were tested at 100 Hz (in gray).

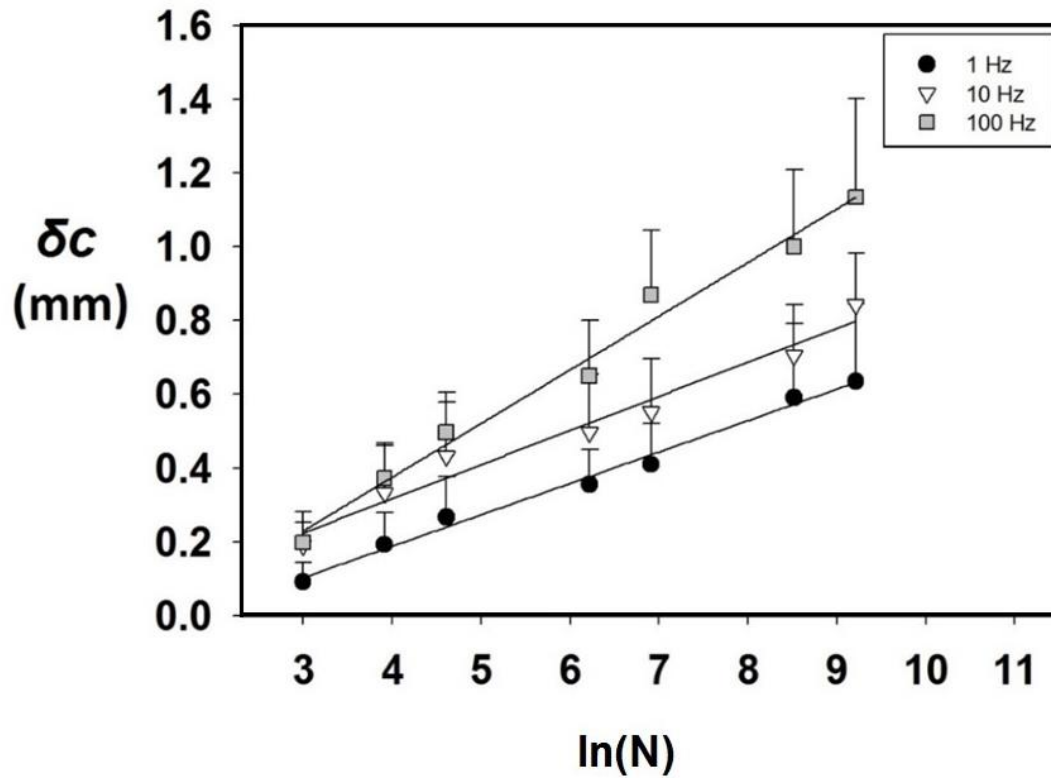


Figure 5.10. Mean crack growth ( $\delta c$ ) against the natural logarithm of the number of cycles ( $N$ ). Logarithmic curves (equation 5.3) fitted the data points well. Error bars represent 95% confidence intervals for the samples. For clarity only positive error bars are include.

Table 5.1. Details of the constants from the mean crack growth against number of cycles curve fits (Figure 5.10). Units for A and B are in mm.

Frequency (Hz)	<i>A</i> (SE)	<i>B</i> (SE)	<i>R</i> <sup>2</sup>
1	0.08 (0.003)	-0.15 (0.02)	0.98
10	0.09 (0.007)	-0.05 (0.04)	0.94
100	0.14 (0.008)	-0.2 (0.05)	0.90

The correlation between crack growth and number of cycles is described by logarithmic curve fits for each loading frequency. Mean crack growth against number of cycles curve fits were statistically significant ( $p < 0.001$ ) for all frequencies. *SE* is the standard error of the coefficients *A* and *B*. *R*<sup>2</sup> is a squared correlation coefficient and shows how well the line fits the data points.

All ten specimens were found to undergo extensive necking during testing at a frequency of 1 Hz (Figure 5.8-a, Figure 5.11). However, necking occurred less compared to the specimens tested at 10 or 100 Hz (Figure 5.8-b, Figure 5.8-c). Necking was also found to progress continually with increased number of cycles from qualitative observations (Figure 5.12). Figure 5.12 shows that mean necking ( $\delta h$ ) increased with increasing number of cycles. However, this value was always higher at a frequency of 1 Hz as opposed to frequencies of 10 and 100 Hz. The trends for mean necking ( $\delta h$ ) against number of cycles ( $N$ ) were described using the logarithmic curve fit:

$$\delta h = C(\ln(N)) + D \quad (5.4)$$

where  $C$  and  $D$  are constants and  $N$  is number of cycles (Table 5.2).

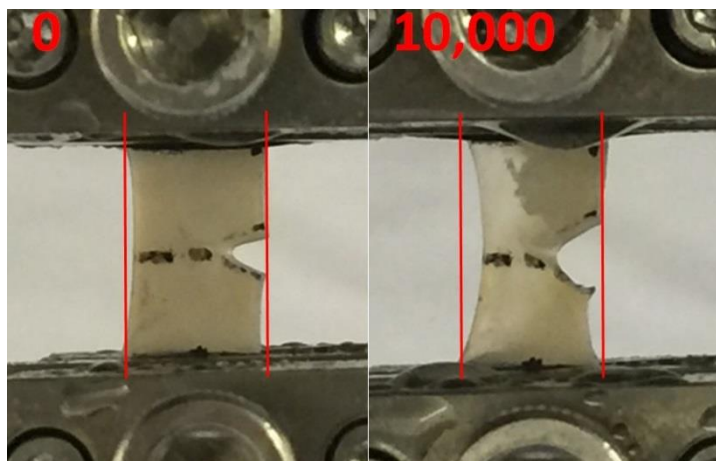


Figure 5.11. Sample images taken from cartilage specimen number 8, tested at a frequency of 1 Hz at the initial testing position and following 10,000 cycles. Vertical lines were inserted in each image in order to show the displacement of the sides of the cartilage specimen relative to their initial position.

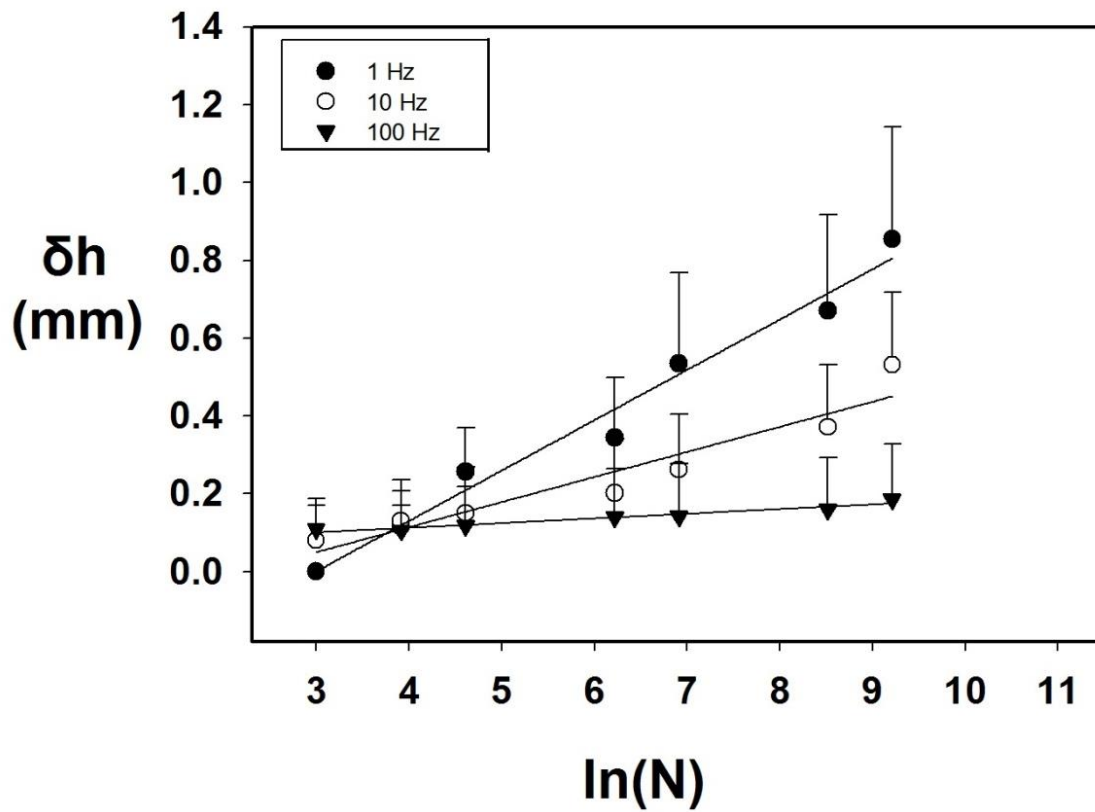


Figure 5.12. Mean necking ( $\delta h$ ) against the natural logarithm of the number of cycles ( $N$ ). Logarithmic curves (equation 5.4) fitted the data points well. The  $R^2$  and  $p$  values of this figure are included in table 2. Error bars represent 95% confidence intervals for the samples. For clarity only positive error bars are include.

Table 5.2. Details of the constants from the mean necking against number of cycles curve fits (Figure 5.12). Units for  $C$  and  $D$  are in mm.

Frequency (Hz)	$C$ (SE)	$D$ (SE)	$R^2$
1	0.12 (0.008)	-0.38 (0.05)	0.97
10	0.06 (0.009)	-0.14 (0.05)	0.9
100	0.01 (0.001)	0.06 (0.008)	0.94

The correlation between mean necking and number of cycles is described by logarithmic curve fits for each loading frequency. Mean necking against number of cycles curve fits were statistically significant ( $p < 0.001$ ) for all frequencies. SE is the standard error of the coefficients  $C$  and  $D$ .  $R^2$  is a squared correlation coefficient and shows how well the line fits the data points.

### 5.3. Discussion

The results from this chapter demonstrate how pre-existing cracks in articular cartilage samples grow when subjected to cyclic strains at different frequencies. In the current chapter, crack growth was found to increase with an increasing number of cycles. Crack growth rate was also found to be greater at higher frequencies. This is a new observation because controlled crack growth experiments have not been used to explain the influence of frequency on the growth of pre-existing cracks in cartilage off-bone samples under tension. Experimental data previously obtained from cartilage-on-bone samples have shown that pre-existing cracks can grow under tension (Stoke *et al.*, 2003 & 2007). In this chapter, the crack length increased with increasing frequency between 1, 10 and 100 Hz, independent of load. Counter wise, more necking was observed at a frequency of 1 Hz compared to the necking at frequencies of 10 or 100 Hz.

In the present chapter, higher crack growth rate of specimen samples occurred at higher frequencies. This could correspond to cartilage approaching a glass transition when subjected to dynamic loading at frequencies above 10 Hz. Cartilage changes from a soft tissue to a “glass-like” (more brittle) material (Fulcher *et al.*, 2009) that could result in the fast growth of cracks in cartilage samples when subjected to frequencies representative of RHS rise times (Kelly *et al.*, 1996). Other studies (Pearson & Espino, 2013; Sadeghi *et al.*, 2015; Fulcher *et al.*, 2009) have also suggested that there might be an increase in cartilage damage with increasing loading frequency. This was suggested through comparing the ability of the tissue to store energy (storage modulus) and to dissipate energy (loss modulus) over a broad range of frequencies (0.001-92 Hz). The suggestion was consistent with the reported increase in energy under impact loading *in vitro* which was suggested to cause cartilage fracture (Jeffrey *et al.*, 2006; Verteramo *et al.*, 2007). Further, measurements of hysteresis (energy dissipation) following drop-tower tests showed that hysteresis could increase with increased loading velocity (Edelsten *et al.*, 2010).

In the current chapter, it was found that specimens subjected to tensile strain at a frequency of 1 Hz underwent necking, while this effect happened to a lesser degree for specimens tested at frequencies of 10 or 100 Hz. Necking represents a lateral displacement, of the intact side of the cartilage, relative to its initial length along the axis of loading. This observation has previously been reported in full thickness cartilage samples following tensile loading (Stok *et al.*, 2003 & 2007). These studies suggested that as cartilage is loaded in tension, the collagen fibrils within the solid matrix align and stretch along the axis of loading. Such necking might be due to the pull of the collagen fibers in response to the tensile strain. However, this effect is more evident in samples tested at 1 Hz as opposed to 100 Hz. Collagen is arranged to provide reinforcement to a highly hydrated proteoglycan gel in cartilage tissue (Aspden *et al.*, 1981). Viscoelastic properties of articular cartilage are associated with the stress transfer mechanism during gel-collagen interaction (Goh *et al.*, 2010; Aspden *et al.*, 1994). Thus, the difference in the behaviour of cartilage samples at the tested frequencies could be the consequence of the variation of the interactions between the structural components of the tissue. This could also be related to before/after glass transition (Fulcher *et al.*, 2009). More necking of the specimens at the frequency of 1 Hz could also suggest that the tissue could flow more readily compared to the glass-like behaviour at the frequency of 100 Hz.

Flachsmann *et al.* (2006) subjected cartilage-on-bone samples to compression using an indenter (8 mm diameter). They found that introducing cracks about 1 mm in length in the superficial layer of cartilage reduced the compressive strength to less than half of the value measured from samples without cracks. Increased compression at the edge of a surface defect (Braman *et al.*, 2005) as well as increased cartilage failure in a joint with a pre-existing defect has also been described in the literature (Hollander *et al.*, 1995; Cicuttini *et al.*, 2005). These findings are in agreement with the current study that showed a pre-existing crack could grow in a cartilage specimen subjected to cyclic strains, which may lead to the complete failure of the specimen. Quinn *et al.* (2001) subjected cartilage-on-bone samples to impact loading at varying strain rates between

$3 \times 10^{-5}$  and  $0.7 \text{ s}^{-1}$ , to maximum stresses in the range 3.5 to 14 MPa, respectively. At the higher strain rates tissue cracks were observed particularly near the superficial layer. However, at lower strain rates no signs of damage were observed. This is consistent with the findings of this chapter that showed crack growth rate is higher at higher loading frequencies. However, the results from Flachsmann *et al.* (2006) and Quin *et al.* (2001) were of cartilage-on-bone samples and tested in compression.

Most studies on the tensile failure of cartilage (Weightman *et al.*, 1976 & 1978; Kempson *et al.*, 1982 & 1991; Mc Cormack *et al.*, 1998) have been concerned with variations in fatigue properties among joints, the effects of repeated load, and age. The tensile loading of human cartilage samples *in vitro* was shown to cause surface fibrillation (Weightman *et al.*, 1976). Cartilage samples from the femoral head were subjected to cyclic tensile stress by Weightman *et al.* (1978). They found that the resistance of the specimen samples decreased with age. Other studies (Kempson *et al.*, 1982 & 1991) documented changes including a decrease in tensile strength and stiffness of cartilage tissue which might make the tissue more predisposed to injury and development of degeneration. While McCormack *et al.* (1998) found that a sufficient number of compressive load cycles under a mean stress of 3.2 MPa, applied to the cartilage surface *in situ*, caused a decrease in tensile strength. After 64,800 cycles of compressive loading their results showed no change in the tensile strength of cartilage, but after 97,200 cycles, tensile strength was reduced significantly. In chapter 3, subjecting bovine cartilage to 10,000 cycles of maximum stress of 4.2 MPa at frequency of 10 Hz and a lower stress of 2.8 MPa but at a higher frequency of 100 Hz, produced cracks on the cartilage surface. This means that at 100 Hz less force is needed to cause cartilage surface damage compared to 10 Hz. In the current chapter the number of cycles was kept constant to understand the effect of altering the loading frequency on crack growth while specimens were subjected to 20% of their maximum tensile strain. Maximum cartilage strains *in vivo* were measured to be 12% occurring when the knee joint is undergoing shear stresses (Chan *et al.*, 2016).

The current study demonstrates that the frequency at which a joint is loaded is an additional factor when assessing crack growth and cartilage failure. Previous studies have shown that high tensile stresses are generated in the knee in flexion (Minns *et al.*, 1979) and these stresses arise in the surrounding regions of the loaded surfaces in contact in the joint (Kelly *et al.*, 1996). Tensile failure of cartilage has been of interest, because it was suggested that vertical cracks in cartilage were initiated by tensile stresses on the articular surface (Eberhardt *et al.*, 1991). Fracture mechanics of cartilage have been studied extensively (Chin-Purcell *et al.*, 1996; Stok *et al.*, 2003 & 2007) by measuring fracture toughness, or the ability of the cartilage to resist crack growth. Stok *et al.* (2003 & 2007) and Chin-Purcell *et al.* (1996) studied crack growth in cartilage with tensile loading, while Wang *et al.* (2001) investigated the strain distribution at compressive loading. Chin-Purcell *et al.* (1996) measured the fracture toughness of cartilage using energy based methods. This study demonstrated that cartilage quickly distributes loads via crack growth when subjected to instantaneous loads to avoid stress concentration.

Stok *et al.* (2003) applied tensile loading at both ends of full thickness cartilage off-bone tissue samples in a single edge notch test. Furthermore, they analysed crack growth at varying rates (1.5, 3.0 and 4.5 mm/min) and found that the energy measured during crack growth did not vary significantly. However, loading rates used by Stoke *et al.*, (2003) might lead to very low strain rates i.e. below 1 Hz. They suggested that it was the structural variations between the diverse zones of the tissue, rather than the rate of loading, that mainly determined the characteristics of fracture in cartilage. However, results from this chapter suggest that when an initial crack grows inside a cartilage specimen, the mechanism by which collagen-gel interaction occurs varies with frequency and hence so do mechanisms of energy dissipation.

An acknowledged limitation of Stoke *et al.* (2003 & 2007) is that the superficial cartilage layer appears to have greater resistance to crack growth than the middle or deep zones of the tissue (Stok *et al.*, 2007). However, Broom *et al.* (1984) reported that cracks perpendicular to the cartilage surface were easier to grow than those parallel to it. This is a limitation because crack growth was

The effect of frequency on crack growth in articular cartilage under tension

investigated through the depth of the cartilage specimen by Stoke *et al.* (2003 & 2007). In the current chapter crack growth was investigated from inside the cartilage specimens and not through all four cartilage zones consecutively. The data from Stok *et al.* (2007) showed an increase in the length of the initial crack from 25 to 100  $\mu\text{m}$  from the superficial layer through the depth of the cartilage. This corresponded to a minor decrease in failure stress, which is consistent with the findings from this current study that has shown increased crack growth with increasing number of cycles.

#### **5.4. Chapter summary**

Crack growth increased with the number of cycles of loading. The crack growth rate of cartilage samples was greater at higher frequencies. The variation of crack growth of cartilage specimen samples at loading frequencies associated with normal (1 Hz), above normal (10 Hz) and up to RHS rise times (100 Hz) may have implications in the early stages of OA. This is because in the early stages of the disease, the cartilage surface becomes inflamed and swollen. This effect is usually accompanied by tissue and water loss that is followed by the appearance of cracks and fissures on the cartilage surface. As the disease progresses, and more tissue is lost and the cartilage starts to stiffen. Thus, it becomes increasingly prone to damage from cyclic loading and injury. The next chapter provides the overall discussion and conclusions based on the work of this thesis.

## 6. Overall Discussion and Conclusions

Chapters 3 and 4 of this thesis reported the experimental failure of articular cartilage-on-bone specimens following the application of sinusoidally varying forces, under compression and bending, respectively. Chapter 5 provided the methods and measurements of failure propagation across the area of cartilage specimens under tension. Failure of cartilage/cartilage-on-bone specimens were assessed, over frequencies representative of normal, above normal and rapid heel-strike rise times. The work of this thesis showed that frequency, independent of load increases the failure of cartilage/cartilage-on-bone specimens subjected to compression, bending and tension.

The results of chapters 3-5 are consistent with the findings of Radin *et al.* (1986 & 1991) that showed RHS rise times during gait have implications in the early onset of OA in lower limb joints. Heel strike rise times in the normal population have been determined to be typically 100-150 ms (Shepherd *et al.*, 1997). However, Radin *et al.* (1986) have shown that at heel-strike, some people exhibit a very high rate of loading with a distinct impulsive peak. These rapid heel-strikes take only 5–25 ms to reach a maximum force (Simon *et al.*, 1981). The duration of the heel-strikes corresponds to loading frequencies of 3–5 Hz for normal and up to 90 Hz for impulsive heel-strike rise times (Fulcher *et al.*, 2009). Previous studies (Fulcher *et al.*, 2009; Sadeghi *et al.*, 2015) have also hypothesised that the possibility of cartilage failure would increase with loading frequency because at higher frequencies the ability of the tissue to store energy increased.

Chapter 3 subjected cartilage-on-bone specimens to 10,000 cycles of compressive loads using a metal indenter (5.2 mm diameter) at frequencies of 1, 10 and 100 Hz. These frequencies were applied with a maximum load in the range of 60-160 N. Application of such loads and frequencies resulted in crack formation on the articular surface of the cartilage-on-bone specimens. Surface damage was quantified and compared at different regions of damage corresponding to the test frequencies. Results from chapter 3 showed that surface damage increased with frequency throughout all load ranges investigated. The increase in crack length with loading frequency and

maximum load can be observed when comparing figure 3.20-a and figure 3.20-c. The dependence of total crack lengths on loading frequency at each load range was described by second order polynomial curve fits (Figure 3.22). The idea that mechanical failure might be a contributory factor in the development of OA and that fatigue is a possible mechanism for this failure is not new and over the years many studies have been conducted in this area (Johnson *et al.*, 1976; Simon *et al.*, 1989; Weightman *et al.*, 1973 & 1975; Kerin *et al.*, 2003). These studies examined the effects of cyclic loading in terms of the damage it induced on the joint surface, i.e. in the presence of surface fibrillation. However, the methods used in chapter 3, for the first time, demonstrated that cartilage surface failure is dependent on the frequency of loading alone, independent of load.

Chapter 4 used cyclic three-point bending to introduce failure into cartilage-on-bone specimens. Sinusoidally varying maximum compressive loads in the range 40-130 N were applied to beam-shaped cartilage-on-bone specimens at frequencies of 1, 10, 50 and 100 Hz. The number of cycles to failure decreased when loading frequency increased from normal and above gait (1 and 10 Hz) to loading frequencies representative of rapid heel-strikes (50 and 100 Hz) (Figure 4.14). It was found that 67% and 27% of the specimens reached run-out at loading of 10,000 cycles at frequencies of 1 and 10 Hz, respectively. However, 0% of the tissue samples reached run-out at loading frequencies of 50 and 100 Hz. Characterization of the bending failure of articular cartilage to variations in loading frequency is somewhat of a neglected area, with the only similar studies by Lafferty *et al.* (1978 & 1979). These studies by Lafferty *et al.* suggested that fatigue strength of cortical bone accelerated with increasing loading frequency via combined numerical and experimental approaches to the failure of bone. However, Lafferty *et al.* have only assessed the fatigue strength of bone in frequencies of 2 and 125 Hz, which resulted in the acceleration of fatigue tests conducted at 125 Hz.

Fatigue curves were used to assess how the peak value of the maximum sinusoidal force applied in the cyclic tests altered the number of cycles to failure of cartilage-on-bone. The curve fits obtained demonstrated a logarithmically decreasing trend with number of cycles to failure. The

findings from chapter 4 were consistent with previous studies that carried out injurious experiments of cartilage under cyclic shear (Tomatsu *et al.*, 1992) and compression (Zimmerman *et al.*, 1988) of cartilage-on-bone specimens. These studies showed that by increasing the number of loading cycles, the extent of cartilage failure on bovine cartilage surface also increases. However, the results from this study goes a step further, showing that the failure of cartilage-on-bone specimens were frequency dependent.

The findings presented in chapter 4 are consistent with those of chapter 3, where subjecting cartilage-on-bone specimens to 10,000 cycles of compressive loads using an impermeable indenter, resulted in surface failure of cartilage-on-bone specimens. Chapter 4 subjected rectangular cartilage-on-bone specimens to cyclic three-point bending. It also showed that increasing the loading frequency from normal and above gait (1 and 10 Hz) to frequencies which can be used to represent rapid heel-strikes (50 and 100 Hz), reduced the ability of the specimen samples to resist fracture. However, those studies focused on cartilage-on-bone, under compression and three-point bending, rather than tensile strains which have been implicated in the growth of superficial cartilage cracks during impact loading (Kelly *et al.*, 1996). Therefore, chapter 5 investigated whether frequencies associated with rapid heel-strikes (100 Hz) might also predispose articular cartilage to increased crack growth under purely tensile conditions and whether it is possible to measure this growth with respect to a certain number of cycles.

Chapter 5 investigated the propagation of an initial crack in cartilage specimens under different frequencies of loading. A 2.26 mm crack was introduced into cartilage specimens and crack growth was achieved by applying a sinusoidally varying tensile strain at frequencies of 1, 10 and 100 Hz. These frequencies were applied with a strain of between 10-20 % and the crack length was measured at 0, 20, 50, 100, 500, 1,000, 5,000 and 10,000 cycles of strain. Crack growth increased with increasing number of cycles. The correlation between crack growth and the number of cycles were described by logarithmic curve fits. The maximum crack growth was  $0.6 \pm 0.3$  (mean  $\pm$  standard deviation),  $0.8 \pm 0.2$  and  $1.1 \pm 0.4$  mm at frequencies of 1, 10 and 100 Hz, respectively.

Mean crack growth rates were 0.08 and 0.09 at frequencies of 1 and 10 Hz, respectively. However, this value increased up to 0.14 at a frequency of 100 Hz. The work conducted in chapter 5 confirms that strain experienced by the specimens at higher frequency e.g. 100 Hz caused a greater crack growth. Increased loading frequency also results in increasing the rate of crack propagation through the depth of cartilage specimens.

In this thesis bovine articular cartilage was used, which is an accepted model for human cartilage (Taylor *et al.*, 2011). A recent study (Temple *et al.*, 2016) showed that frequency-dependent viscoelastic trends of bovine articular cartilage were consistent with those of human articular cartilage; this includes a similar frequency dependency and higher-frequency plateau. However, bovine cartilage has been found to be approximately twice as stiff as human cartilage. Therefore, it is possible that if the protocols of this thesis were repeated on human cartilage the same patterns of failure would be achieved. However, previous observations following drop-tower impact tests suggested that human cartilage behaved differently from bovine and that the two forms of end to the impactor commonly used, a plane-ended impactor or an indenter, produced different characteristic damage (Burgin *et al.*, 2003; Jeffrey *et al.*, 2006). This might be because of the differences in the arrangement of collagen fibril network along the depth of cartilage tissue between human and other mammals (Kääb *et al.*, 1998). However, although the patterns of failure might vary, the same failure trends with increasing the loading frequency might be obtained under all loading types of compression, bending and tension covered in this thesis.

Future work could concern deeper analysis of the cartilage failure, with the variation of frequency, particularly similar to the full limb behaviour. This could include subjecting the whole joint to different frequencies without removing the cartilage from the joint which could provide data under more realistic conditions. Thus, the full limb behaviour could combine well with strategies to reduce failure in human subjects. These frequencies could be in the range as used in chapters 3-5 (1-100 Hz) and the number of cycles could be 10,000 cycles as it was shown to cause failure in cartilage. The failure characteristics of cartilage/cartilage-on-bone specimens with respect

to loading frequency and number of cycles provides valuable information in planning strategies to prevent the initiation/progression of OA in human joints. These could involve specific cushioning for shoes or developing specific systems to reduce heel-strike impulse during gait and thus prevent cartilage degeneration. Another strategy is to target the composition of articular cartilage. For instance, increased cross-linking (Verzijl *et al.*, 2002) or altering the state of hydration of cartilage (Fick *et al.*, 2011) has been shown to reduce the initiation of failure in cartilage.

Previous studies (Radin *et al.*, 1973 & 1984) have attempted to observe the changes in cartilage and subchondral bone metabolism after the application of cyclic impulsive loads using experimental animals such as rabbits. A comparable study (Radin *et al.* 1982) has investigated the changes in chondrocyte metabolism of sheep cartilage after experimental animals were subjected to prolonged walking on concrete. However, none of these studies have observed the variation of surface failure or failure through the depth of cartilage subsequent to being subjected to loads with frequencies representative of RHS. Therefore, it would be useful to have data on experimental failure of cartilage following RHS frequencies in the joint, and not removed from it. However, using such methods has a number of limitations. One of the limitations could be that the contact area is difficult to control as opposed to indentation in which the area of contact is the same during testing. The second limitation is that holding the full joint during high loading frequencies such as 100 Hz would require a test rig with specific adjustable geometries given that each joint is different in size, length, etc.

The overall conclusions of this thesis are as follows:

- Frequency alone is a factor in the failure and progression of failure in articular cartilage.

- Cyclic loading of cartilage-on-bone specimens using an indenter resulted in a significant increase ( $p < 0.05$ ) in the cartilage surface crack length with frequency throughout all load ranges.
- Increasing the frequency from normal (1 and 10 Hz) to frequencies which can be used to represent rapid heel-strikes (50 and 100 Hz), reduced the ability of rectangular shaped cartilage-on-bone specimens to resist failure during cyclic three-point bending tests.
- Growth of an initial crack in cartilage specimens under tension were found to increase with number of cycles. Strain experienced by the specimens at higher frequency e.g. 100 Hz caused a greater crack growth. The rate of crack propagation across the cartilage specimens was also higher at frequencies representative of RHS.

## REFERENCES

Adams DJ, Brosche KM, Lewis JL. Effect of specimen thickness on fracture toughness of bovine patellar cartilage. *J Biomech Eng* 2004;125:927–928.

Adams MA, Kerin AJ, Winsom MR. Sustained loading increases the compressive strength of articular cartilage. *Connect Tissue Res* 1998;39:245–256.

Adams MA, Merrill AK, Kerin AJ. Mechanically-induced proteoglycan loss from damaged articular cartilage in-vitro. *Trans Orthop Res Soc* 1997;43:409.

Ahmed AM, Burke DL. In-vitro measurement of static pressure distribution in synovial joints part I: tibial surface of the knee. *J Biomech Eng* 1983,105:216–25.

Ahsan T, Sah RL. Biomechanics of integrative repair. *Osteoarthritis Cartilage* 1999;7:29–40.

Akizuki S, Mow VC, Müller F, Pita JC, Howell DS, Manicourt DH. Tensile properties of human knee joint cartilage, I: influence of ionic conditions, weight bearing and fibrillation on the tensile modulus. *J Orthop Res* 1986;4:379–392.

Alford JW, Cole BJ. Cartilage restoration, part I: basic science, historical perspective, patient evaluation and treatment options. *Am J Sports Med.* 2005;33:295–306.

Armstrong CG, Lai MW, Mow VC. An analysis of the unconfined compression of articular cartilage. *J Biomech Eng* 1984;106:165–173.

Armstrong CG. An analysis of the stresses in a thin layer of articular cartilage in a synovial joint. *Eng Med* 1986;15:55–61.

Aspden RM, Hukins DWL. Collagen organization in articular cartilage, determined by x-ray diffraction, and its relationship to tissue function. *Proc R Soc Lond Ser B* 1981;212:299–304.

Aspden RM, Jeffrey JE, Burgin LV. Impact loading: physiological or pathological? *Osteoarthritis Cartilage* 2002;10:588–589.

Aspden RM. Constraining the lateral dimensions of uniaxially loaded materials increases the calculated strength and stiffness: application to muscle and bone. *J Mater Sci Mater Med* 1990;1:100–4.

Aspden RM. Fiber reinforcing by collagen in cartilage and soft connective tissues. *P Roy Soc Land B Bio* 1994;258:195–200.

ASTM D7774–12, Standard test method for flexural fatigue properties of plastics, ASTM International, 2012.

Ateshian GA. The role of interstitial fluid pressurization in articular cartilage lubrication. *J Biomech* 2009;42:1163–1176.

Athanasίου KA, Darling EM, Jerry CH, DuRaine DG, Reddi AH. *Articular cartilage*. CRC Press/Taylor & Francis Group, LLC 2013.

Ayis S, Dieppe P. The natural history of disability and its determinants in adults with lower limb musculoskeletal pain. *J Rheumatol* 2009;36:583–591.

Baltzopoulos V. Muscular and tibiofemoral joint forces during isokinetic concentric knee extension. *Clin Biomech* 1995;10:208–214.

Barker MK, Seedhom BB. Articular cartilage deformation under physiological cyclic loading apparatus and measurement technique. *J Biomech* 1997; 30:377–81.

Barker MK, Seedhom BB. The relationship of the compressive modulus of articular cartilage with its deformation response to cyclic loading: does cartilage optimize its modulus so as to minimize the strains arising in it due to the prevalent loading regime? *Rheumatology* 2001;40:274–284.

Bassey EJ, Littlewood JJ, Taylor JG. Relations between compressive axial forces in an instrumented massive femoral implant, ground reaction forces, and integrated electromyographs from vastus lateralis during various ‘osteogenic’ exercises. *J Biomech* 1997; 30:213–23.

Bellucci G, Seedhom BB. Mechanical behaviour of articular cartilage under tensile cyclic load. *Rheumatology* 2001;40:1337–1345.

Bergmann G, Bender A, Graichen F, Dymke J, Rohlmann A, Trepczynski A, Heller MO, Kutzner I. Standardized loads acting in knee implants. *PLoS One* 2014;9:e86035.

Bergmann G, Deuretzbacher G, Heller M, Graichen F, Rohlmann A, Strauss J, Duda GN. Hip contact forces and gait patterns from routine activities. *J Biomech* 2001;34:859–71.

Bigley RF, Gibeling JC, Stover SM, Hazelwood SJ, Fyhrie DP, Martin RB. Volume effects on fatigue life of equine cortical bone. *J Biomech* 2007;40:3548–3554.

Borrelli J, Torzilli PA, Grigiene R, Helfet DL. Effect of impact load on articular cartilage: development of an intra-articular fracture model. *J Orthop Trauma* 1997;11:319-326.

Braman JP, Bruckner JD, Clark JM, Norman AG, Chansky HA. Articular cartilage adjacent to experimental defects is subject to atypical strains. *Clin Orthop* 2005;430:202–207.

Broom ND. Further insights into the structural principals governing the function of articular cartilage. *J Anat* 1984;139:275–294.

Broom ND. The collagenous architecture of articular cartilage--a synthesis of ultrastructure and mechanical function. *J Rheum* 1986;13:142–152.

Brown TD, Shaw DT. *In vitro* contact stress distributions in the natural human hip *J Biomech* 1983;16:373–84.

Buckwalter JA. Articular cartilage injury and repair. In injury and repair of the musculoskeletal soft tissues. SLY. Woo, JA Buckwalter, eds, American academy of orthopaedic surgeons, Park Ridge, IL, 1988;465–482.

Buckwalter JA. Mechanical injuries of articular cartilage. *Iowa Orthop J* 1992;12:50–57.

Buckwalter JA. Sports, joint injury, and posttraumatic osteoarthritis, *J Orthop Sports Phys Ther* 2003;33:578–88.

Burgin LV, Aspden RM. Impact loading of human articular cartilage. *J Biomech* 2001;34:S39–S40.

Burgin LV, Aspden RM. Impact testing to determine the mechanical properties of articular cartilage in isolation and on bone. *J Mater Sci: Mater Med* 2008; 19:703–711.

Burgin LV. *Impact loading of articular cartilage*, PhD thesis, university of Aberdeen, 2003.

Byers PD, Hoaglund FT, Purewal GS, Yau AC. Articular cartilage changes in Caucasian and Asian hip joints. *Ann Rheum Dis* 1974;33:157–61.

Byers PD, Maroudas A, Ozlop F, Stockwell R, Venn MF. Histological and biochemical studies on cartilage from osteoarthritic femoral heads with special reference to surface characteristics. *Connect Tissue Res* 1977;5:41–49.

Byers PD. What is osteoarthritic cartilage? In proceedings of the symposium, Normal and osteoarthritic articular cartilage (ed. SY Ali, MW Elves, DH Leaback) 1974;131–139. London: Institute of orthopaedics.

Canal CE, Hung CT, Ateshian GA. Two-dimensional strain fields on the cross-section of the bovine humeral head under contact loading. *J Biomech* 2008;41:3145–3151.

Chan DD, Cai L, Butz KD, Trippel SB, Nauman EA, Neu CP. *In vivo* articular cartilage deformation: noninvasive quantification of intratissue strain during joint contact in the human knee. *Sci Rep* 2016;6:19220.

Chiang EH, Laing TJ, Meyer CR, Boes JL, Rubin JM, Adler RS. Ultrasonic characterization of *in vitro* osteoarthritic articular cartilage with validation by confocal microscopy. *Ultrasound Med Biol* 1997;23:205–13.

Chin-Purcell MV, Lewis JL. Fracture of articular cartilage. *J Biomech Eng* 1996;118:545–556.

Cicuttini F, A Wluka J, Hankin J, Wang Y. Longitudinal study of the relationship between knee angle and tibiofemoral cartilage volume in subjects with knee osteoarthritis. *Rheumatology* 2004;43:321–324.

Cicuttini F, Ding C, Wluka A, Davis S, Ebeling RR, Jones G. Cartilage defects are associated with knee cartilage loss in healthy, middle-aged adults: a prospective study. *Arthritis Rheum* 2005;52:2033–2039.

Clark JM, Simonian PT. Scanning electron microscopy of ‘fibrillated’ and ‘malacic’ human articular cartilage: technical considerations. *Microsc Res Tech* 1997;37:299–313.

Clark JM. Variation of collagen fiber alignment in a joint surface: a scanning electron microscope study of the tibial plateau in dog, rabbit, and man. *J Orthop Res* 1991;9:246–257.

Clements KM, Bee ZC, Crossingham GC, Adams MA, Sharif M. How severe must repetitive loading be to kill chondrocytes in articular cartilage? *Osteoarthritis Cartilage* 2001;9:499–507.

Cooper C, McAlindon T, Coggon D, Egger P, Dieppe P. Occupational activity and osteoarthritis of the knee. *Ann Rheum Dis* 1994;53:90–3.

Creamer P, Hochberg MC. Osteoarthritis. *Lancet* 1997;350:503–509.

DeFrate LE, Sun H, Gill TJ, Rubash HE, Li G. In vivo tibiofemoral contact analysis using 3D MRI-based knee models. *J Biomechanics* 2004;37:1499–1504.

Dekel S, Weissman SL. Joint changes after overuse and peak overloading of rabbit knees in vivo. *Acta Orthop Scand* 1978;49:519–528.

Dickinson JA, Cook SD, Leinhardt TM. The measurement of shock waves following heel strike while running. *J Biomech* 1985;18:415–422.

Ding C, Garnerio P, Cicuttini F, Scott F, Cooley H, Jones G. Knee cartilage defects: association with early radiographic osteoarthritis, decreased cartilage volume, increased joint surface area and type II collagen breakdown. *Osteoarthritis Cartilage* 2005;13:198–205.

DiSilvestro MR, Suh JF. A cross-validation of the biphasic poroviscoelastic model of articular cartilage in unconfined compression, indentation, and confined compression. *J Biomech* 2001;34:519–525.

Dominick KL, Athern FM, Gold CH, Heller DA. Health-related quality of life and health service use among older adults with osteoarthritis. *Arthritis Rheum* 2004;51:326–331.

Draper ERC, Goodship AE. A novel technique for four-point bending of small bone samples with semi-automatic analysis. *J Biomech* 2003;36:1497–1502.

Eberhardt AW, Lewis JL, Keer LM. Normal contact of elastic spheres with two elastic layers as a model of joint articulation. *J Biomech Eng* 1991;113:410–417.

Edelsten L, Jeffrey JE, Burgin LV, Aspden RM. Viscoelastic deformation of articular cartilage during impact loading. *Soft Matter* 2010;6:5206–5212.

Espino DM, Shepherd DET, Hukins DWL. Viscoelastic properties of bovine knee joint articular cartilage: dependency on thickness and loading frequency. *BMC Musculoskelet Disord* 2014;15:205.

Ewers BJ, Dvoracek-Driksna D, Orth MW, Haut RC. The extent of matrix damage and chondrocyte death in mechanically traumatized articular cartilage explants depends on rate of loading. *J Orthop Res* 2001;19:779–84.

Eyre DR. The collagens of articular cartilage. *Semin Arthritis Rheum* 1991;21(Suppl 2):2–11.

Ferry JD. *Viscoelastic properties of polymers*. John Wiley & Sons, New York 1980.

Fick JM, Espino DM. Articular cartilage surface failure: an investigation of the rupture rate and morphology in relation to tissue health and hydration. *P I Mech Eng H* 2012;226:389–96.

Fick JM, Espino DM. Articular cartilage surface rupture during compression: Investigating the effects of tissue hydration in relation to matrix health. *J Mech Behav Biomed* 2011;4:1311–1317.

Fick JM. How the structural integrity of the matrix can influence the microstructural response of articular cartilage to compression. *Connect Tissue Res* 2013;54:83–93.

Flachsmann ER, Broom ND, Oloyede A. A biomechanical investigation of unconstrained shear failure of the osteochondral region under impact loading. *Clinic Biomech* 1995;10:156–165.

Flachsmann R, Broom ND, Hardy AE. Deformation and rupture of the articular surface under dynamic and static compression. *J Orthop Res* 2001;19:1113–1139.

Flachsmann R, Kim W, Broom N. Vulnerability to rupture of the intact articular surface under with respect to age and proximity to site of fibrillation: a dynamic and static investigation. *Connect Tissue Res* 2005;46:159–169.

Flachsmann R, Kistler M, Rentzios A, Broom ND. Influence of an initiating microsplit on the resistance to compression-induced rupture of the articular surface. *Connect Tissue Res* 2006;47:77–84.

Folman Y, Wosk J, Voloshin A, Liberty S. Cyclic impacts on heel-strike: a possible biomechanical factor in the etiology of degenerative disease of human locomotor system. *Arch Orthop Trauma Surg* 1986;104:363–365.

Freeman MAR. *Modern Trends in Orthopaedics*. Butterworths, London;40:1972.

Fulcher GR, Hukins DWL, Shepherd DET. Viscoelastic properties of bovine articular cartilage attached to subchondral bone at high frequencies. *BMC Musculoskelet Disord* 2009;10:61.

Ghosh S, Bowen J, Jiang K, Espino DM, Shepherd DET. Investigation of techniques for the measurement of articular cartilage surface roughness. *Micron* 2013;44:179–84.

Gillespie KA, Dickey JP. Determination of the effectiveness of materials in attenuating high frequency shock during gait using filterbank analysis. *Clin Biomech* 2003;18:50–59.

Goh KL, Meakin JR, Hukins DWL. Influence of fibre taper on the interfacial shear stress in fibre-reinforced composite materials during elastic stress transfer. *Compos Interface* 2010;17:74–80.

Green TP, Adams MA, Dolan P. Tensile properties of the annulus fibrosus. Part II: Ultimate tensile strength and fatigue life. *Eur Spine J* 1993;2:209–214.

Griffin TM, Guilak F. The role of mechanical loading in the onset and progression of osteoarthritis. *Exerc Sport Sci Rev* 2005;33:195–200.

Hargrave-Thomas E, Van Sloun F, Dickinson M, Broom N, Thambyah A. Multi-scalar mechanical testing of the calcified cartilage and subchondral bone comparing healthy versus early degenerative states. *Osteoarthritis Cartilage* 2015;23:1755–1762.

Hayes WC, Bodline AJ. Flow-independent viscoelastic properties of articular cartilage matrix. *J Biomech* 1978;11:407–419.

Hayes WC, Mockros LF. Viscoelastic properties of human articular cartilage. *J Appl Physiol* 1973;31:562–568.

Hodge WA, Carlson KL, Fijan RS, Mann RW. Contact pressures from an instrumented hip endoprosthesis *J Bone Joint Surg* 1989;71:1378–86.

Hollander AP, Pidoux I, Reiner A, Rorabeck C, Bourne R, Poole AR. Damage to type II collagen in aging and osteoarthritis starts at the articular surface, originates around chondrocytes and extends into the cartilage with progressive degeneration. *J Clin Invest* 1995;96:2859–2869.

Hukins DWL, Aspden RM, Yarker YE. Fibre reinforcement and mechanical stability in articular cartilage. *P I Mech Eng H* 1984;13:153–156.

Hukins DWL, Aspden RM. Composition and properties of connective tissues. *Trends Biochem Sci* 1985;10:260–4.

Hukins DWL, Leahy JC, Mathias KJ. Biomaterials: defining the mechanical properties of natural tissues and selection of replacement materials. *J Mater Chem* 1999;9:629–636.

Hurwitz DE, Ryals AR, Block JA, Sharma L, Schnitzer TJ, Andriacchi TP. Knee pain and joint loading in subjects with osteoarthritis of the knee. *J Orthop Res* 2000;18:572–579.

Huyghe JM, Wilson W, Malakpoor K. On the thermodynamical admissibility of the triphasic theory of charged hydrated tissues. *J Biomech Eng* 2009;131:245–258.

Huyghe JMRJ, Wilson W, Malakpoor K. Reply to discussion On the thermodynamical admissibility of the triphasic theory of charged hydrated tissues. (Mow V.C., Lai W.M., Setton L.A., Gu W., Yao, H., Lu X.L., *ASME J. Biomech. Eng.* 2009, 131, p.095501). *J Biomech Eng ASME*, 2010;132:065501-1/1.

Jeffrey AK, Blunn GW, Archer CW, Bentley G. Three dimensional collagen architecture in bovine articular cartilage. *J Bone Joint Surg* 1991;73:795–801.

Jeffrey JE, Aspden RM. The biophysical effects of a single impact load on human and bovine articular cartilage. *Proc Inst Mech Eng Part H J Eng Med* 2006;220:677–686.

Jeffrey JE, Gregory DW, Aspden RM. Matrix damage and chondrocyte viability following a single impact load on articular cartilage. *Arch Biochem Biophys* 1995;322:87–96.

Jeffrey JE, Thompson LA, Aspden RM. Matrix loss and synthesis following a single impact load on articular cartilage in vitro. *Biochim Biophys Acta* 1997;1334:223–232.

Johnson GR, Dowson D, Wright V. The fracture of articular cartilage under impact loading. In: *Proc. 3rd Leeds-Lyons Symposium on Tribology*. 1976 University of Leeds, Leeds, UK.

Johnson-Nurse C, Dandy DJ. Fracture-separation of articular cartilage in the adult knee. *J Bone Joint Surg* 1985;67:42–43.

Jones G, Ding C, Scott F, Glisson M, Cicuttini F. Early radiographic osteoarthritis is associated with substantial changes in cartilage volume and tibial bone surface area in both males and females. *Osteoarthritis Cartilage* 2004;12:169–174.

Kääb MJ, Gwynn IA, Nötzli HP. Collagen fibre arrangement in the tibial plateau articular cartilage of men and other mammalian species. *J Anat* 1998;93:23–34.

Kafka V. Surface fissures in articular cartilage: new concepts, hypotheses and modeling. *Clin Biomech (Bristol, Avon)* 2002;17:73–80.

Kelly PA, JJ O'Connor. Transmission of rapidly applied loads through articular cartilage Part 1: uncracked cartilage, *Proc Inst Mech Eng* 1996; 210:27–37.

Kelly PA, O'Connor JJ. Transmission of rapidly applied loads through articular cartilage, Part 2: cracked cartilage. *Proc Inst Mech Eng* 1996;210:39–49.

Kempson GE. Age-related changes in the tensile properties of human articular cartilage: a comparative study between the femoral head of the hip joint and the talus of the ankle joint. *Biochim Biophys Acta* 1991;1075:223–230.

Kempson GE. Relationship between the tensile properties of articular cartilage from the human knee and age. *Ann Rheum Dis* 1982;41:508–511.

Kempson GE. The mechanical properties of articular cartilage. Ch 5: the joint and synovial fluid, Academic press, Inc 1980;177–239.

Kennedy JC, Grainger RW, McGraw RW. Osteochondral fractures of the femoral condyles. *J Bone Joint Surg* 1966;48:436–440.

Ker RF. The design of soft collagenous load-bearing tissues. *J Exp Biol* 202:3315-3324.

Kerin AJ, Coleman A, Winsom MR, Adams MA. Propagation of surface fissures in articular cartilage in response to cyclic loading in vitro. *Clin Biomech (Bristol Avon)* 2003;18:960–8.

Kerin AJ, Wisnom MR, Adams MA. The compressive strength of articular cartilage. *Proc Inst Mech Eng H* 1998;212:273–280.

Kiefer GN, Sundby K, McAllister D, Shrive NG, Frank CB, Lam T, Schachar NS. The effect of cryopreservation on the biomechanical behaviour of articular cartilage. *J Orthop Res* 1989;7:494–501.

Korhonen RK, Laasanen MS, Toyas J, Rieppo J, Hirvonen J, Helminen HJ. Comparison of the equilibrium response of articular cartilage in unconfined compression, confined compression and indentation. *J Biomech* 2002b;35:903–909.

Korhonen RK, Wong M, Arokoski J, Lindgren R, Helminen HJ, Hunziker EB. Importance of the superficial tissue layer for the indentation stiffness of articular cartilage. *Med Eng Phys* 2002a;24:99–108.

Kovach IS. A molecular theory of cartilage viscoelasticity. *Biophys Chem* 1996;59:61–73.

Kovach IS. The importance of polysaccharide configurational entropy in determining the osmotic swelling pressure of concentrated proteoglycan solution and the bulk compressive modulus of articular cartilage *Biophys Chem* 1995;53:181–7.

Kraus VB, Collins JE, Hargrove D, Losina E, Nevitt M, Katz JN, Wang SX, Sandall LJ, Hoffmann SC, Hunter DJ. Predictive validity of biochemical biomarkers in knee osteoarthritis: Data from the FNIH OA biomarkers consortium. *Ann Rheum Dis* 2017;76:186-195.

Lafferty JF, Analytical model of the fatigue characteristics of bone. *Aviat Space Environ Med* 1978;49:170–174.

Lafferty JF, Raju PV. The Influence of stress frequency on the fatigue strength of cortical bone. *J Biomech Eng* 1979;101:112-113.

Lafortune MA, Hennig EM. Cushioning properties of footwear during walking: accelerometer and force platform measurements. *Clin Biomech* 1992;7:181–184.

Larson P. Foot strike in runners: Influence on injury risk. *LER* 2012;4(6):31-35.

Lawrence RC, Felson DT, Helmick CG, Arnold LM, Choi H, Deyo RA. Estimates of the prevalence of arthritis and other rheumatic conditions in the United States. Part II, Arthritis Rheum 2008;58:26–35.

LeBaron RG, Athnasiou KA. *Ex vivo* synthesis of articular cartilage. *Biomaterials* 2000;21:431–440.

Leslie L, Kukureka S, Shepherd DET. Crack growth of medical-grade silicone using pure shear tests. *Proc Inst Mech Eng H* 2008;222:977–982.

Lewis JL, Johnson SL. Collagen architecture and failure processes in bovine patellar cartilage. *J Anat* 2001;199:483–492.

Light LH, McLellan GE, Klenerman L. Skeletal transients on heel strike in normal walking with different footwear. *J Biomech* 1980;13:477–480.

Loeser RF, Goldring SR, Scanzello CR, Goldring MB. Osteoarthritis: a disease of the joint as an organ. *Arthritis Rheum* 2012;64:1697–1707.

Lu X, Mow VC. Biomechanics of articular cartilage and determination of material properties. *Med Sci Sports Exerc* 2008;40:193–9.

Lu XL, Sun DDN, Guo XE, Chen FH, Lai WM, Mow VC. Indentation determined mechanochemical properties and fixed charged density of articular cartilage. *Ann Biomed Eng* 2004;32:370–379.

Mankin HJ. The response of articular cartilage to mechanical injury. *J Bone Joint Surg Am* 1982;64:460–6.

Maroudas A, Bullough P. Permeability of articular cartilage. *Nature* 1968;219:1260–1261.

Maroudas A, Venn M. Chemical composition and swelling of normal and osteoarthritic femoral head cartilage. *Ann Rheum Dis* 1977;36:399–406.

Martin JA. and Buckwalter JA. Aging, articular cartilage chondrocyte senescence and osteoarthritis. *Biogerontology* 2002;3:257–64.

Mathews MB, Decker L. Comparative studies of water sorption of hyaline cartilage. *Biochim Biophys Acta* 1977;497:151–9.

McCormack T, Mansour JM. Reduction in tensile strength of cartilage precedes surface damage under repeated compressive loading *in vitro*. *J Biomech* 1998;31:55–61.

McNary SM., Athanasiou KA, Reddi AH. Engineering lubrication in articular cartilage. *Tissue Eng Pt B-Rev* 2012;18,88–100.

Meachim G, Denham D, Emery IH, Wilkinson PH. Collagen alignments and artificial splits at the surface of human articular cartilage. *J Anat* 1974;118:101–118.

Meachim G. Light microscopy of indian ink preparations of fibrillated cartilage. *Ann Rheum Dis* 1972;31:457–464.

Meakin JR, Hukins DWL, Aspden RM, Imrie CT. Rheological properties of poly(2-hydroxy methacrylate) (pHEMA) as a function of water content and deformation frequency. *J Mater Sci Mater Med* 2003;14:783–7.

Mente PL, Lewis JL. Elastic modulus of calcified cartilage is an order of magnitude less than that of subchondral bone. *J Orthop Res* 1994;12:637–647.

Milentijevic D, Rubel IF, Liew AS, Helfet DL, Torzilli PA. An in vivo rabbit model for cartilage trauma: a preliminary study of the influence of impact stress magnitude on chondrocyte death and matrix damage. *J Orthop Trauma* 2005;19:466–473.

Minns RJ, Birnie AJM, Abernethy PJ. A stress analysis of the patella, and how it relates to patellar articular cartilage lesions. *J of Biomech* 1979;12:699–711.

Minns RJ, Steven FS. The collagen fibril organization in human articular cartilage. *J Anat* 1977;123:437–457.

Morel V, Mercay A, Quinn TM. Prestrain decreases cartilage susceptibility to injury by ramp compression in vitro. *Osteoarthritis Cartilage* 2005;13:964–970.

Morel V, Quinn TM. Cartilage injury by ramp compression near the gel diffusion rate. *J Orthop Res* 2004;22:145–151.

Mow V, Rosenwasser M. Articular cartilage: bio-mechanics. In: Woo SLY, Buckwalter JA, Ed. *Injury and Repair of the Musculoskeletal Soft Tissues*. Park Ridge, IL: American Academy of Orthopaedic Surgeons 1988:427–63.

Mow VC, Ateshian GA, Spilker RL. Biomechanics of diarthrodial joints: a review of twenty years of progress. *J Biomech Eng* 1993;115:460–467.

Mow VC, Kuei SC, Lai WM, Armstrong CG. Biphasic creep and stress relaxation of articular cartilage in compression: theory and experiments. *J Biomech Eng* 1980;102:73–84.

Mow VC, Ratcliffe A. Structure and function of articular cartilage and Meniscus. In: V.C. Mow, W.C.H (ed.), *Basic orthopaedic biomechanics*. Lippincott-Raven, New York 1997; p.113–178.

Mow VC, Homes MH, and Lai WM. Fluid transport and mechanical properties of articular cartilage. A review. *J Biomech* 1984;17: 377.

Muir IHM. The chondrocyte, architect of cartilage. *BioEssays* 1995;17:1039–1048.

Murray RC, Birch, HL, Lakhani K, Goodship AE. Biochemical composition of equine carpal articular cartilage is influenced by short-term exercise in a site-specific manner. *Osteoarthritis Cartilage* 2001;9:625–632.

National Collaborating Centre for Chronic Conditions. *Osteoarthritis: national clinical guideline for care and management in adults*. London: Royal college of physicians; 2008.

Natoli RM, Scott CC, Athanasiou KA. Temporal effects of impact on articular cartilage cell death, gene expression, matrix biochemistry, and biomechanics. *Ann Biomed Eng* 2008;36:780–792.

Oloyede A, Broom ND, The generalized consolidation of articular cartilage: an investigation of its near-physiological response to static load. *Connect Tissue Res* 1994a;31:75–86.

Oloyede A, Broom ND. Complex nature of stress inside loaded articular cartilage. *Clin Biomech* 1994b;9:149–156.

Oloyede A, Flachsmann R, Broom N. The dramatic influence of loading velocity on the compressive response of articular cartilage. *Connect Tissue Res* 1992;27:211–224.

Park S, Kerbs DE, Mann RW. Hip muscle co-contraction: evidence from concurrent in vivo pressure measurement and force estimation. *Gait Posture* 1999;10:211–22.

Paul IL, Munro MB, Abernethy PJ, Simon SR, Radin EL. Musculoskeletal shock absorption: relative contribution of bone and soft tissues at various frequencies. *J Biomech* 1978;11:237–239.

Paul JP. Forces transmitted by joints in the human body. *P I Mech Eng H* 1966; 181:8–15.

Pearson B, Espino DM. The effect of hydration on the frequency-dependant viscoelastic properties of articular cartilage *P I Mech Eng H* 2013;227:1246–52.

Quinn TM, Morel V. Microstructural modelling of collagen network mechanics and interactions with the proteoglycan gel in articular cartilage. *Model Mechanobiol* 2007;6:73–82.

Radin EL, Ehrlich MG.; Chernack, Robert; Abernethy, Peter; Paul; I. L; Rose RM. Effect of repetitive impulsive loading on the knee joints of rabbits. *Clin Orthop* 1978;131:288–293.

Radin EL, Martin RB, Burr DB, Carterson B, Boyd RD, Goodwin C. Effects of mechanical loading on the tissues of the rabbit knee. *J Orthop Res* 1984;2:221–234.

Radin EL, Orr RB, Kelman JL, Paul IL, Rose RM. Effect of prolonged walking on concrete on the knee of sheep. *J Biomech* 1982;15:487–492.

Radin EL, Parker HG, Pugh JW, Steinberg RS, Paul IL, Rose RM. Response of joints to impact loading – III. Relationship between trabecular microfractures and cartilage degeneration. *J Biomech* 1973;6:51–57.

Radin EL, Paul IL, Lowy M. A comparison of the dynamic force transmitting properties of subchondral bone and articular cartilage. *J Bone Joint Surg* 1970;52:444–456.

Radin EL, Rose RM. Role of subchondral bone in the initiation and progression of cartilage damage. *Clin Orthop Relat Res* 1986b;213:34–40.

Radin EL, Whittle MW, Yang KH, Jefferson R, Rodgers MM, Kish VL, O'Connor JJ. The heelstrike transient, its relationship with the angular velocity of the shank, and effects of quadriceps paralysis. In *Advances in Bioengineering*. Edited by Lantz SA, King AI. New York: American Society of Mechanical Engineering; 1986:121–123.

Radin EL, Yang KH, Riegger C, Kish VL, O'Connor JJ. Relationship between lower-limb dynamics and knee-joint pain. *J Orthop Res* 1991;9:398–405.

Radin EL. Who gets Osteoarthritis and why? *J Rheumatol Suppl* 2004;70:10–5.

Ranstam J. Repeated measurements, bilateral observations and pseudoreplicates, why does it matter? *Osteoarthritis Cartilage* 2012;20:473-475.

Repo RU, Finlay JB. Survival of articular cartilage after controlled impact. *J Bone Joint Surg* 1977;59:1068–1076.

Roberts S, Weightman B, Urban J, Chappell D. Mechanical and biochemical properties of human articular cartilage in osteoarthritic femoral heads and in autopsy specimens. *J Bone Joint Surg Br* 1986;68: 278-288.

Roth V, Mow VC. The intrinsic tensile behaviour of the matrix of bovine articular cartilage and its variation with age. *J Bone Joint Surg Am* 1980;62:1102–1117.

Sadeghi H, Espino DM, Shepherd DET. Variation in viscoelastic properties of bovine articular cartilage below, up to and above healthy-gait relevant loading frequencies. *P I Mech Eng H* 2015;229:115–23.

Sasazarki Y, Shore R, Seedhom BB. Deformation of failure of cartilage in the tensile mode. *J Anat* 2006;208:681–694.

Schmidt MB, Mow VC, Chun LE, Eyre DR. Effects of proteoglycan extraction on the tensile behaviour of articular cartilage. *J Orthop Res* 1990;8:353–363.

Seldin ED, Hirsch C. Factors affecting the determination of physical the properties of femoral cortical bone. *Acta Orthop Scand* 1966;37:29–48.

Shepherd DET, Seedhom BB. Technique for measuring the compressive modulus of articular cartilage under physiological loading rates with preliminary results. *P I Mech Eng H* 1997;211:155–165.

Shepherd DET, Seedhom BB. Thickness of human articular cartilage in joints of the lower limb. *Ann Rheum Dis* 1999;58:27–34.

Shrive NG, Frank CB. Articular cartilage. In: Nigg, B.M., Herzog, W. (Ed.), *Biomechanics of the musculo-skeletal system*. John Wiley & sons, Toronto, 1999; p. 86–106.

Shultz SJ *Examination of musculoskeletal injuries*. 2nd ed, North Carolina: Human Kinetics, 2005;P. 55–60.

Silyn-Roberts H, Broom ND. Fracture behaviour of cartilage-on-bone in response to repeated impact loading *Conn Tiss Res* 1990;24:143–56.

Simon SR, Paul IL, Mansour J, Munro M, Abernethy PJ, Radin EL. Peak dynamic force in human gait. *J Biomech* 1981;14:817–822.

Simon WH, Mak A, Spirt A. The effect of shear fatigue on bovine articular cartilage. *J Orthop Res* 1990;8:86–93.

Sophia Fox AJ, Bedi A, Rodeo SA. The basic science of articular cartilage: structure, composition and function. *Sports Health* 2009;1:461–467.

Sowers MR, Karvonen-Gutierrez CA. The evolving role of obesity in knee osteoarthritis. *Curr Opin Rheumatol* 2010;22:533–537.

Stockwell RA. Cartilage failure in osteoarthritis: Relevance of normal structure and function. *A Review Clinic Anat* 1991;4:161–191.

Stok K, Oloyede A. A qualitative analysis of crack propagation in articular cartilage at varying rates of tensile loading. *Connect Tissue Res* 2003;44:109–120.

Stok K, Oloyede A. Conceptual fracture parameters for articular cartilage. *Clin Biomech* 2007;22:725–735.

Summers GC, Merrill A, Sharif M, Adams MA. Swelling of articular cartilage depends on the integrity of adjacent cartilage and bone. *Biorheology* 2008;45:365–374.

Sutherland DH. *Gait disorders in childhood and adolescence*, Williams & Wilkins, Baltimore 1984, p. 201.

Swann AC. The effect of mechanical stress on the stiffness articular cartilage and its role in the aetiology of osteoarthritis. In *PhD* thesis University of Leeds;1988.

Szarko M, Muldrew K, Bertram JEA. Freeze-thaw treatment effects on the dynamic mechanical properties of articular cartilage. *BMC Musculoskelet Disord* 2010;11: 231.

Taylor SD, Tsiridis E, Ingham E, Jin Z, Fisher J, Williams S. Comparison of human and animal femoral head chondral properties and geometries. *P I Mech Eng H*, 2011;226:55–62.

Temple DK, Cederlund AA, Lawless BM, Aspden RM, Espino DM. Viscoelastic properties of human and bovine articular cartilage: a comparison of frequency-dependent trends. *BMC Muskuloskelet Disord* 2016;17:419.

Tomatsu T, Imai N, Takeuchi N. Experimentally produced fractures of articular cartilage and bone: the effect of shear forces on the pig knee *J Bone and Joint Surg* 1992;74:457–62.

Torzilli PA, Grigiene R, Borrelli J, Helfet DL. Effect of impact load on articular cartilage: cell metabolism and viability, and matrix water content. *J Biomech Eng* 1999;121:433-441.

Turner S. *Mechanical testing of plastics*, 2nd ed. New York:Longman 1983:134–135.

Toyra J, Lyyra -Laitinen T, Niinimäki M, Lindgren R, Nieminen MT, Kiviranta I, Jurvelin JS. Estimation of the Young's modulus of articular cartilage using an arthroscopic indentation instrument and ultrasonic measurement of tissue thickness *J Biomech* 2001;34: 251–256.

Verteramo A, Seedhom BB. Effect of a single impact loading on the structure and mechanical properties of articular cartilage. *J Biomech* 2007;40:3580–3589.

Verzijl N, DeGroot J, Ben ZC, Brau-Benjamin O, Maroudas A, Bank RA, Mizrahi J, Schalkwijk CG, Thropes SR, Baynes JW, Bijlsma JW, Lefeber FP, TeKoppele JM. Crosslinking by advanced glycation end products increases the stiffness of the collagen network in human articular cartilage:

a possible mechanism through which age is a risk factor for osteoarthritis. *Arthritis Rheum* 2002;46:114–123.

Voloshin AS, Wosk J. Influence of artificial shock absorbers on human gait. *Clin Orthop Relat Res* 1981;160:52–56.

Wainwright SA, Biggs WD, Currey JD, Gosline JM. *Mechanical designs in organisms*. Edward Arnold, London. (Ed.) 1976.

Wang Y, Liu H, Gao L, Xu B, Zhang C. Test the mechanical properties of articular cartilage using digital image correlation technology. *Procedia Environ Sci* 2011;8:191–196.

Weightman B, Chappell DJ, Jenkins EA. A second study of tensile fatigue properties of human articular cartilage. *Ann Rheum Dis* 1978;37:58-63.

Weightman B, Freeman MAR, Swanson SAV. Fatigue of articular cartilage. *Nature* 1973;224:303.

Weightman B, Kempson GE. Load carriage. In: Freeman, M.A.R. (Ed.), *Adult Articular cartilage*. Pitman Medical Publishing, London, 1979 pp. 291–329.

Weightman B. *In vitro* fatigue testing of articular cartilage. *Ann Rheum Dis* 1975;34:108–110.

Weightman B. Tensile fatigue of human articular cartilage. *J Biomech* 1976;9:193–200.

Whittle MW. Generation and attenuation of transient impulsive forces beneath the foot: a review. *Gait Posture* 1999;10:267–275.

Wolf AD, Pflieger B. Burden of major musculoskeletal conditions. *Bull World Health Organ* 2003;81:646–656.

Xin H, Shepherd DET, Dearn KD. Strength of poly-ether-ether-ketone: Effects of sterilisation and thermal ageing. *Polym Test* 2013;32:1001–1005.

Zimmerman NB, Smith DG, Pottenger LA, Cooperman DR. Mechanical disruption of human patellar cartilage by repetitive loading in vitro *Clin Orthop Relat Res* 1988; 229:302–307.